INFORMATION TO USERS

This manuscript has been reproduced from the microfilm master. UMI films the text directly from the original or copy submitted. Thus, some thesis and dissertation copies are in typewriter face, while others may be from any type of computer printer.

The quality of this reproduction is dependent upon the quality of the copy submitted. Broken or indistinct print, colored or poor quality illustrations and photographs, print bleedthrough, substandard margins, and improper alignment can adversely affect reproduction.

In the unlikely event that the author did not send UMI a complete manuscript and there are missing pages, these will be noted. Also, if unauthorized copyright material had to be removed, a note will indicate the deletion.

Oversize materials (e.g., maps, drawings, charts) are reproduced by sectioning the original, beginning at the upper left-hand corner and continuing from left to right in equal sections with small overlaps.

Photographs included in the original manuscript have been reproduced xerographically in this copy. Higher quality 6" x 9" black and white photographic prints are available for any photographs or illustrations appearing in this copy for an additional charge. Contact UMI directly to order.

Bell & Howell Information and Learning
300 North Zeeb Road, Ann Arbor, MI 48106-1346 USA
800-521-0600

DESIGN AND CONSTRUCTION OF A HIGH-BANDWIDTH COMPUTER CONTROLLED ROTARY VANE VENTILATOR

Mohsen Ahmadi

Department of Biomedical Engineering

McGill University, Montreal

April, 1999

A thesis submitted to the Faculty of Graduate Studies
and Research in partial fulfillment of the requirements
for the degree of

Doctor of Philosophy

Abstract

Abstract

The precise assessment of respiratory mechanics in intensive care unit (ICU) patients can potentially be of great benefit to their management. Some commercial ventilators now offer methods for determining values for lung compliance and resistance at a single frequency, however ongoing research in animals has shown that much more valuable information can be extracted from an analysis of the mechanical input impedance spectrum over a range of frequencies. To do this, it is essential to be able to control the characteristics of the input flow waveform into the lungs (i.e. frequency and amplitude). A new type of mechanical ventilator that measures respiratory impedance over a broad frequency range has been designed and built. It allows for simultaneous application of different ventilatory modes. The design has overcome some of the problems associated with the current experimental systems, such as the use of flow transducers between the patient and the flow source, or the temporary disconnection of the patient during the application of forced oscillations in flow. Generation of flow oscillations is based around a vane that rotates inside a semi-circular housing. The computer-controlled vane can generate volume displacements as low as 20 ml for frequencies from 0.5 to 10 Hz. The new ventilator may serve as a flexible research tool for mechanics studies in ICU patients, and ultimately as a device for routine assessment of respiratory mechanical status.

French abstract

Résumé

La possibilité d'évaluer avec précision l'état mécanique des voies respiratoires de patients admis en soins intensifs serait extrêmement bénéfique pour leur traitement. Actuellement, certains ventilateurs commerciaux offrent la possibilité de déterminer la valeur de l'élasticité et de la résistance des voies respiratoires mais seulement à une seule fréquence. De récentes études sur des animaux ont démontré qu'une grande quantité d'informations se trouve dans l'impédance mécanique des voies respiratoires mais sur une bande de fréquences. Pour obtenir ces informations, il est essentiel de pouvoir contrôler les caractéristiques du débit d'air allant dans les poumons. Cette thèse aborde la conception et la construction d'un nouveau type de ventilateur qui permet de mesurer l'impédance des voies respiratoires sur une large bande de fréquences. Avec ce concept, on a résolu certains des problèmes qui existent dans les systèmes actuellement sur le marché. Entre autres, on a éliminé l'utilisation d'un capteur de débit d'air entre le patient et le ventilateur, de même que le besoin de déconnecter le patient pendant l'application d'une ventilation forcée. Le débit d'air est produit par une vane qui oscille à l'intérieur d'un enclos semi-circulaire. Un moteur électrique produit le torque nécessaire pour déplacer la vane. Le système, entièrement contrôlé par un ordinateur, peut produire un débit d'air de 20 ml à une fréquence de 10 Hz. Ce nouveau ventilateur se présente, à ce jour, comme un instrument de recherche mais notre objectif est qu'il devienne un outil de routine pour l'évaluation de l'état mécanique des voies respiratoires.

Acknowledgments

Acknowledgments

I would like to thank Dr. Jason H.T. Bates for his help, guidance and supervision of this work. My thanks to Mr. Serge Filatrault for his valuable help in the mechanical workshop at Meakins Christie Laboratories. I would also like to express my gratitude to the Department of Physics, McGill University, in allowing the use of their facilities at their machine shop and in particular I like to thank Mr. Steven Kacani for his kind help with the CNC lathe machine. My thanks are due to Dr. Robert E. Kearney and other members of Biomedical Engineering Department for providing me with the opportunity to learn and produce this work. I like to express my deep appreciation to my colleagues Dr. Ross Wagner and Mr. Andrzej Kozakiewicz for many lively discussions on computing and signal processing matters. My thanks also go to Miss Eve Bijavi for her kind help with translation of the French abstract as well as her assistance during many experiments. Finally, my thanks go to the Medical Research Council of Canada for their financial support for this project.

TC

Table of contents

Abstract ii

Résumé iii

Acknowledgments iv

Table of Contents v

List of symbols x

1. Introduction 1

1.1 Mechanical ventilation 1

1.2 Rotating Vane Ventilator (RVV) objectives and design features 3

1.2.1. Objectives 3

2. Review of respiratory mechanics 5

2.1 Respiratory Fundamentals 5

2.1.1. Pulmonary Function 5

2.1.2. Physiology of the respiratory system 6

2.1.3. Mechanisms of respiration 7

2.1.4. Lung pressures during inspiration and expiration 8

2.1.5. Pulmonary compliance and elastance 8

2.2 Diseases affecting the respiratory system 9

2.2.1. Lung Mechanics 9

2.2.2. Lung mechanics - diseased conditions 9

2.2.3. Lung diseases 9

2.3 Mathematical modeling of the respiratory system 10

2.3.1. The single compartment linear model 13
2.4 Multi-Compartment Models 15
2.4.1. Two compartment model 15
2.5 Nonlinear Models 17
2.6 Respiratory Impedance 18
2.6.1. Fourier transformation 18
2.6.2. The impedance of the respiratory system 18
2.7 Respiratory mechanics parameter estimation techniques 21
2.7.1. Simultaneous equation technique 21
2.7.2. Loop flattering 21
2.7.3. Multiple linear regression 21
2.7.4. Flow interrupter technique 23
2.7.5. Forced oscillation 24
2.8 Characteristics of respiratory data 25
2.8.1. Precision of flow measurements 26
2.8.2. Perturbation signals 26
2.9 Closing remarks 27
3. Review of ventilator design 28
3.1 Mechanical ventilators 28
3.1.1. Historical overview 28
3.2 Basic features of a respiratory ventilator 29
3.2.1. Ventilator general basic functions 29
3.2.2. Classification of ventilators 29
3.3 Ventilation Modes 34
3.3.1. Pressure support 34
3.3.2. Synchronized intermittent mandatory ventilation (SIMV) 35
3.3.3. Adaptive lung ventilation (ALV) 36
3.3.4. Proportional assist- ventilation (PAV) 36
3.4 Gas compression technique in ventilators 37
3.4.1. Drive mechanisms 37
3.4.2. Weighted bellows 38
3.4.3. Spring-Loaded bellows 39
3.4.4. Linear driven piston 39
3.4.5. Nonlinear driven pistons 40
3.4.6. Pressure reducing valves 40

3.4.7. Blowers 41
3.4.8. Injectors 41
3.5 Ventilator circuits 42
3.5.1. Single circuit 42
3.6 High Frequency Ventilators 43
3.6.1. Historical overview 43
3.6.2. Terminology 45
3.6.3. High-frequency positive pressure Ventilator 46
3.6.4. High-frequency jet ventilator 47
3.6.5. High-frequency oscillator 48
3.6.6. High-frequency chest wall compressor 48
3.6.7. Small animal ventilator (SAV) 49
3.7 Mechanisms of gas transport during high-frequency ventilation 50
3.7.1. Physiological mechanisms of HFV 50
3.7.2. Mechanisms of gas transport involved in HFO 51
3.7.3. Clinical Application of High Frequency Ventilation 52
3.8 Technical problems common to most high frequency ventilators 54
3.9 Closing remarks 55
4. RVV: Mechanical design 56
4.1 RVV overview 56
4.1.1. RVV design 59
4.1.2. Calculation of Resistance to Back-Flow 63
4.1.3. Mathematical model of the ventilator 66
4.2 DC Motor 68
4.3 Shaft coupling 69
4.4 Valves 69
4.5 Compartmentalized support box 70
4.6 Electronic board installation 71
4.7 Position sensor 71
4.8 Closing remarks 72
5. RVV: Electronics setup 73
5.1 The Power amplifier 73
5.1.1. Assessment of power requirements 73
5.2 Power supply for the amplifier 75

5.2.1. Power supply 75
5.3 Data acquisition 78
5.3.1. Data acquisition circuitry 78
5.3.2. Optimized current source for resistive bridge sensors 79
5.3.3. The pressure channels 80
5.3.4. Signal conditioning within the control loop 83
5.3.5. Analog-to-digital converter board 83
5.3.6. PCMCIA board installation 88
5.4 Position sensor 89
5.5 Power supplies 90
5.6 Valve drivers 90
5.7 Information display panel 91
5.8 Air circulation fan 92
5.9 Closing remarks 93
6. RVV: System control analysis 94
6.1 RVV System Analysis and Control 94
6.2 Linear Model Development 95
6.2.1. Plant model 95
6.2.2. Dynamic analysis of the plant 98
6.2.3. PID controllers 99
6.2.4. Controller design 100
6.2.5. Proportional-Derivative compensation 103
6.3 The Nonlinear plant 108
6.3.1. Nonlinearities 108
6.4 Discrete realization 110
6.5 Implementing and tuning the controller 112
6.6 Closing remarks 116
7. RVV: Software design 117
7.1.1. Overview 117
7.1.2. User interaction 121
7.1.3. Programming language and operating system 122
7.1.4. Hardware requirements 123
7.2 Realization 123
7.2.1. Main Program 123
7.2.2. Menu system 124

7.2.3. Function modules 125
7.3 Setup and autocalibration **126**
7.3.1. Hardware initialization 126
7.3.2. Position and pressure channel calibration 127
7.4 Data acquisition function **128**
7.4.1. Perturbation signals 130
7.4.2. Interrupt service routine (ISR) 130
7.4.3. Data storage 132
7.5 Utility functions **133**
7.6 Closing remarks **133**
8. RVV: Validation 134
8.1 Characterization of the flow through opening C ($\dot{V}$) 135
8.2 Validation of flow ($\dot{V}$) computation by RVV **139**
8.2.1 Single frequency sinusoidal volume input waveforms 139
8.2.2 Chirp input waveforms 142
8.3 Load impedance estimation by RVV **144**
8.3.1 Theoretical analysis of the load 148
8.3.2 Estimation of the load by RVV versus the computer controlled piston oscillator 149
8.4 Respiratory impedance in normal subjects 151
8.5 Closing remarks 153
9. Discussion and conclusions 154
9.1 Applications scope: present and future **155**
9.1.1. Ventilation control 156
9.1.2. Modeling respiratory mechanics 156
9.1.3. Evaluation of bronchial pharmacology 156
9.2 Future directions **157**
9.3 Original contributions **158**
9.4 Publications arriving from this work **159**
References 161

List of symbols

List of symbols

ADC	Analog to Digital Converter
ADV	Adaptive Lung Ventilation
ARDS	Adult Respiratory Distress Syndrome
CMV	Conventional Mechanical Ventilation
COPD	Chronic Obstructive Pulmonary Disease
CPAP	Continuous Positive Airway Pressure
CSS	Card Socket Services
DAC	Digital to Analog Converter
DMA	Direct Memory Access
DOS	Disk Operating System
DTF	Disturbance Transfer Function
FIFO	First In First Out
FRC	Functional Residual Capacity
HFCWC	High Frequency Chest Wall Compression
HFFI	High Frequency Flow Interrupter
HFJV	High Frequency Jet Ventilation
HFO	High Frequency Oscillation
HFPPV	High Frequency Positive Pressure Ventilation
HFV	High Frequency Ventilation
IMV	Intermittent Mandatory Ventilation
I/O	Input-Out data lines
ISR	Interrupt Service Routine

LSB	Least Significant Bit
MMV	Mandatory Minute Ventilation
MTF	Motor Transfer Function
OVW	Optimal Ventilatory Waveform
PAV	Proportional Assist-Ventilation
PCMCIA	Compliant Personal Computer Memory Card International Association
PD	Proportional-Derivative
PEEP	Positive End Expiratory Pressure
PI	Proportional-Integrative
PID	Proportional-Integrative-Derivative
RAM	Random Access Memory
RVDT	Rotational Variable Differential Transformer
RVV	Rotary Vane Ventilator
SIMV	Synchronized Intermittent Mandatory Ventilation
TSR	Terminate and Stay Resident
C_L	Lung compliance
D	Viscous friction torque
E_L	Lung elastance
E_{tis}	Tissue elastance
E_{st}	Static elastance
f	Frequency
G	Tissue resistance
G_a	Amplifier gain
G_C	Controller gain
H	Tissue elastance
I	Inertance of gas
i	Motor armature current
L	Motor coil inductance
M	Motor constant
P_A	Alveolar pressure
P_a	Atmospheric pressure
P_{AW}	Airway pressure
P_{LC}	Pressure in the left chamber
P_{PL}	Pleural pressure
P_{RC}	Pressure in the right chamber
P_{sur}	Exterior absolute pressure
P_{tp}	Transpulmonary pressure
P_{tr}	Tracheal absolute pressure
R_{AW}	Airway resistance
R_L	Lung resistance
R_{tis}	Tissue resistance

V	Lung volume
$\dot{V}$	Air flow
V_t	Respiratory tidal volume
V_{RC}	Volume of compressed gas in the right chamber
V_{LC}	Volume of compressed gas in the left chamber
U_{offs}	Offset voltage
U_m	Motor input voltage
$Z(f)$	Impedance
Z_{ti}	Impedance of the tissue
Z_{AW}	Impedance of the airway
α	Phase of tissue compartment
λ	System's pole
μ	Air viscosity
θ	Angular displacement

1

Introduction

A flexible computer controlled high-bandwidth Rotating Vane Ventilator (RVV) is presented in this thesis. The RVV is intended for research in respiratory mechanics in larger experimental animals and adult humans.

1.1 Mechanical ventilation

Respiratory failure is a common cause of admission to the intensive care unit (ICU), and the subsequent weaning of the patients from the ventilator support is a major preoccupation. Despite this, current monitoring of respiratory mechanical function is essentially limited to examination of peak airway pressures and flow-volume curves. The mechanical properties of the lungs are crucial determinants of its ability to function properly, and may change adversely in a number of common situations (such as pulmonary edema, bronchoconstriction, and mechanical blockage of a major airway). The use of more sophisticated methods for assessing lung mechanics are beginning to appear in the ICU, and generally provide values for lung compliance and resistance. However, the mechanical functioning of the lung is far too complex to be adequately captured in a

pair of numbers. For example, the elastic and dissipative properties of the organ change greatly with the frequency of ventilation, and with tidal volume.

It is well known that much valuable information can be obtained by perturbing the respiratory system at frequencies higher than those found in breathing (Pelsin et al. 1986). Recent work in animals has shown quite clearly that one can infer a considerable amount about the site of airway obstruction, for example, by examining how the apparent resistance and elastance of the lung vary with frequencies from 0.1 to 10 Hz. The estimation of respiratory mechanics, in essence, involves the application of perturbations (in either flow or pressure) to the respiratory system and the measurement of the resulting output (either pressure or flow). The inputs and outputs are related in terms of mechanical models whose parameters are taken to embody quantities of physiological interest (like resistance or compliance). Thus, ideally the perturbations applied should be chosen appropriate to the kind of information required. For example, high frequency respiratory impedance (>5 Hz) tends to reflect properties of airways, while at low frequencies (<2 Hz) the properties of the respiratory tissues tend to dominate. Currently the estimation of respiratory mechanics in the ICU can be described as an *ad hoc* process in which one tries to make the best of whatever ventilator waveform is available (Bates et al. 1993). To be able to identify pulmonary mechanics, it is essential to have a means of applying flow waveforms into the lungs that have the appropriate frequency content and amplitude range. Current experimental systems in operation for application of forced oscillations in flow to the lungs use loudspeakers, piston pumps and a variety of other devices, connected in series with a conventional mechanical ventilator. However, these usually require that the patient be temporarily disconnected from the ventilator. Furthermore, if the flow oscillations are superimposed on top of the ventilator or spontaneous breathing waveforms, it is invariably necessary to interpose a flow transducer between the patient and the flow source.

Flow is usually measured by a pneumotachograph, which senses the differential pressure across a calibrated resistance. A pneumotachograph is incorporated into some single-patient monitoring systems, such as the *Siemens-Elma* ventilator. However incorporation of pneumotachographs into ventilator systems introduces an entirely new

set of problems, including increased dead space, mucous plugging of the pneumotachograph and problems of calibration changes caused by varying gas concentration. Pneumotachographs are also sensitive to temperature, humidity, and flow, and should be frequently calibrated under clinical conditions for reliable results. Moreover, they have limited frequency responses due to inertive and elastic properties of the gas inside them.

1.2 Rotating Vane Ventilator (RVV) objectives and design features

1.2.1. Objectives

It was the principal objective of this work to design and construct a new kind of mechanical ventilator that will overcome all of the limitations outlined in section 1.1. In particular the design goals were to

- Have maximum flexibility in terms of the flow waveforms available.
- Be able to accurately calculate the mechanical impedance of the ventilated load at flow oscillation frequencies up to 10 Hz.
- Avoid the use of pneumotachographs to measure flow.

To achieve these objectives, an innovative *drive mechanism* design for gas compression (see section 4.1.1) was developed and constructed. Generation of flow oscillations is achieved through the use of a vane rotating in a closed semi-circular housing, driven by a high torque, fast responding dc motor controlled by a computer (see 4.1.1). Air displacement of up to 20 ml at 15 Hz is easily achieved. The flow is estimated from the angular position and the pressures on either side of the vane. The ventilator is fully computer controlled and so has considerable flexibility; it can apply broadband ventilation and/or perturbation flow waveforms into the respiratory system. The waveforms merely need to be specified in software and exported to the ventilator drive. Precise estimation of the mechanical impedance of a ventilated load is possible from the ventilator's unique design (section 4.1.1.1), and does not require the use of any flow or pressure transducers interposed between the endotracheal tube and the ventilator tubing.

This is achieved without the temporary disconnection of the patient from the ventilator during the application of forced oscillations in flow, in contrast to most current experimental systems.

An information panel continually indicates the status of the valves, power supplies and other parameters. With the exception of the vane's position signal, pressure signals on either side of the vane and any other data from up to four channels are amplified, anti-alias filtered and digitized using a 12-bit A/D converter. A 90 MHz Pentium Laptop computer performs valve and motor control together with display panel update and data storage.

Naturally, the ventilator must maintain adequate ventilation to the patient as its highest priority. This means that computer control of the vane's position has to have priority over other tasks, such as data storage and graphic updates. This is realized by the use of a software/hardware programming technique called the *interrupt service routine (ISR)*, where a timing counter on the computer motherboard is programmed to give a clock pulse at a specific frequency which then activates the ISR where the motor control code is actually executed. All user interactions with software have to be checked to avoid a possible stall or crash of the program. The design of the software includes various graphics, safety features and alarms. Further ideas, computing tasks, ventilation modes as well as changes in control algorithms can be incorporated in the future relatively easily. The ventilator can thus serve as a flexible research tool for mechanics studies in ICU patients, with potential for use for routine assessment of respiratory mechanical status.

This thesis contains a detailed description of all the hardware and software components of the RVV and presents a validation study of the RVV's performance. In the next chapter a review of respiratory mechanics is given, beginning with a brief introduction to respiratory fundamentals and leading to a discussion of various proposed models as well as estimation techniques currently used for measurement of respiratory mechanics.

2

Review of respiratory mechanics

In this chapter, the basic respiratory system components are first presented. This is followed by a survey of the diseases affecting the lung and a literature review of mathematical models of the respiratory system. Techniques of parameter estimation applied to respiratory mechanics, types of data, the precision of flow measurements and perturbation signals are also discussed.

2.1 Respiratory Fundamentals

2.1.1. Pulmonary Function

The exchange of gases in any biological process is termed respiration. To sustain life, the human body must take in oxygen, which combines with hydrogen, carbon and various nutrients to produce heat and energy for the performance of work. The human respiratory system is made up of a number of components including the upper airways, the lungs and the chest wall. The function of the lung is to oxygenate the blood and to

eliminate carbon dioxide in a controlled manner. As fresh air enters the respiratory tract during inspiration it displaces the gases already present in the trachea and bronchi and then mixes with the gases in the alveoli. Gas exchange takes place when oxygen diffuses from the alveoli to the pulmonary capillary blood. Carbon dioxide, on the other hand, diffuses from the blood to the alveoli. The blood circulation system carries oxygen from the lungs and distributes it among the various cells of the body and at the same time returns carbon dioxide to the lungs.

2.1.2. Physiology of the respiratory system

Air enters the lungs via nasal cavities, pharynx, larynx, trachea, bronchi and bronchioles, as shown in Figure 2-1. The airways form a system of branching tubes, whose diameters decrease from the trachea to the periphery. The trachea is about 1.5 to 2.5 cm in diameter and approximately 11 cm long, extending from the larynx to the upper boundary of the chest, where it bifurcates into the right and left main stem bronchi. Starting from the trachea on average there are 23 bifurcations in the human. The first branching separates the flow to the right and left lung. The most peripheral generations of these airways are provided with alveoli. Like air bubbles with an average diameter of 0.3 mm, they are very densely packed and are separated by thin septa which maintain a close network of blood capillaries. This is the region where gas exchange takes

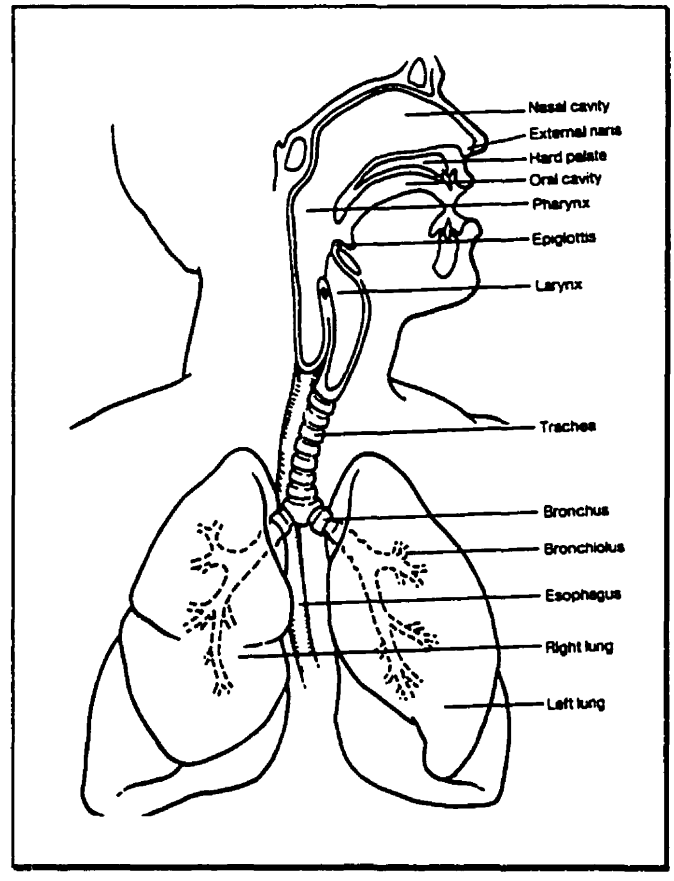

Figure 2-1: Air passages of the human respiratory system. (Adapted from Van De Graaff et al. 1987)

place (West 1977). The airway system has three distinct zones as seen in Figure 2-2. The conducting zone consists of airways that distribute and conduct the flow of inspired air into the gas exchange region and contain no alveoli. Gas transport in this region takes place as bulk flow. The intermediate or transitional zone includes airways very tightly associated with alveoli to form the link between conducting and respiratory airways. Finally, the respiratory zone or alveolar duct region contains all alveoli together with the pulmonary capillary network in their walls. At this level, diffusion is the mechanism by which gas is transported (West 1977).

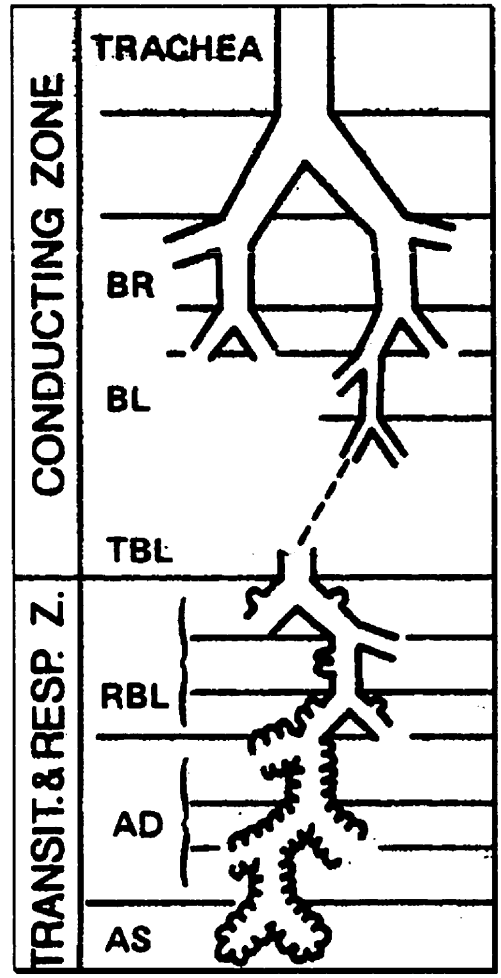

Figure 2-2: Human respiratory airways (Adapted from West 1977)

2.1.3. Mechanisms of respiration

Breathing is accomplished by musculature that changes the volume of the thoracic cavity and, in so doing, creates negative and positive pressures that move air into and out of the lungs.

The primary muscle of inspiration is the diaphragm. It forms a highly curved basal floor of the thoracic cavity which, when contracted, pulls downward to enlarge the thorax. While this happens, a group of external intercostal muscles lifts the rib cage and sternum to increase the effective diameter of the thoracic cavity and hence create a negative pressure in the thorax. This negative pressure (vacuum) is then relieved by air entering the lungs. At rest expiration is passive. On relaxation of the inspiratory muscles, the elastic energy stored in the lung and the chest wall reduces the volume of the thorax, developing a positive alveolar pressure that forces

air out of the lungs. When ventilation is increased, or during forced expiration, a set of abdominal muscles contribute actively to expiration.

2.1.4. Lung pressures during inspiration and expiration

During inspiration alveolar pressure reaches –1 cm H_20 while pleural pressure falls to about –11 cmH_2O. For exhalation, the pleural pressure increases to -7.5 cm H_20 and the alveolar pressure rises to +1 cm H_20 approximately.

2.1.5. Pulmonary compliance and elastance

Compliance indicates the relationship between the change in the volume of a closed system and the pressure distending it. In the respiratory case, the ability of the lungs and thorax to expand during breathing is influenced by their combined compliance, which is expressed as the volume increase ΔV in the lungs per unit increase in intra-alveolar pressure ΔP;

$$C_L = \frac{\Delta V}{\Delta P} \tag{2.1A}$$

Where C is compliance in L/cm H_2O, ΔV is the change in volume in liters and ΔP is the change in pressure in cm H_2O. Note the total compliance (C_T) of the respiratory system is made up of chest wall compliance (C_{cw}) and lung compliance (C_L). They add reciprocally:

$$\frac{1}{C_T} = \frac{1}{C_{CW}} + \frac{1}{C_L} \tag{2.1B}$$

Elastance, on the other hand, is the mathematical inverse of the compliance. It is defined as pressure increase ΔP in the lungs per unit increase in lung volume ΔV. The resistance of the airways to flow of air $\dot{V}$ into and out of the lungs is called *Airway* resistance R_{aw} and is expressed as the pressure drop ΔP between the mouth and the alveoli divided by $\dot{V}$.

$$R_{aw} = \frac{\Delta P}{\dot{V}} \tag{2.2}$$

Where R_{aw} is usually expressed in units of cm H_2O/L/sec; ΔP is pressure in cm H_2O and $\dot{V}$ is in L/sec. Lung tissue resistance (R_t) is determined by relating the difference between alveolar and lung surface pressure to the rate of change of the lung volume (Macklem et al. 1986).

2.2 Diseases affecting the respiratory system

2.2.1. Lung Mechanics

Lung mechanics concerns the study of the mechanical properties of the lung and chest wall. The mechanical characteristics of a lung under iso-volume conditions are referred to as lung statics. The application of Newton's laws of motion, for the determination of airflow into and out of the lung, is termed lung dynamics. As air is a fluid, fluid dynamics therefore govern its movement into and out of the lung.

2.2.2. Lung mechanics - diseased conditions

Several diseases can affect the ability to breathe by changing the mechanical properties of the lungs, chest wall or other components of the respiratory system. Pulmonary diseases are generally classified into two categories; restrictive and obstructive. Restrictive diseases limit the volume changes of the lung and hence reduce its compliance and increase the elastic work of breathing. Obstructive diseases, on the other hand, increase the flow-resistive work of breathing.

2.2.3. Lung diseases

Chronic obstructive pulmonary disease (COPD) refers to any longstanding obstructive process. However, the term is generally used to describe patients who exhibit *Emphysema*, *Chronic Bronchitis* or a combination of the two. Narrowing and collapsing of the airways, inflammation and increased mucous production are some of the problems

associated with COPD. A direct consequence of COPD is a severe increase in airway resistance and a somewhat lesser increase in lung elastance (West 1992). Asthma, on the other hand, is a condition where lung elastance and airway resistances increase significantly due to reversible bronchoconstriction as hyperresponsive airway smooth muscle constricts to an abnormal extent. The stimuli and underlying mechanisms of this phenomenon are still poorly understood. *Pulmonary Fibrosis* is one of the most common diseases of the lung parenchyma. Fibrous scar tissue is formed in the interstitium of the alveolar wall. The lung becomes stiff and nondistensible. Providing that the scar does not involve the airways, there is no significant increase on the airflow resistance.

Another disease associated with the lungs is the disorder of the Pleura, which is characterized by the loss of the vacuum of the intrapleural space. This happens when liquid (*Pleural Effusion*) or air (*Pneumothorax*) penetrates into the pleural space. In both cases resistance and elastance are increased.

2.3 Mathematical modeling of the respiratory system

Throughout the literature, the study of respiratory function is based almost universally on a class of models termed lumped-parameter, input-output relations. In these models, spatial distributions or variations of the parameters within the respiratory system are either ignored or incorporated as discrete values associated with hypothesized subsystems. The simplest such model reduces the whole respiratory system to a single flow conducting conduit and a single elastic compartment. While this greatly simplifies any description of its behavior in terms of easily measured variables, a certain degree of detail and insight is lost at the same time.

The pressure-volume relation of the lungs can be expressed as a mathematical relation of the form

$$P_A - P_{PL} = f(V) \tag{2.3}$$

where P_A is alveolar pressure and P_{PL} is pleural pressure. The pressure-volume relationship of the respiratory system can be evaluated independently from its pressure-

flow relation. To do this, for a range of volume changes, the pressure measured at the mouth when all flow throughout the system has died out represents the pressure difference. Pressure measured at the airway opening, P_{AO}, under zero flow conditions has no component due to airway resistance and so is due to elastic properties of the system only. Figure 2-3 is a plot of P_{AO} versus the range of lung volume. This is a nonlinear relationship, although for a restricted range of volumes a linear fit can be considered. If an operating point corresponding to the volume at functional residual capacity (FRC) or *end-expiration* is chosen, for variations in volume equivalent to tidal volume, the pressure is well approximated as a linear function of volume and the *static elastance* (E) is defined as the slope of the linear relationship. It is referred to as *static* because the measurements are made when the system is motionless. Equation 2.3 can now be written as

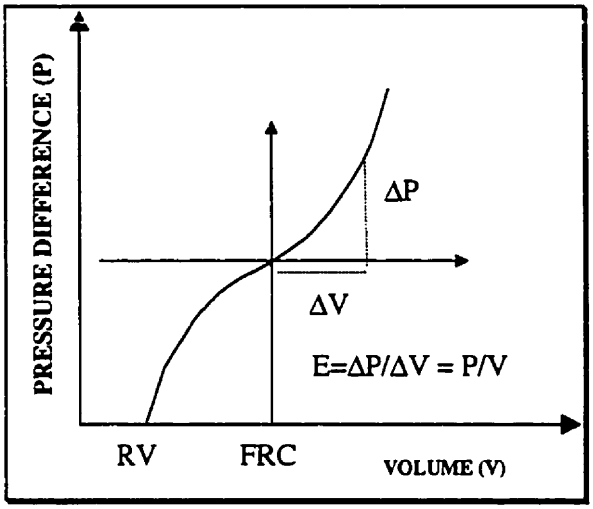

Figure 2-3: Airway pressure versus long volume

$$(P_A - P_{PL}) - (P_A - P_{PL})_{\text{at FRC}} = E(V - FRC) \tag{2.4}$$

If compliance is substituted for elastance, one obtains

$$(P_A - P_{PL}) - (P_A - P_{PL})_{\text{at FRC}} = (1/C)(V - FRC). \tag{2.5}$$

A general mathematical model in which pressure difference is expressed as a linear function of volume can be written as

$$(P_2 - P_1) - (P_2 - P_1)_0 = (1/C)(V - V_0) \tag{2.6}$$

or

$$p_2 - p_1 = (1/C)v \tag{2.7}$$

where p_1, p_2 and v are measured relative to defined operating points. P_o and V_o represent the values of pressure and volume at the chosen operating point. Furthermore, it is assumed that all variables are measured relative to their values at *FRC* or end-expiration.

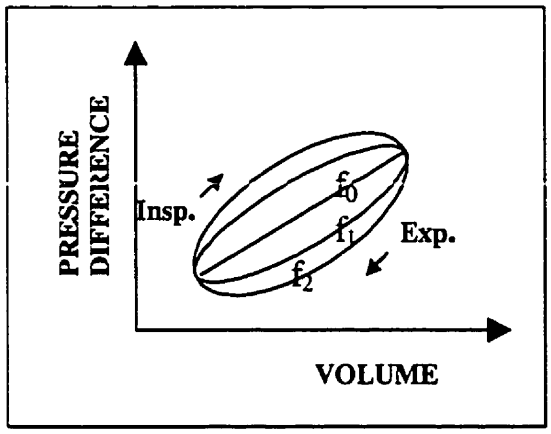

Figure 2-4: Pressure-volume relation for different frequencies

To describe the behavior of the respiratory system during spontaneous breathing or mechanical ventilation, the effects of flow have to be included in the model. If, for convenience, the breathing pattern can be taken to be approximately of sinusoidal nature, a plot of the pressure-volume relation for a range of breathing frequencies similar to Figure 2-4 is obtained. As seen in the Figure 2-4, the pressure difference necessary to inflate the lungs under dynamic conditions is greater than that of static conditions. It should also be noted that for any given tidal volume, with an increase in the breathing frequency, the flow and corresponding pressure difference also increase. Equation 2.8 incorporates the effect of flow:

$$p_1 - p_2 = V/C + f(\dot{V}) \tag{2.8}$$

Examination of pressure, volume and flow generated during breathing and subtracting a component equal to V/C from each value of pressure difference yields a pressure-flow relationship as in Figure 2-5. This is a nonlinear relationship, although it can be approximated by a linear function over a limited range of flows. Equation 2.8 can thus be written as

$$p_1 - p_2 = V/C + R\dot{V} \tag{2.9}$$

where R the constant of proportionality, is defined as *resistance*. Since volume, flow and pressure change continuously during a breathing cycle, Equation 2.9 can be rewritten as

$$p_1(t) - p_2(t) = V(t)/C + R\dot{V}(t) \tag{2.10}$$

Equation 2.10 is frequently used in the respiratory literature to describe respiratory mechanics. It is a linear differential equation with constant coefficients and is identical in form to that used in basic electronic circuit analysis to describe linear RC circuits.

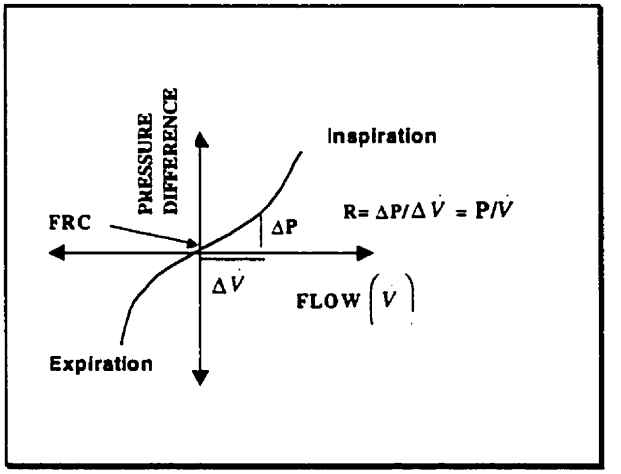

Figure 2-5: Pressure-flow relationship

2.3.1. The single compartment linear model

The simplest model of respiratory mechanics is that of a *Single Compartment Linear Model* shown in Figure 2-6 (Pelsin et al. 1986; Rodarte et al. 1986). The mathematical representation for this model is given by

$$P_{tp}(t) = P_{tr} - P_{sur} = EV + (R_{aw} + R_{tis})V + I\ddot{V} + K \tag{2.11}$$

where the variables are defined as

P_{tp} Transpulmonary pressure

P_{tr} Tracheal absolute pressure

P_{sur} Exterior absolute pressure, equivalent to atmospheric pressure if the chest wall is taken into account or representing that of the pleural space if only lung is modeled

I Inertance of the flowing gas

K Baseline pressure, i.e. the pressure at zero flow and tidal volume
The same as Positive End Expiratory Pressure (PEEP).

The effect of inertance is usually negligible at low frequencies close to those of normal breathing (0 to 4 Hz in dogs) but it has significance at higher frequencies. For low frequency purposes, the term $I\ddot{V}$ can therefore be negiected and Equation 2-11 is simplified to

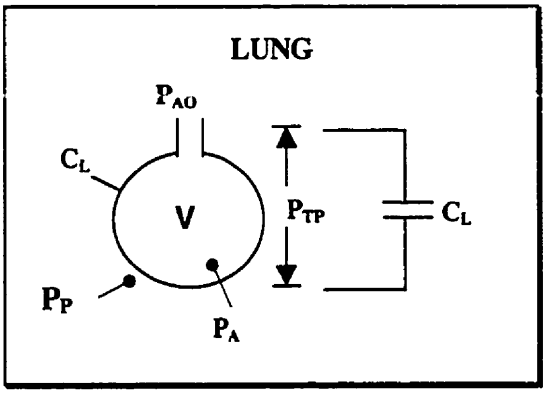

Figure 2-6: Single compartment model

$$P_{tp}(t) = P_{tr} - P_{sur} = EV + (R_{aw} + R_{tis})\dot{V} + K \tag{2.12}$$

or

$$P_{tp}(t) = P_{tr} - P_{sur} = EV + R\dot{V} + K \tag{2.13}$$

The first-order single compartment linear model (Figure 2-6) characterized by Equation 2.13 is the form most frequently referred to in the literature and is used both in drug response studies and in clinical applications. It is simple to visualize and understand. However representing the complexity of the respiratory system by this model has some drawbacks. To start with, it does not distinguish between the airway resistance due to gas flow, and the viscous effects in the parenchymal tissue. Nonlinearities such as flow dependence of airway resistance and dependence of the elastance on lung volume are not taken into consideration either.

2.4 Multi-Compartment Models

2.4.1. Two compartment model

In order to describe the respiratory system more accurately, a somewhat more complicated model is needed. One such model was first introduced by *OTIS* et al in 1956, and has been used in respiratory mechanics ever since. In this model the lungs are assumed to behave as two mechanically distinct units acting independently and connected in parallel, having elastances E_1 and E_2 and airway resistances R_1 and R_2. The two units are connected to a common central airway of resistance R_c (Figure 2-7a).

In 1969, *MEAD* suggested an alternative two-compartment representation for respiratory mechanics, consisting of compartments connected in series as shown in Figure 2-7b. In this model the proximal compartment represents the alveolar regions of the lung while the central compartment represents the finite compliance of the conducting airways. The impedance of this model has the same form as that of Figure 2-7a and can be made equal if the parameters are chosen appropriately. Figure 2-7 shows sketches of typical resistance and elastance as functions of frequency for the two-compartment model of the respiratory system.

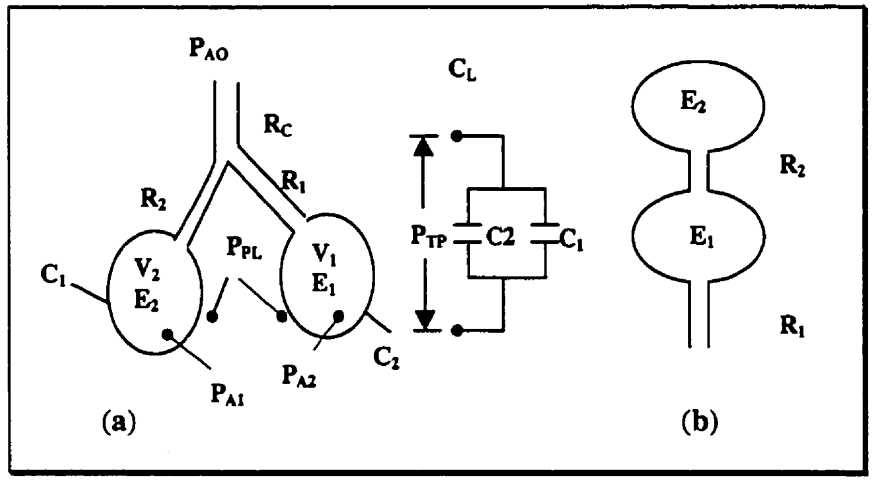

Figure 2-7: Two compartment model, a: Parallel, b: In series

There exists a third model of the respiratory mechanics where a single compartment model may be expanded to second order. *BATES* (1986) used a single uniformly ventilated alveolar compartment ventilated by a single rigid airway, but the tissues of the parenchyma are considered as having viscoelastic properties and so generate a recoil pressure that depends on volume and its history (Figure 2-9). The mathematical representation of this model can be written in the Laplace (s) domain as

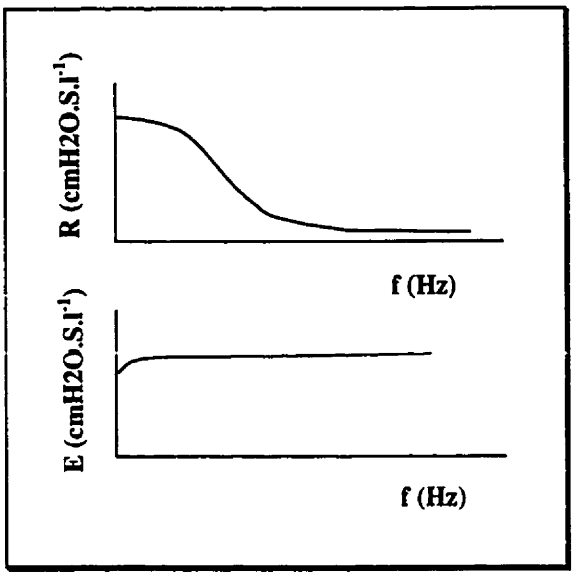

Figure 2-8: Hypothetical frequency dependence and resistance and reactance

$$\frac{P_{tr}(s)}{V(s)} = R_{aw} + \frac{E_{st}}{s} + \frac{R_{tis}E_{tis}}{sR_{tis} + E_{tis}} \tag{2.14}$$

Where P_{tr} and $\dot{V}$ are tracheal pressure and flow respectively. This model has been shown to fit the data identically to the other two compartment models shown previously, but is superior when alveolar pressure measurements are involved (Bates et al. 1986). The three models discussed above thus give a good estimation of respiratory mechanics for 0 to 2 Hz in normal lungs. At higher frequencies the effect of inertance must be included. Moreover in the case of disease the lungs invariably become inhomogeneous and the corresponding

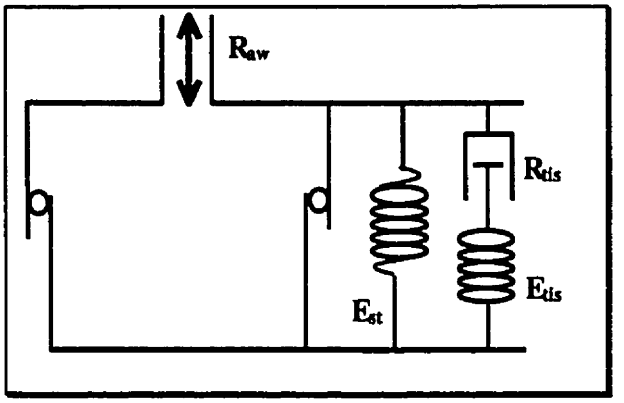

Figure 2-9: Second order elastic model

model should account for many alveolar compartments, each with different time constants and viscoelastic properties.

2.5 Nonlinear Models

Linear models, are valid for small amplitude perturbations in flow and volume. However the respiratory system acts in a nonlinear fashion when amplitude become large. It is believed that *ROHRER* (1915) proposed the first nonlinear description of respiratory mechanics. He postulated a pressure-flow relationship in the conducting airways:

$$\Delta P_{aw} = K_1 \dot{V} + K_2 V \left|\dot{V}\right| \tag{2.15}$$

ΔP_{aw} is the pressure drop across an airway. This equation is still being used to characterize airflow in airways and endotracheal tubes for ventilated patients (Bates et al. 1993).

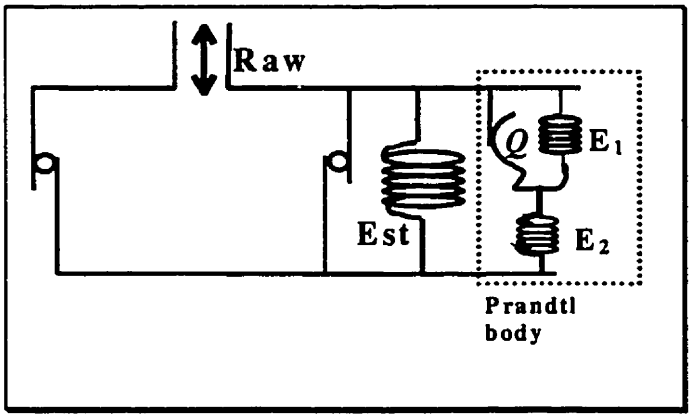

Figure 2-10: Second order viscoelastic model

HILDERBRANDT (1970) attempted to explain the quasi-static hysteresis observed experimentally in pressure-volume relations. Here the first order single compartment model has been extended by a plastoelastic *Prandtl* body, as shown in Figure 2-10. Due to the dry friction element Q within the Prandtl body, the total elastance varies in a very nonlinear fashion, since Q and E_1 will only move when the applied force exceeds the threshold value of Q.

Finally *HANTOS* (1982) used a polynomial formulation for pressure P_{tp}

$$P_{ip} = \sum_{k=0}^{K} e_k V^{k} + \sum_{l=1}^{L} r_l \dot{V}^{l} + \sum_{m=1}^{M} i_m \ddot{V}^{m} \tag{2.16}$$

good fits to experimental data has been reported for selection of K,L and M. The model is restricted to a single alveolar compartment.

2.6 Respiratory Impedance

2.6.1. Fourier transformation

Equation 2.13 can be Fourier transformed to give

$$P(f) = R\dot{V}(f) + \frac{E}{j2\pi f}\dot{V}(f) = R\dot{V}(f) - \frac{jE}{2\pi f}\dot{V}(f) \tag{2.17}$$

$$\therefore P(f) = \dot{V}(f)\left[R - jE/2\pi f\right] \tag{2.18}$$

where j is the square root of -1.

2.6.2. The impedance of the respiratory system

The impedance $Z(f)$ of the respiratory system is a complex function of frequency and is obtained from the relation

$$P(f) = Z(f)\dot{V}(f) \tag{2.19}$$

$Z(f)$ consists of two independent parts, a real and an imaginary part, for every value of f. Thus we have

$$Z(f) = \frac{P(f)}{\dot{V}(f)} = R(f) + jX(f) \tag{2.20}$$

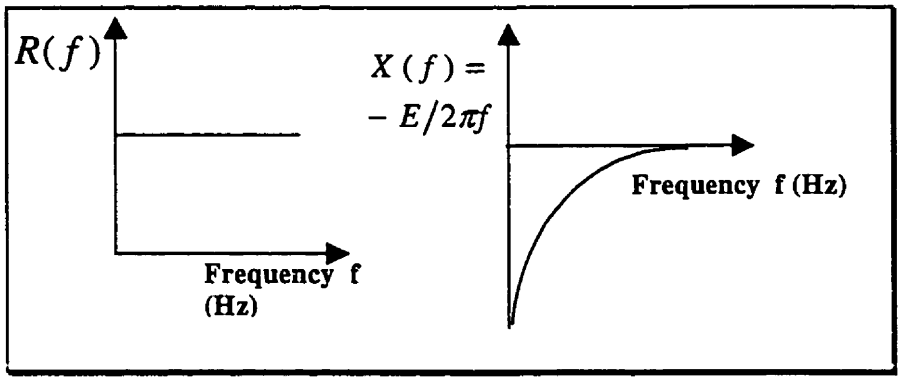

Figure 2-11: Hypothetical frequency dependence of resistance and reactance

The real part of impedance $R(f)$ is called resistance, because comparison of Equations 2.18 and 2.19 shows that, for the single compartment model:

$$R(f) = R \tag{2.21}$$

The imaginary part of $Z(f)$ is called reactance and is equal to $-E/2\pi f$. In the case of a single compartment model the reactance is negative and hyperbolic with frequency (Figure 2-11).

2.6.2.1 Constant-phase model

This is a model of pulmonary impedance (Z_L) that includes a constant-phase tissue part. It describes the lung impedance (Z_L) as

$$Z_L = R + jwI + \frac{(G - jH)}{(2\pi f)^{\alpha}} \tag{2.22}$$

$$\alpha = (2/\pi)\arctan(H/G) \tag{2.23}$$

Where R is resistance; I is pulmonary inertance; and G and H is reflect tissue resistance and elastance respectively. Z_L is made up of impedance of the tissue (Z_{ti}) and that of the

airways (Z_{aw}).α is an indicator of the phase of the tissue compartment (Z_{ti}) which is independent of the frequency, hence, the term constant-phase. It also controls the degree of coupling between tissue resistance and elastance. The model of Equation 2.22 was successfully applied to data obtained from dogs to separate airway and tissue properties by the use of what is referred to as the optimal ventilator waveform (OVW), where frequency content and the energy associated with those frequencies are specially selected (Lutchen et al. 1994). The constant-phase model was originally applied to pulmonary impedance in dogs (Hantos et al. 1990). Recently, the same model was also used to investigate the effects of lung volume on lung and chest wall mechanics in rats (Hirai et al. 1999).

2.6.2.2 Lung impedance: normal and bronchoconstrictioned

Recent work aiming to separate the contribution of all individual resistive and elastic components of the respiratory system to the overall lung impedance has shown that at typical breathing frequencies, R_{ti} makes up approximately 40% of the total R_L (Kaczka et al. 1997). However, under induced bronchoconstriction, R_{aw} is responsible for most of the increase in R_L. As the degree of constriction increases and for all frequencies, E_L and R_L increase, although the increase in E_L is more pronounced at higher frequencies (Kaczka et al. 1997).

Results obtained from the analysis of airway and tissue mechanics during physiological breathing and bronchoconstriction in dogs (Lutchen et al. 1994) indicates that there is a large increase in R_{ti} and tissue elastance (E_{ti}) when constriction of the lung occurs. Furthermore, in the case of severe constriction a significant increase in R_{aw} as well as airway inhomogeneities occurs. Further recent work has used a morphometric model of the human lung to predict flow distributions among the acini under heterogeneous bronchoconstriction (Lutchen et al. 1997), and investigated possible relations between those distributions and abnormalities in the mechanical properties of the lung. It was concluded that the ventilation distribution in the normal lung is homogenous over the frequency range of 0.1-5.0 Hz, and at frequencies below 0.1 Hz the ventilation seems fairly homogenous with mild constriction. However, with an increase in

the frequency, ventilation rapidly becomes heterogeneous. Moreover, severe constriction results in heterogeneous ventilation at all frequencies, and random airway closure is also probably produced (Lutchen et al. 1997).

2.7 Respiratory mechanics parameter estimation techniques

2.7.1. Simultaneous equation technique

The first method for estimating respiratory mechanic parameters is credited to *NEERGAARD* and *WIRTZ* (1927). It is based on the solution of simultaneous equations. For a first-order single compartment model, Equation 2.11 is evaluated at two points in order to obtain the unknown parameters R and E. If the two sampling points are chosen when flow is zero, (i.e. end of inspiration and end of expiration) then one of the variables vanishes in each equation and results are then available immediately. This method is sensitive to noise since only two isolated points per breath are used.

2.7.2. Loop flattening technique

The *Loop Flattening Technique* (Mead et al. 1953) is based on a graph of pressure against flow, a loop, that in the case of sinusoidal input to a first order model becomes an ellipse. In this technique the loop is flattened out to a line by rearranging Equation 2.13 and plotting $\Delta P - \hat{E}V$ against $R\dot{V}$. $\hat{E}$ is now the estimate of E adjusted by the operator and equals E exactly when the loop is flattened out to a line. The slope of the line then represents the resistance R. Precision and speed limit this technique.

2.7.3. Multiple linear regression technique

Recently implementation of the so-called *multiple linear regression and recursive least squares* techniques have found application in respiratory mechanics (Chapman et al. 1989; Lauzon et al. 1991). Both techniques relate system outputs to the inputs in a linear fashion. In general a linear (static) system may be expressed as follows,

$$\mathbf{y} = \mathbf{xA} + \varepsilon \tag{2.24}$$

where $\mathbf{y}$ is the output vector (N×1), $\mathbf{x}$ is the vector of independent input variables (N×M), $\mathbf{A}$ is the system matrix (M×1) and ε is un-correlated noise. The system of Equation 2.24 is modeled as

$$\hat{\mathbf{y}} = \mathbf{x}\hat{\mathbf{A}} \tag{2.25}$$

where $\hat{\mathbf{y}}$ is the estimated output and $\hat{\mathbf{A}}$ is the estimated system matrix. The sum of the squared errors between the model estimate and the experimental data is given by

$$\mathbf{e}^{\mathsf{T}}\mathbf{e} = \left[\mathbf{y} - \hat{\mathbf{y}}\right]^{\mathsf{T}}\left[\mathbf{y} - \hat{\mathbf{y}}\right] = \left[\mathbf{y} - \hat{\mathbf{A}}\mathbf{x}\right]^{\mathsf{T}}\left[\mathbf{y} - \hat{\mathbf{A}}\mathbf{x}\right] \tag{2.26}$$

Superscript $\mathbf{T}$ denotes matrix transposition. Minimizing Equation 2.26 with respect to $\hat{\mathbf{A}}$ gives a matrix that contains the model parameters

$$\hat{\mathbf{A}} = \left[\mathbf{x}^{\mathsf{T}}\mathbf{x}\right]^{-1}\mathbf{x}^{\mathsf{T}}\mathbf{y} = \mathbf{P}\mathbf{x}^{\mathsf{T}}\mathbf{y} \tag{2.27}$$

The matrix $\mathbf{P}$ is referred to as the information matrix. Equation 2.27 is the multiple linear regression algorithm.

A recursively updated version of this equation were recently applied to respiratory mechanics (Avanzolini et al. 1985; Chapman et al. 1989; Lauzon et al. 1991). The version of this algorithm used by *LAUZON* and *BATES* (1991) included a weighting parameter or "forgetting factor" $\rho, 0 < \rho < 1$, that essentially decreases the contributions of older values to the parameter estimates. The algorithm is as follows

$$\hat{\mathbf{A}}_{n+1} = \hat{\mathbf{A}}_n + \mathbf{P}_n\mathbf{x}_{n+1}\frac{\mathbf{y}^{\mathsf{T}}{}_{n+1} - \mathbf{x}^{\mathsf{T}}{}_{n+1}\hat{\mathbf{A}}_n}{\rho + \mathbf{x}^{\mathsf{T}}{}_{n+1}\mathbf{P}_n\mathbf{x}_{n+1}} \tag{2.28}$$

and for $\mathbf{P}$

$$\mathbf{P}_{n+1} = \frac{1}{\rho}\left[\mathbf{P}_n + \frac{\mathbf{P}_n \mathbf{x}_{n+1} \mathbf{x}^T{}_{n+1} \mathbf{P}_n}{\rho + \mathbf{x}^T{}_{n+1} \mathbf{P}_n \mathbf{x}_{n+1}}\right] \tag{2.29}$$

The choice of forgetting factor should be a trade-off between smooth parameter estimates and low noise sensitivity. When this technique is applied to Equation 2.13, representing a single compartment linear model of the respiratory system, the following is obtained

$$\begin{pmatrix} P_1 \\ P_2 \\ P_3 \\ . \\ . \end{pmatrix} = \begin{pmatrix} V_1 & \dot{V}_3 \\ V_2 & \dot{V}_2 \\ V_3 & \dot{V}_3 \\ . & \\ . & \end{pmatrix} \begin{pmatrix} E \\ R \end{pmatrix} + \begin{pmatrix} n_1 \\ n_2 \\ n_3 \\ . \\ . \end{pmatrix} \tag{2.30}$$

The algorithm described by Equations 2.28 and 2.29 were used successfully to estimate respiratory mechanics in vivo both in dogs (Bates et al. 1992; Lauzon et al. 1992) and humans (Bates et al. 1993).

2.7.4. Flow interrupter technique

The Flow Interrupter Technique was also proposed by *NEERGARD* and *WIRTZ* (1927). The idea is to suddenly occlude the subject's airway so that flow is forced to zero and the term $R_{aw}\dot{V}$ in the Equation 2.13 disappears. This produces a step change in tracheal pressure, ΔP_{init}, that gives R_{aw} if $\dot{V}$ just prior to occlusion is known. If the airway closure remains, further reduction in tracheal pressure will take place until a plateau is reached. The pressure drop ΔP_{diff} in normal lungs is almost entirely due to viscoelastic properties of the respiratory tissues (Figure 2-12) (Bates et al. 1988). If airway resistance is of interest, the occlusion can be brief enough not to cause discomfort

to the subject, but the compliance of the upper airways (cheeks, nose and pharynx) influence the measurements significantly

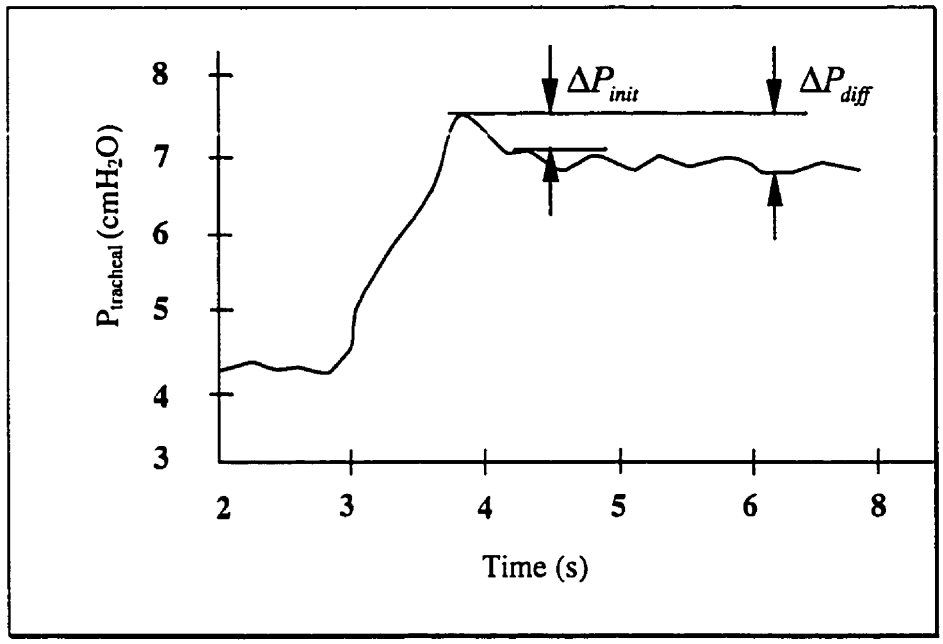

Figure 2-12: Flow interrupter technique

2.7.5. Forced oscillation technique

In recent years, Forced Oscillation Techniques have been increasingly used in respiratory mechanics (DuBois et al. 1956; Jackson et al. 1987; Sato et al. 1991). In this method normally a broadband composite flow signal is applied to the airway opening of the subject. The resulting pressure is also measured at the airway opening. The flow oscillation signal can be applied on top of spontaneous breathing, although it must not contain any frequency components that might exist in the breathing pattern. Data obtained are processed using the Fast Fourier Transform (FFT) to calculate the input impedance of the respiratory

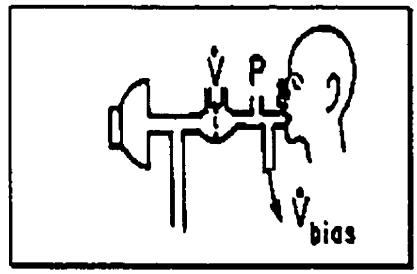

Figure 2-13: experimental setup for the application of forced oscillation technique

system. Figure 2-13 shows a typical experimental setup used in this technique. Piston oscillators and loudspeakers are some of the most common devices that are used to generate sinusoidal flow signals. Assuming pressure and flow transducers have linear responses over the range of interest, their signals are amplified and anti-alias filtered before digitization.

The input flow signal is usually composed of frequencies of interest with appropriate amplitudes and phases. However a sinusoidal input to a nonlinear dynamic system gives an output signal which contains power at other frequencies, in particular at the harmonics of the input frequencies. Moreover, if the power in the input signal to such a system occurs at a fundamental frequency and its first harmonic, it is not possible to see what effects in the output signal come from the fundamental and what are due to the harmonic. To solve this problem, the input signal may be composed of mutually prime frequencies where the power in the input signal occurs at a fundamental frequency and a second higher frequency that is not an integer multiple of the fundamental (see section 2.8.2).

2.8 Characteristics of respiratory data

In order to be able to describe the dynamics and other features of the respiratory system, identification of respiratory mechanics is essential. In developing a mathematical model of respiratory system mechanics, relevant physiological variables that can be used to describe the mechanical behavior of the system have to be defined and acquired. Ultimately, these variables must be traceable to forces, displacement, and their rates of change. The variables most commonly used to describe respiratory mechanics are pressure (a generalized force), volume (displacement), and flow.

Data can be acquired during regular ventilation (spontaneous or mechanical). It is also possible to temporarily suppress ventilation and apply a specific perturbation flow signal. In both cases, the input due to respiratory muscular forces is unknown, when the subject attempts to breathe voluntarily. Although, in experimental situations or in the case of animal experiments, subjects can be anesthetized and paralyzed to remove the input from the muscular forces, this may not always be possible in clinical practice. In those

circumstances an esophageal balloon can be used to measure esophageal pressure as an estimate of pleural pressure. However, in animal experiments, direct measurement of alveolar pressure is possible through alveolar capsules, where a small capsule containing a pressure transducer is placed on the lung surface. Small puncture holes on the pleural surface then establish direct connection between alveoli and pressure transducer (Fredberg et al. 1984; Fredberg et al. 1985; Bates et al. 1988; Ludwig et al. 1990).

2.8.1. Precision of flow measurements

In most conventional setups, a pneumotachograph and a differential pressure transducer are used to measure tracheal flow. These are placed between the subject and the ventilator. Pneumotachographs are known to perform poorly when small flows at high frequencies are being measured. This is mainly due to the additional inertive and elastic properties of the entrained air inside the transducer and the connecting tubes. The dynamic behavior of the Fleisch type 0 and 00 pneumotachographs have been shown not to be ideally flat up to 15 Hz (Schuessler et al. 1993). Although it may be possible to characterize the frequency response of the transducer and correct for it, in practice this is problematic and generally prone to noise.

2.8.2. Perturbation signals

To identify the parameters of a model, an appropriate flow signal has to be applied to the respiratory system. For example, a linear low-order model might produce a good fit to data obtained from a quasi-sinusoidal and not a broad band input signal.

In general, when the parameters of a model are being identified, the frequency of the applied signal to the system must exceed those of the dominant poles that govern the system under identification. To avoid harmonic distortion and minimize harmonic cross talk, the signal may be constructed so that none of the frequencies containing energy is an integer multiple of the fundamental frequency or the difference or sum of the other frequencies. At each frequency the phase may be optimized to yield a minimum peak to peak volume excursion (Lutchen et al. 1994). This is known as non-sum non-difference optimal ventilatory waveform (OVW-NSND).

2.9 Closing remarks

In this chapter an introduction to respiratory fundamentals was given and certain diseases associated with the respiratory system were also touched upon. Mathematical models relating pressure and flow for single- and multi-compartmental systems were discussed and the chapter concluded with a survey of various techniques used for estimation of respiratory mechanics as well as the types of perturbation signals that are most suited for this process.

The next chapter focuses on the design of ventilators. Their basic features, functions, and classification will be discussed and some of the more common ventilation modes presented. Gas compression techniques and common mechanisms used are a principal component of any ventilator, so this will be investigated exhaustively. Ventilators that move gas at high frequencies will also be discussed. The chapter will conclude with a survey of some of the problems associated with these types of ventilators.

3

Review of ventilator design

This chapter starts with an introduction to mechanical ventilators. The basis of classification and some of the ventilation modes that they can deliver are described. A full survey of gas compression techniques, a major feature of all ventilators, will be addressed. Next, ventilators that are capable of delivering air at high frequencies and their corresponding characteristics will be discussed. Mechanisms of gas transport during high frequency ventilation and clinical applications of this mode of ventilation will also be presented. Some of the common problems associated with these devices will bring the chapter to a close.

3.1 Mechanical ventilators

3.1.1. Historical overview

A ventilator is basically a device used to deliver gas volumes to the lungs. Positive pressure ventilation applies positive pressure to the airway opening, while negative pressure ventilators apply a relative vacuum round the chest wall. These techniques result in bulk flow of gas through the airways and into the gas exchanging

units of the lung. A mechanical ventilator is usually employed with a mask or endotracheal or tracheostomy tube. Widespread use of artificial ventilatory support began with the poliomyelitis epidemic of the 1950s. Today, the crude devices of the1950s have been replaced by more practical and efficient devices as a result of technological advances. Positive pressure ventilation has become common-place and at the same time newer techniques and technologies have further enhanced the ability to maintain artificial breathing for long periods of time.

3.2 Basic features of a respiratory ventilator

3.2.1. Ventilator general basic functions

In general, there are four phases within a respiratory cycle that a ventilator has to control. As shown in Figure 3-4 these are

- Inflate the lungs — Inspiratory phase
- Stop lung inflation — The changeover from inspiratory to expiratory phase
- Allow lungs to empty — The expiratory phase
- Start lung inflation — The changeover from expiratory to inspiratory phase

3.2.2. Classification of ventilators

3.2.2.1 Type of pressure gradients

Classification of ventilators has been described in various formats in the medical literature for over two decades. One of the bases of theoretical classification of these devices is pressure. This is the type of force that the ventilator applies to the subject to achieve ventilation. There are three major divisions of ventilators based on pressure, they are:

- ***Negative-pressure*** ventilators, where application of negative pressure around the chest wall generates a force which causes a pressure gradient of atmospheric to sub atmospheric, which expands the chest and moves the gas into the lungs (Figure 3-1). The Iron Lung and Cuirass are examples of this type of ventilator.

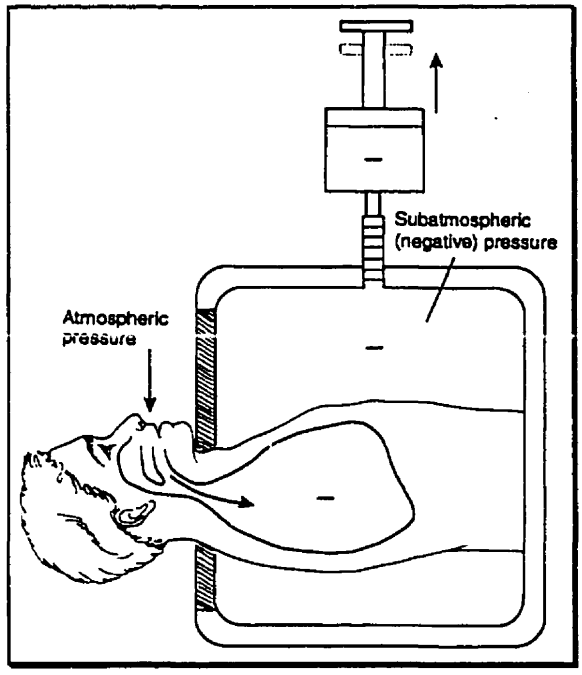

Figure 3-1: Negative pressure ventilation (Adopted from McPherson 1995)

- ***Positive-pressure*** ventilators, where the device creates a positive pressure at the airway opening. This leads to a force that expands the chest and lungs (Figure 3-2). Pressure-limited and volume-limited ventilators are examples of this type.

- ***Positive/negative-pressure ventilators*** where a combination of the forces stated above creates negative extrathoracic pressure and positive intrathoracic pressure to provide the necessary force to move gas into the lungs (Figure 3-3).

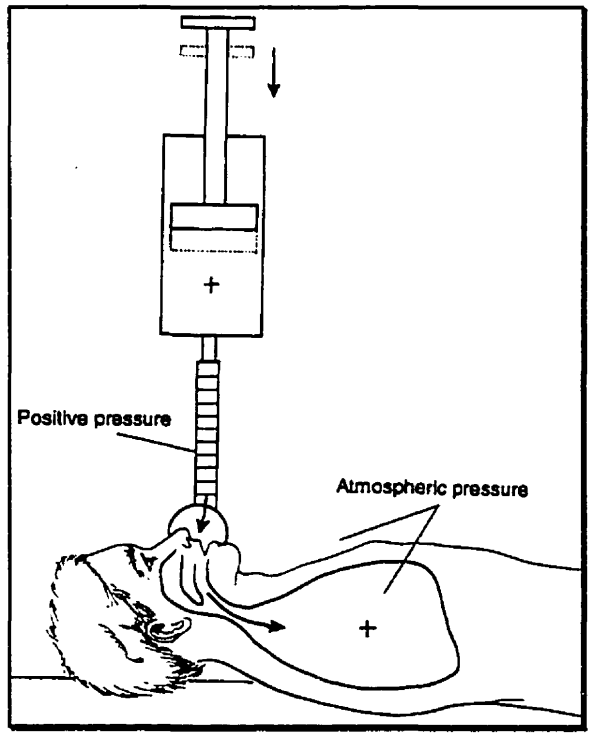

Figure 3-2: Positive pressure ventilation (Adapted from McPherson 1995)

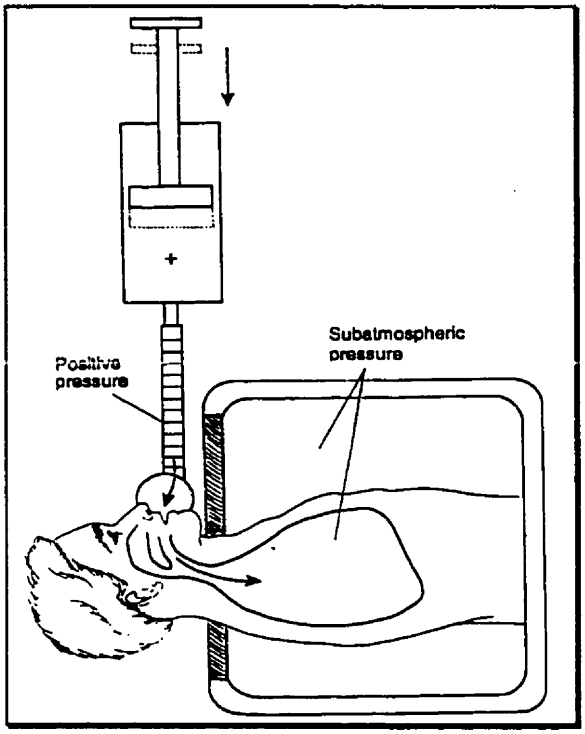

Figure 3-3: Positive/negative inspiration (Adapted from McPherson 1995)

3.2.2.2 Starting inspiration

The initiation of inspiration in any of the three ventilator divisions described above can include one or any combination of the following methods:

- ***Assist*** mode where a pressure sensor responds to the slight airway pressure change that occurs each time the patient attempts to inhale. This triggers the apparatus to begin inflating the lungs (Figure 3-4).
- ***Control*** mode where the respiration rate is set by a timer mechanism.
- ***Assist-Control*** mode which is essentially the same as assist mode but if the patient fails to breathe within a predetermined time, a timer automatically triggers the device to initiate inspiration.
- ***Manual*** mode where the patient or an operator triggers the inspiratory phase manually.

3.2.2.3 Ending inspiration-initiating expiration

One further basis of classification of ventilators is the mechanism by which the device terminates the inspiratory phase. This is referred to as the changeover from inspiratory phase to expiratory phase. This factor has a considerable effect on how a ventilator is designed, influencing the electronics and the mechanisms involved in control, the physical size of the air chamber, and a whole series of other features. The following is a list of the four cycling mechanisms used in the design of automatic ventilators:

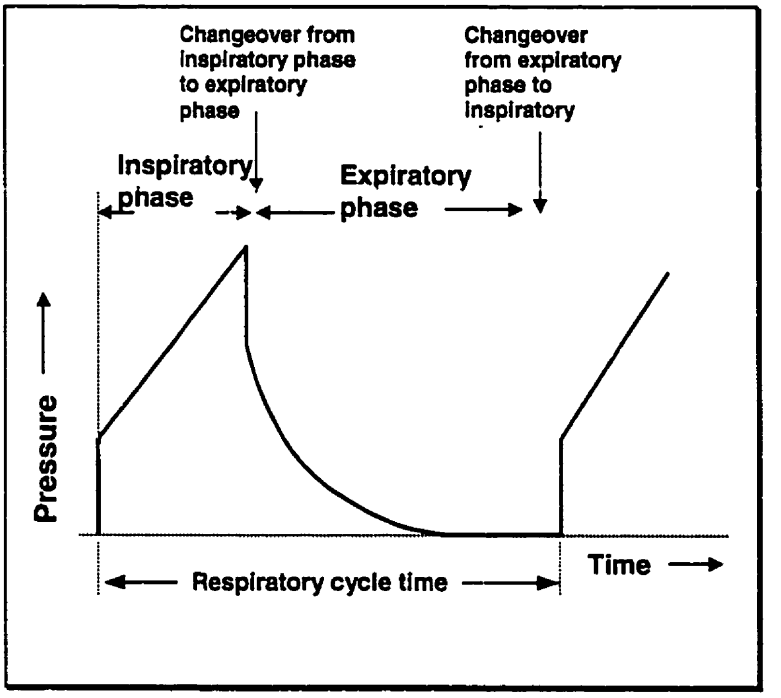

Figure 3-4: Four phases of respiratory cycle on controlled ventilation

- Pressure cycled
- Flow cycled
- Volume cycle
- Time cycled

3.2.2.4 Pressure-cycled mechanisms

A ventilator is said to be pressure cycled if the inspiratory phase is terminated when a pressure sensing mechanism, within the ventilator, detects a predetermined pressure set by the operator. Note that other parameters such as the volume of air delivered, the flowrate and the time taken to deliver the volume may all vary from one

respiratory cycle to other. This happens when any pressure-cycled ventilator is confronted with changes in lung mechanics (Dupuis 1992). This mechanism may be pneumatic, electronic, or a combination of both.

3.2.2.5 Flow-cycled mechanisms

In flow cycled ventilators, the inspiratory phase ends when the flowrate, detected by a flow sensitive valve incorporated within the ventilator, falls to a critical level. As is the case with pressure-cycled ventilators, at the moment of flow cycling, the volume and pressure in the lungs and the time it may take to end the inspiratory phase can all change from one inspiratory cycle to the next. The only parameter which remains constant is the terminal flowrate.

3.2.2.6 Volume-cycled mechanisms

When the inspiratory phase in a ventilator is controlled via delivery of a predetermined volume set by the operator, the ventilator is said to be volume cycled. During cycling, the time taken to deliver the volume, the pressure developed in the patient circuit, and the flowrate can all change within different respiratory cycles. However volume always remains constant. The volume-cycling mechanism can be pneumatic or electric.

3.2.2.7 Time-cycled mechanisms

With a time cycled ventilator, the inspiratory phase is controlled through a timing mechanism. Although other parameters, such as pressure, flow and volume, can constantly change from one respiratory cycle to another, preset inspiratory time remains constant. The timing mechanism is usually pneumatic or electromechanical, and electronic or microprocessor controlled.

3.3 Ventilation Modes

As mentioned in section 3.2.2.2, the ventilation mode is concerned with the way the ventilator interacts with the patient in the inspiratory phase of the breathing cycle. In this section some of these modes are described.

3.3.1. Pressure support

Pressure support ventilation (PSV) is a spontaneous breathing mode where the patient triggers the ventilator to receive a pressure-supported breath. During the inspiration phase the ventilator adjusts the flow continuously to supply the patient's inspiratory demands, while maintaining the airway pressure at a constant positive level. As with any spontaneous breathing mode, PSV should be initiated at a level that provides the desired volume exchange, usually set between 10 and 12 ml/kg of body weight, and is

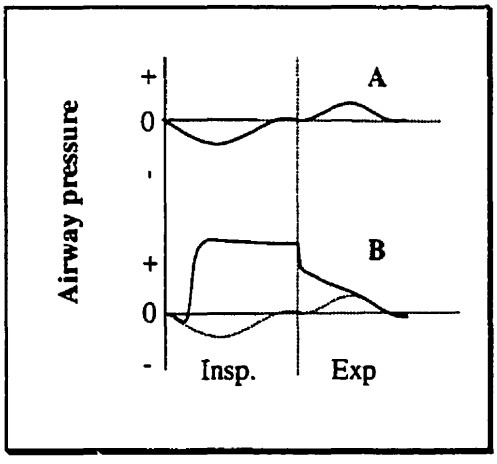

Figure 3-5: Airway pressure during spontaneous breathing (A) and pressure support (B)

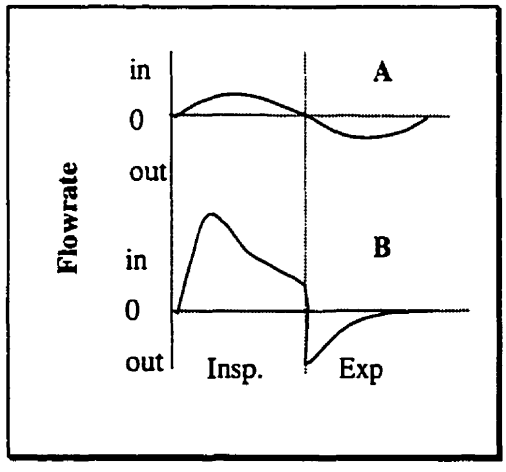

Figure 3-6: Flowrate during spontaneous breathing (A) and pressure support (B)

normally considered only for subjects that have the drive to initiate respiration on their own. Figure 3-5A and B show sketches of the airway pressure during spontaneous and pressure supported ventilation, respectively. As seen in Figure 3-5, the support of pressure within the ventilator is turned off as spontaneous inspiration approaches its end. However, with most ventilators this happens when the flowrate during inspiration falls to 25% of the maximum flow attained during the same breath (Figure 3-6B). It is worth

noting that in PSV mode, most ventilators normally operate in flow-cycling mode (see section 3.2.2.5), although other mechanisms are also used for patient safety. PSV can be used to reduce the work of breathing (WOB). This is the work the patient has to perform to overcome viscous and airflow resistance and elastance of the airways and the lungs. PSV is also utilized with other modes of ventilation such as synchronized intermittent mandatory ventilation (SIMV), mandatory minute ventilation (MMV) and continuous positive airway pressure (CPAP).

3.3.2. Synchronized intermittent mandatory ventilation (SIMV)

A ventilatory mode that permits the patient to breathe spontaneously between controlled positive pressure breaths is called intermittent mandatory ventilation (IMV). During IMV, the spontaneous and the mandatory breaths are not necessarily synchronized; a mandatory breath may be delivered anywhere in the patient's respiratory cycle. This can lead to stacking of breaths as shown in Figure 3-7B. However, if delivery of IMV is synchronized with spontaneous breathing, the procedure is referred to as

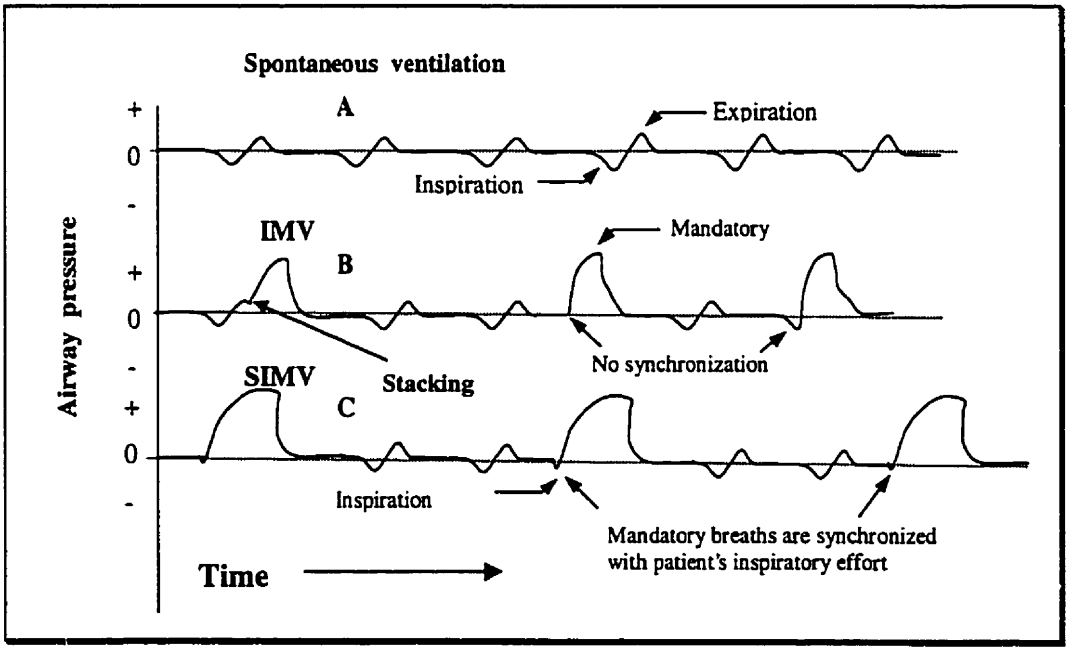

Figure 3-7: Pressure waveforms for A, spontaneous ventilation. B, Intermittent mandatory ventilation (IMV). C, Synchronized intermittent mandatory ventilation (SIMV)

SIMV. In other words, during SIMV the ventilator recognizes the patience's respiratory cycle through various mechanisms and delivers the mandatory breath at a pre-determined point in that cycle. In this way, the stacking of the breaths is avoided. Figure 3-7 illustrates the essential differences between spontaneous ventilation, IMV and SIMV. Mandatory minute ventilation (MMV) is a special form of SIMV where the patient is guaranteed to receive a certain minimum minute ventilation, either through spontaneous breathing, by the ventilator or by a combination of both. These techniques of ventilation have been presented as an alternative to the standard method of patient weaning (Dupuis 1992).

3.3.3. Adaptive lung ventilation (ALV)

For many years, the controllers used for mechanical ventilation were based on mean expired CO_2, end-tidal CO_2, arterial CO_2, or arterial pH. The controlled variables were inspiratory pressure, tidal volume or mechanical rate, or both (Laubscher et al. 994). Using such controllers can be hazardous in certain circumstances. For example the end-tidal CO_2 controller does not take into account physiologic deadspace ventilation in patients with lung emboli. Furthermore, these controllers used simple modes of mechanical ventilation, not suitable for assisted ventilation or spontaneous breathing. In the case of pressure support ventilation this presents an unacceptable limitation.

ALV is based on closed loop controlled ventilation. it is a pressure controlled ventilation mode suitable for spontaneous breathing as well as paralyzed subjects. The controlled variables are the breathing rate and inspiratory pressure level. The ALV controller attempts to achieve a desired level of alveolar ventilation based on the measurement of the patient's lung mechanics and series dead space (Laubscher et al. 994).

3.3.4. Proportional assist- ventilation (PAV)

PAV is an experimental mode of partial ventilatory support in which the ventilator generates flow to compensate for the resistive load (flow assistance) and volume to compensate for the elastic load (volume assistance). In both cases, the ventilator pressure increases either in proportion to the volume or to the flow of spontaneous breathing. The

ventilator pressure thus follows a pattern similar to that of the patient-generated pressure. In effect, the ventilator amplifies the patient effort. The degree of assistance is proportional to inspiratory muscle effort and can vary from zero to a maximal level at which the ventilator produces almost all the pressure required to maintain instantaneous volume and flow. Naturally, since the ventilator-generated pressure is a function of the patient's effort at any time, the patient remains in control over all parameters of the ventilator output (i.e. tidal volume, flowrate, inspiratory-expiratory ratio and so on). This makes PAV an ideal tool for the study of the pattern of breathing in patients with various respiratory diseases. Other potential benefits with PAV are (Younes 1992):

- Greater patient comfort
- Reduction of peak airway pressure to maintain ventilation and, hence, potential for avoiding intubation
- Improved efficiency of negative pressure ventilation
- Less over-ventilation
- Preservation and enhancement of patient's own behavioral, reflex, and homeostatic control mechanisms
- Insights into the control of breathing of patients

3.4 Gas compression techniques in ventilators

3.4.1. Drive mechanisms

A major design feature of ventilators, positive or negative, is the pressure compression/decompression system or drive mechanism. The scope of applications of a ventilator depends critically on its drive mechanism. The following is a list of the most common techniques currently used for pressurizing air in ventilators.

- Weighted bellows
- Spring-loaded bellows
- Linear-drive pistons
- Nonlinear-drive pistons

- Pressure-reducing valves
- Blowers
- Injectors

3.4.2. Weighted bellows

In this setup (Figure 3-8A), the pressure generated within the bellows is a function of the weight acting on the cross-sectional area of the bellows. The greater the weight, the greater the pressure generated. This mechanism generates constant pressure. This is due to the fact that the downward force of the weight causes the bellows to empty, as the stopcock is opened (Figure 3-8B) and the pressure inside it remains unchanged because the relationship of force per area does not change. The Brompton-Manley BM-2 ventilator incorporates this drive mechanism.

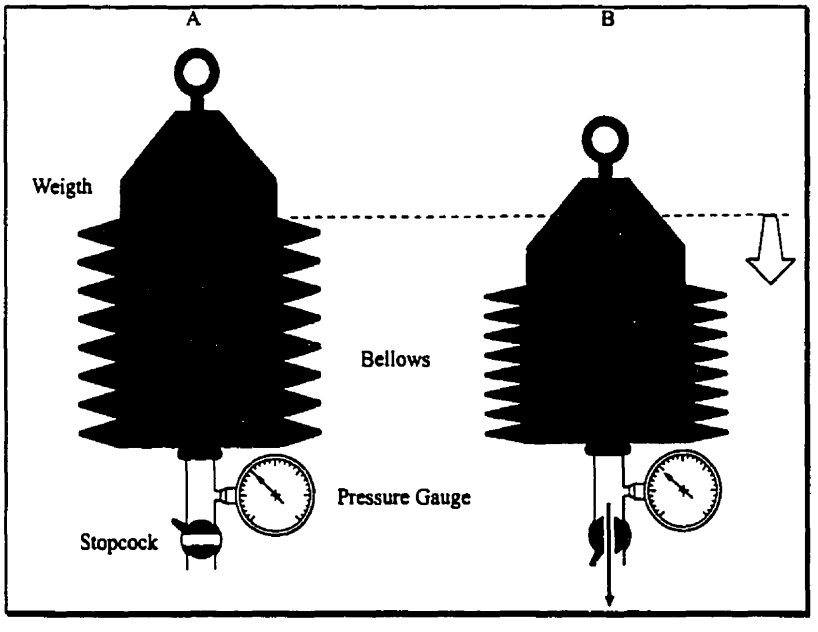

Figure 3-8: Weighted bellows drive mechanism (Adapted from Dupuis 1992)

3.4.3. Spring-Loaded bellows

This is a mechanism used in the Siemens Servo 900 series ventilators. As shown in Figure 3-9, the tension of a spring applies a continuous downward force at the top of an expanded bellows. The pressure generated is a function of the cross-sectional area of the bellows and the force within the spring. However, unlike the weighted bellows, as the bellows empties the spring relaxes and hence the pressure within the bellows decreases.

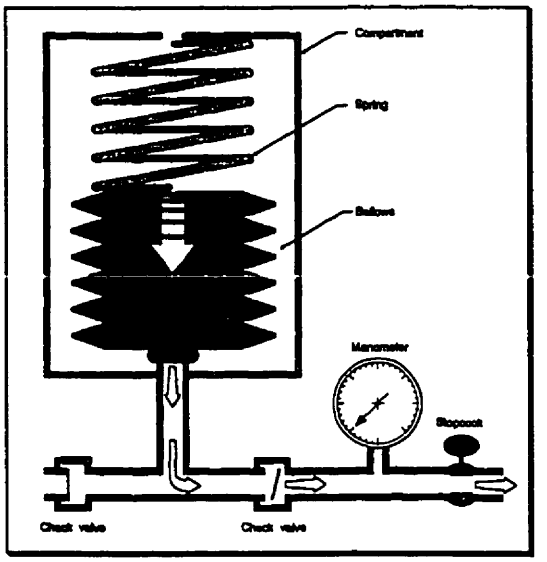

Figure 3-9: spring-loaded bellows (Adapted from Dupuis 1992)

3.4.4. Linear driven piston

In this method of pressure generation, an electric motor drives a piston in a closed cylinder through a linear screw lead assembly as shown in Figure 3-10. The piston's linear forward stroke leads to the creation of positive pressure. This drive mechanism is used in some electronic pediatric ventilators.

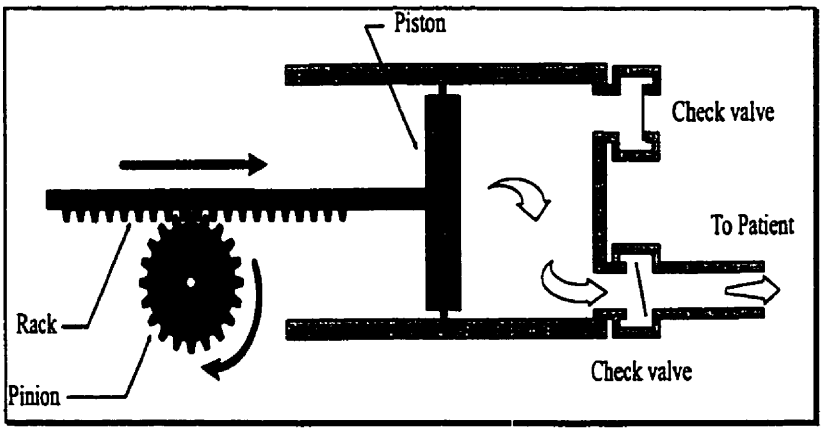

Figure 3-10: Linear driven piston for gas compression (Adapted from Dupuis 1992)

3.4.5. Nonlinear driven pistons

The piston is attached to a rod, connected off center to a large rotating wheel, which is rotated at constant speed by an electric motor (Figure 3-11). Air compression is generated during the forward stroke of the piston. In this assembly the pressure and flow developed change with the motion of the piston which moves quasi-sinusoidally. This drive mechanism is used particularly with home care ventilators, and in animal ventilators.

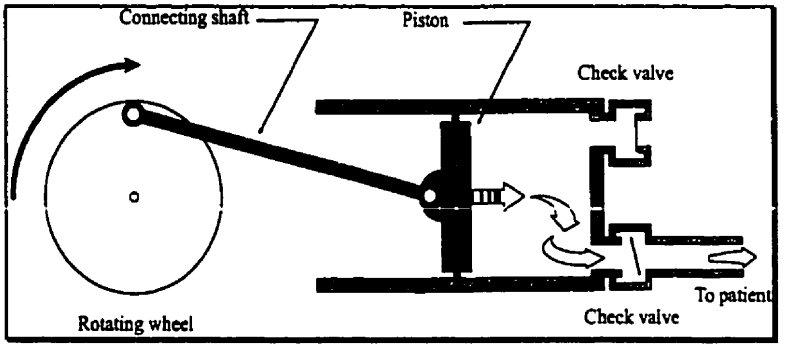

Figure 3-11: Nonlinear driven piston (Adapted from Dupuis 1992)

3.4.6. Pressure reducing valves

This is a very popular drive mechanism, used extensively in microprocessor-controlled ventilators. Here, a high input pressure source coming from high-pressure cylinders in excess of 14000 kPa (2000 psig) or from wall outlets in the hospitals usually at 344.75 kPa (50 psig), is reduced to a lower constant pressure which can be adjustable or preset. The output pressure adjustment is achieved by varying the tensions in the two springs as seen in Figure 3-12. In the case of the adjustable spring being totally relaxed, the smaller spring acts as a seal to prevent the source pressure from entering and reaching the outlet.

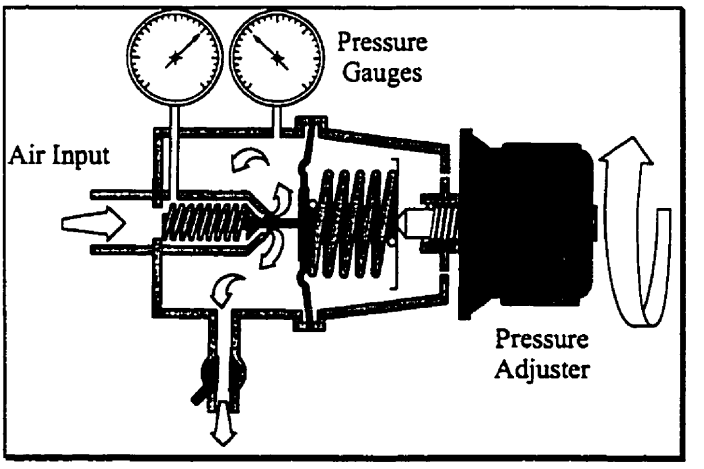

Figure 3-12: Pressure reducing valve mechanism (Adapted form Dupuis 1992)

3.4.7. Blowers

This mechanism is based on the use of an electric motor rotating a fan at high constant speed, propelling air forward and generating a steady level of pressure (Figure 3-13). It should be noted that, since the motor runs continuously, two solenoid valves direct the flow of air to the patient or the vent, during inspiration and expiration respectively. This drive mechanism type was very common in early electronic ventilators. However, it is now more frequently used as a back up air compressor for other drive mechanisms.

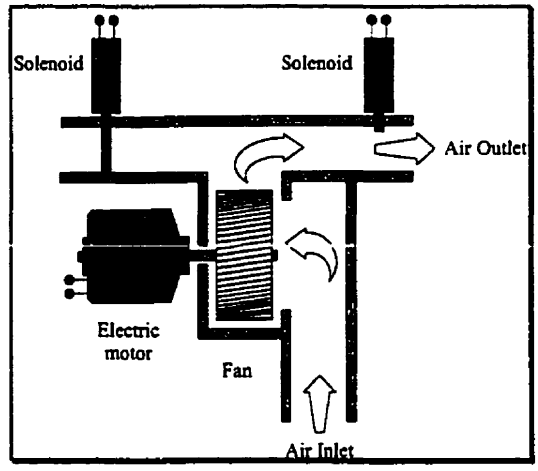

Figure 3-13: Motor driven blower for gas compression (adapted from Dupuis 1992)

3.4.8. Injectors

Injectors, often referred to as *Venturi,* use a high constant pressure source, such as pressure-reducing valves or blowers, as an input forcing gas to leave the output nozzle at a high velocity as shown in Figure 3-14. This causes the pressure on the right-hand side

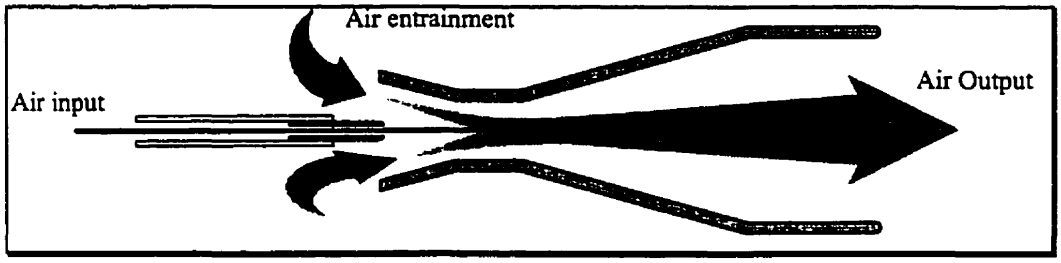

Figure 3-14: Injector or venturi mechanism used for gas compression

of the constriction to drop below atmospheric pressure. Consequently, gases are drawn in around the jet of gas (i.e. air entrainment). The result is an increase in the total flowrate leaving the injector. The pressure generated at the outlet is constant and determined by the flowrate of the gas applied to the injector.

3.5 Ventilator circuits

3.5.1. Single circuit

A further important design aspect of ventilators is whether they have a direct acting (single-circuit) or an indirect acting (double-circuit) drive mechanism. In the former type, the gas from the drive mechanism enters the patient's lung directly. However in an indirect acting mechanism, a direct acting drive is used to operate another circuit (secondary) to generate the pressure source to inflate lungs. Secondary circuits may be a bellows or a bag, and can be powered by any drive mechanism. The principal reason for the development and use of a double circuit ventilator is to provide a reliable method for the delivery of predictable tidal

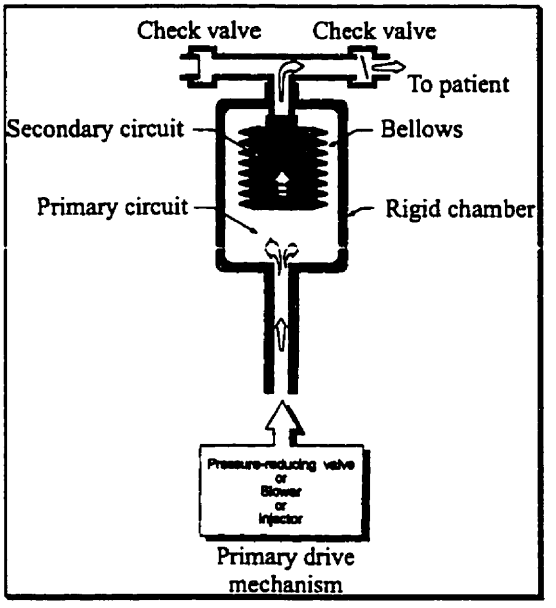

Figure 3-15: An indirect acting drive mechanism (Adapted from Dupuis 1992)

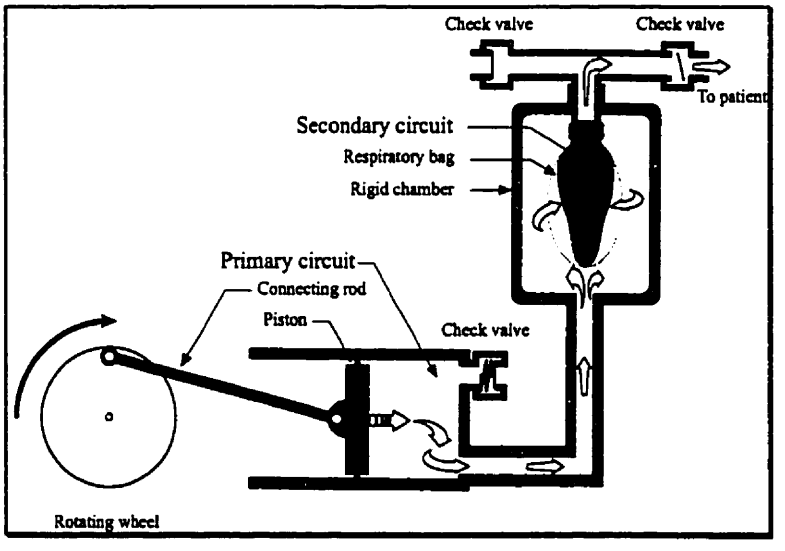

Figure 3-16: Double-circuit ventilator with a nonlinear piston acting as the primary drive mechanism (Adapted from Dupuis 1992)

volumes. Figure 3-15 shows an indirect acting ventilator where the primary drive may be a pressure-reducing valve, a blower, or an injector (see 3.4.7-8). Figure 3-16 shows another double circuit ventilator where the primary drive mechanism is a nonlinear-driven piston and the secondary circuit consists of a large bag enclosed within a rigid chamber.

3.6 High Frequency Ventilators

3.6.1. Historical overview

High frequency ventilation (HFV) is a method of ventilation in which respiratory frequencies in excess of normal physiological respiratory rates (e.g. 60-3000 breaths/min) and tidal volumes close to or less than the anatomical dead space are used (Ribeiro et al. 1998). There are certain clinical conditions that can benefit from HFV. Although to date it has not been demonstrated convincingly in clinical trials, it is believed that the potential for barotrauma is less with HFV than with other conventional ventilatory techniques.

There are certain areas where better ventilatory solutions are still needed. For example, impact of variation of intrathoracic pressure during intermittent positive pressure breathing (IPPB) has adverse effects on cardiovascular function. Furthermore, there are situations where CO_2 elimination and oxygenation with conventional mechanical ventilation proves futile. Finally lung injuries have to be minimized and the outcome of acute respiratory failure in neonates (RDS) or adults have to improve. See Nochomovitz (1987) for details.

The motivations for finding new modes of mechanical ventilation in general, and of HFV in particular, was to overcome a number of limitations and adverse effects associated with conventional pressure or volume ventilation. Techniques of HFV have been viewed as a new and innovative respiratory approach. Although reports of investigation with high frequency ventilation are said to date back to 1915 when *HENDERSON* and colleagues (1915) made observations of panting dogs. They proposed that adequate gas diffusion in larger species could take place even with tidal volumes smaller than dead space. Emerson, in 1959, hypothesized that improved diffusion can be achieved by vibrating a column of gas, yielding more effective distribution within the

lungs. High frequency ventilation was first developed in Sweden when *OBERG* and *SJOSTRAND* (1969), during studies on the carotid sinus reflex, anticipated improved experimental control once the effect of respiratory synchronous variations in blood pressure were eliminated. To achieve this condition a ventilatory method was developed that did not have this effect on the blood pressure. This technique formed the basis of high-frequency positive pressure ventilation (HFPP), and resulted in low tidal volumes that gave sufficient alveolar ventilation with no adverse effects on the circulation. In 1972, they reported the successful ventilation of 15 patients undergoing abdominal surgery using this mode of ventilation.

Observations of *LUNKENHEIMER* and colleagues (1972) reported improved gas exchange with transtracheal pressure oscillations, and gave birth to a technique called high-frequency oscillation (HFO). In their early experiments, they found that oscillations at 1380-2400 breath/min (23-40 Hz) gave adequate ventilation.

KLAIN and *SMITH*, (1977) used a modified Sanders jet injector technique, where respiratory gases were injected under pressure through a percutaneous transtracheal cannula which also allowed air entrainment. They reported adequate ventilation with rates up to 6000 breath/min (Ribeiro et al. 1998). This technique was later developed to produce another variation of high frequency ventilation termed high-frequency jet ventilation (HFJV).

During the past few years several types of high frequency ventilators have been described. Although the mechanisms used to produce flow waveforms in these ventilators are different, a common characteristics of all such systems is the use of small tidal volumes and high ventilatory frequencies, i.e. greater than 60 breaths per minute. Short inspiratory times, typically less than 0.3 seconds, is another common feature of such devices. This contrasts to the 0.8-1.2 seconds seen with spontaneous respiration and used in conventional ventilation. However, some of the problems currently associated with HFV are: (Nochomovitz et al. 1987)

- Lack of satisfactory understanding of how high-frequency ventilation works to produce gas exchange.

- Incomplete knowledge of the physiological effects or potential complications of high-frequency ventilation.
- Lack of an optimal design of equipment for high-frequency ventilation. There is also generally little knowledge of the mechanics of specific ventilators among clinicians.
- Lack of a recognized protocol with respect to optimal frequency, tidal volume, flow pattern and rate, and inspiratory and expiratory pressures.
- Lack of reliable monitoring devices to assure that ventilation is adequate at all times.
- Poor humidification and inadequate safety features.
- Insufficient experience and confidence in the case of HFV by nurses. This means physicians are necessary for continual bedside monitoring (Nochomovitz et al. 1987).

Finally, the existence of a wide variety of custom-made devices capable of delivering ventilation at high frequencies has contributed to further confusion surrounding the subject.

3.6.2. Terminology

High-frequency techniques are usually classified in four categories: (a) high-frequency positive-pressure ventilation (HFPPV); (b) high-frequency jet ventilation (HFJV) or high-frequency flow interruption (HFFI); (c) high-frequency oscillatory ventilation and (d) high-frequency chest wall compression (HFCWC). Each of these systems operates over a different range of tidal volumes and ventilatory frequencies. At the same time, they also require a different gas delivery system. Table 3-1 gives a brief comparison of conventional and high-frequency ventilation in so far as major parameters of interests are involved.

Table 3-1: comparison of Conventional and High-Frequency ventilation

Type of ventilation	Conventional Ventilation	High-Frequency Ventilation
Frequency	10-20/minutes	60-3000/minute
Peak pressure	High	Low
Tidal volume	Greater than dead space	May be less than dead space
Gas distribution	Highly dependent on regional compliance and resistance	May be less dependent on regional compliance and resistance

3.6.3. High-frequency positive pressure Ventilator

HFPPV refers to the use of a low compliance ventilator to deliver tidal volumes a little smaller than those of conventional ventilators (3-5 cc/kg) at ventilatory frequencies (60-150 breaths/minute) through a small airway. The device used for this purpose utilizes a special pneumatic valve to control inspiratory and expiratory airflow (Figure 3-17). Conventional ventilators using high frequencies and low volumes can also deliver HFPPV. While peak inspiratory pressure is proportionately low, high flow rates (175-250) liters/min are used. Adequate gas exchange can be achieved with no gas entrainment. The inspiratory-to-expiratory ratio is less than 0.3 seconds.

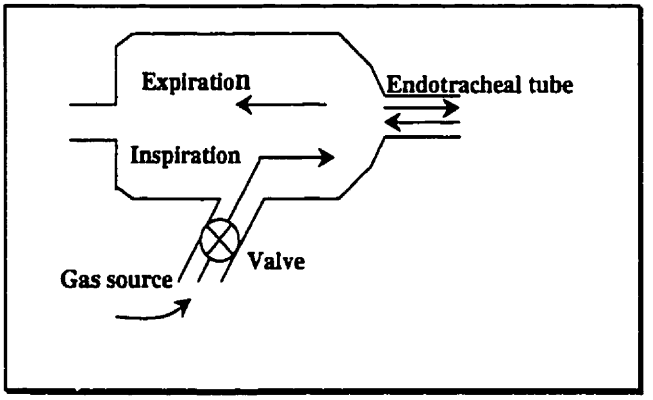

Figure 3-17: High frequency positive pressure ventilator

3.6.4. High-frequency jet ventilator

The high-frequency jet ventilator (HFJV) (Figure 3-18) employs the principal of the jet injector. By the use of a high-pressure source (50-2000 mmHg), the resistance of a narrow cannula is overcome to deliver short bursts of gas (100-200 msec) into the upper airways while expiration is passive. A solenoid valve of pneumatic or fluid gating type controls gas flow to the patient. Respiratory rates in the range of 100-200 breaths/min and higher can be achieved. Tidal volume is 3-5 ml/kg and peak inspiratory pressure depends on flow. It is worth noting that, in this mode of ventilation, inspiratory volumes are generally lower than those used in HFPPV, while significantly higher respiratory frequencies are used. The high frequency flow interrupter (HFFI or HIFI) ventilators aer similar to HFJV and once again some control mechanism chops gas from a high pressure source into pulses usually directed into the top of the endotracheal tube. Often HFFI devices are employed clinically in the presence of a backup level of conventional mechanical ventilation.

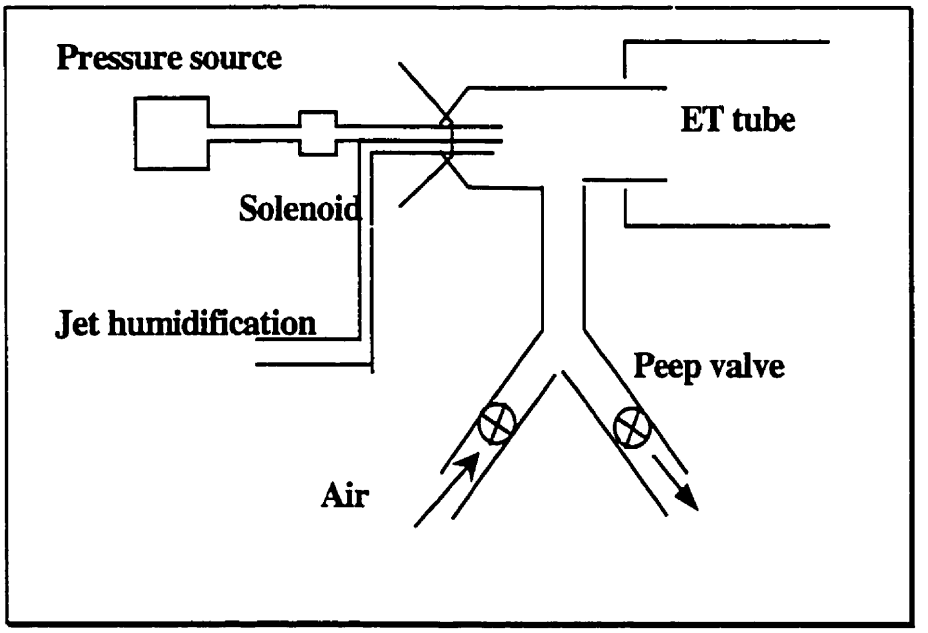

Figure 3-18: High frequency jet ventilator

3.6.5. High-frequency oscillator

If the column of air in the trachea is given an oscillatory motion by the reciprocating pump of a piston or diaphragm, such as a loudspeaker or bellows generating an approximately sinusoidal waveform, HFO will occur. As illustrated in Figure 3-19, since no net displacement of gas into the lung occurs, a bias gas flow must be provided into a side intake port. Expiration is also through a side port placed at right angles to the piston. In this technique ventilatory frequencies and tidal volumes are in the range of 90-3000 cycles/minute and 50 cc, respectively. The frequency range in HFO is higher than that of HFPPV or HFJV while tidal volume is lower.

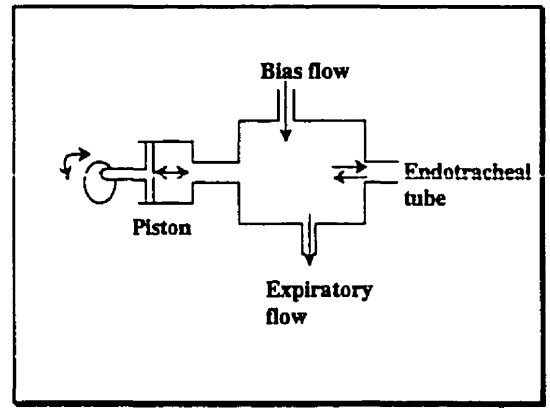

Figure 3-19: High frequency oscillator

3.6.6. High-frequency chest wall compressor

Another described technique of high-frequency ventilation is high frequency chest wall compression (HFCWC) (Lyle et al. 1986). In this technique an inflatable harness is used to surround the chest wall. Air is then pumped into and out of the harness at rates of 3 to 11 Hz or 360-660 cycles/minute, yielding an oscillatory motion of the chest wall, which in turn mixes gases in the airways and alveoli (Figure 3-20).

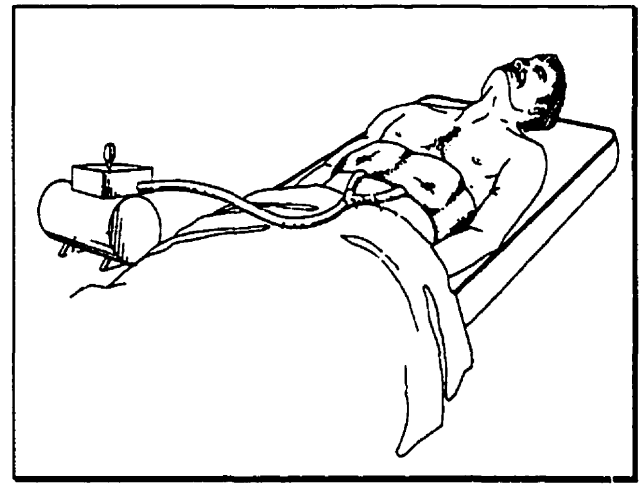

Figure 3-20: High frequency chest wall compressor

3.6.7. Small animal ventilator (SAV)

This is a ventilator which uses a piston driven in a cylinder to create air pressure (see section 3.4.4). The SAV has been designed for ventilation and load impedance measurements in small animals (Schuessler et al. 1993). The SAV can deliver small flow oscillations at up to 50 Hz and uses direct load measuring technique to estimate the respiratory impedance. The flow need not be directly measured and hence the SAV does not use a pneumotachograph.

In addition to the major high frequency ventilators and devices discussed above, there has also been an assortment of other devices, some of which are "home-made" (Figure 3-21).

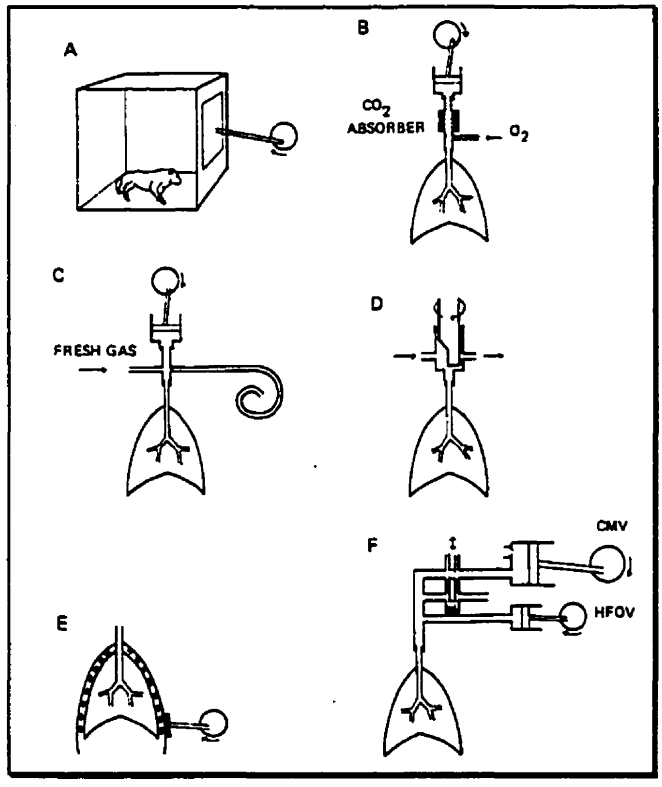

Figure 3-21: An assortment of high-frequency devices. (A) Whole-body oscillator. (B) Bias flow oscillator with CO2 absorber to meet metabolic demand. (C) Bias flow oscilator. (D) Rotating valve. (E) Thorax oscillator. (F) HFOV combined with CMV (Adapted from Carlon et al. 1985)

3.7 Mechanisms of gas transport during high-frequency ventilation

3.7.1. Physiological mechanisms of HFV

The process of high-frequency ventilation has been the subject of investigation by many researchers. Classic pulmonary physiology presumes that respiratory frequency and alveolar volume determine alveolar ventilation, thus

*Alveolar Ventilation = (Tidal volume - Dead space volume) * Ventilatory frequency.*

If applied to HFV when the tidal volume is less than the dead space, alveolar ventilation is predicted to be zero, yet adequate alveolar ventilation has been demonstrated using a wide variety of techniques. Thus gas exchange during HFV must occur via alternative mechanisms. There are two questions which need to be addressed:

- A: "How can gas exchange in the lung be maintained when tidal volumes are less than those of the dead space?"
- B: "Which are the mechanisms of gas transport during high-frequency ventilation?"

HENDERSON et al. in 1915 (1915), probably for the first time, speculated that "there may easily be a gas exchange sufficient to maintain life even when the tidal volume is less than the dead space". It is believed the first attempt to demystify the process systematically was carried out by *FREDBERG* (1980) who used *TAYLOR*'s concept (1954) of longitudinal dispersion caused by the interaction between axial velocities and radial transports due to turbulent eddies possibly combined with swirling motions (Figure 3-22).

In 1954, *BRISCOE* et al. (1954) observed that "with small inspiration, the air penetrates the dead space into alveoli without washing all the gas present in the dead space into the alveoli." Hence, some patients can live while breathing very small tidal volumes. To date, a clear understanding of gas transport during HFO does not exist but numerous studies in recent years are qualitatively indicating that gas transport appears to

be the result of a number of different mechanisms. As in the case of normal breathing, bulk convection and molecular diffusion (Chang et al. 1973; Schied et al. 1982) are two basic mechanisms of gas transport in the lung during HFO.

3.7.2. Mechanisms of gas transport involved in HFO

In normal spontaneous breathing, air is transported in the large proximal airways primarily by convection at least up to the eighth bronchial generation (Chang 1984). In the case of HFO, it is generally agreed that most possible mechanisms involved in the process are as follows.

1. ***Pendelluft***: At high frequency, gas distribution is influenced by asynchronous filling and emptying of parallel lung units due to their time-constant inequalities. The rate of filling and emptying of the units is governed by their mechanical properties, characterized by R and C. The time constant is simply the product of these two quantities ($= R \times C$)
2. ***Taylor dispersion***: *HENDERSON* et al. (1915) showed that when convective flow is superimposed on a diffusive process, dispersion of tracer molecules increases. *FREDBERG* (1980), based on this assumption in turbulent flow, predicted that CO_2 elimination was proportional to $V_t \times F$, although subsequent studies have shown that gas exchange is more strongly influenced by V_t (Alison et al. 1987).
3. ***Cardiogenic* Mixing**: Due to oscillations induced in the lung from the pounding action of the heart, peripheral gas mixing takes place (Slutsky 1981).
4. ***Convective transport of gases as a result of the asymmetry of inspiratory and expiratory velocity profiles***: *HAZELTON* and *SCHERE* (1980) have proposed that material may be transported during oscillatory flow through a bifurcating network. By using a visualizing technique, they observed a steady streaming displacement of fluid elements during repeated cycles of oscillatory flow through a Y-shaped bifurcation similar to that of the human bronchial tree.
5. ***Molecular Diffusion***: Random thermal oscillations of a molecule gives rise to a transport mechanisms known as molecular diffusion. As in normal ventilation, this probably dominates the flux of gas in the terminal air spaces. It is generally

recognized that molecular diffusion is not only responsible for gases exchange across the alveolar capillary membrane, but also contributes to the transport of O_2 and CO_2 within the membrane (Chang et al. 1973; Schied et al. 1980). There have been some studies concerned with optimizing the frequency/tidal volume combination for CO_2 exchange during HFO, but its elimination seems to be a function of $V_t^a \times F^b$ where "a" is greater than "b" (i.e. tidal volume has the predominant effect). These exponents vary between circuits and probably between species (Kolton 1984).

6. ***Bulk Convection***: When a small tidal volume is inspired, there will be direct alveolar ventilation mostly closer to the mouth. Depending on the inspired tidal volume and on the distribution of pathway lengths from the mouth to the alveoli, with each tidal breath, a certain member of alveoli are reached and ventilated.

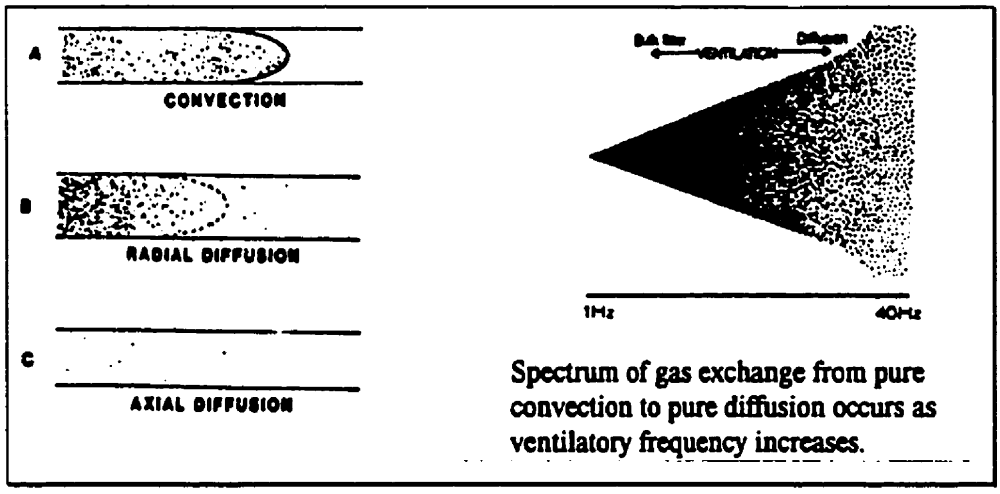

Figure 3-22: (A) Convective or bulk flow predominates in large airways. (B) As the airway decreases in caliber, convective velocity decreases and radial diffusion becomes a prominent mode of transport. (C) Beyond the 12th generation, air transport occurs by convective bulk flow and axial diffusion.

3.7.3. Clinical Application of High Frequency Ventilation

It is believed that by using a three-fold increase in frequency from 20 to 60 breath/min, normocabria can be achieved with a 35% decrease in tidal volume (Sjostrand 1980). Consequently lower peaks and mean intratracheal pressures than conventional

ventilation, accompanied by slight PEEP of ~2.5 CmH_2O, are produced. It has been shown that this pattern of ventilation has less effect on cardiac output than conventional techniques. *CARLON* and co-workers (1981) successfully reported the first treatment of bronchopleural fistula when a massive air leak prevents adequate minute volumes from getting to the alveolar surface to support gas exchange. Many different HFV systems operating with or without gas entrainment have been used since, and indeed have proven effective in the treatment of bronchopleural fistulas in adults and infants (Frantz et al. 1983; Boynton et al. 1984). *BUTLER* et al. (1980) ventilated 12 patients for periods of up to 1 hour using very-high-frequency (15 Hz) sinusoidal oscillations with a volume less than 50% of dead space. He reported improvement in shunt fraction and cardiac output. In 19881, *GOLDSTEIN* et al (1981) used a sine wave generator, amplifier and 30.5 cm loudspeaker at a frequency of 4-10 Hz to achieve adequate ventilation in eight normal subjects. *CARLON* et al. (1981) carried out extensive comparisons of HFJV and conventional volume-cycled ventilation in adult respiratory insufficiency. The study included 300 patients and demonstrated that HFJV was safe. There are many reports of satisfactory use of HFJV for laryngoscopy, brochoscopy and tracheal surgery (El-Baz et al. 1982; Flatau et al. 1982). To date there is no evidence based on clinical studies that HFV is more effective than CMV in treatment of the lung with diffusive injury at modest airway pressures. However, *ROUBY* (1983) and other researchers have demonstrated that in a disease such as adult respiratory distress syndrome (ARDS), oxygenation is strongly affected by the mean airway pressures applied. *BUTLER* and colleagues (1980) in brief trials have demonstrated that HFO can support gas exchange in patients with respiratory failure of varied etiology. *MARCHAK* et al. (1981) found that infants with RDS had a lower FiO_2 requirement when HFO was used at mean airway pressures greater than those during CMV, while no apparent clinical impairment of cardiac function was observed.

It has been some years since investigators first noticed the novel mechanisms of adequate oxygenation and CO_2 removal by small tidal volumes associated with HFV. Assumptions were made that CO_2 in was comparable to O_2 out. Equally it was assumed that small tidal volumes meant less barotrauma. While these expectations have not been completely fulfilled, HFV is now clinically recognized. Its role in anesthesia during

surgery requiring motionless operating field, situations of bronchopleural fistula (lower $PaCO_2$ with least pressure cost) and pulmonary interstitial emphysema is acknowledged (Alison et al. 1987). Furthermore a major area where HFV could be of immense use is in the recruitment of alveoli suffering from atelectasis, exploiting the CO_2 elimination capability of HFV techniques.

The future role of high-frequency ventilation in respiratory care is difficult to predict with certainty. Without a clear understanding of how high-frequency ventilation works, its use is not widely inspired. Uncertainty regarding the physiological effects or complications involved in HFV is a further problematic area. There is not yet an established optimal design protocol for HFV equipment. Finally, the demand for the development of HFV is not compelling, perhaps because of some of the above mentioned reasons.

3.8 Technical problems common to most high frequency ventilators

Many different ventilators have been used to deliver high frequency oscillatory ventilation (HFOV). Usually these devices have been designed to gain better control of variables such as P_{AW} and V_t. Ventilators have also been developed to improve the ways oscillations can be coupled to the respiratory system. However, there are certain problems and limitations that seem to be common to most of these devices, as follows:

- The internal compressible volume and impedance of a ventilator are relatively unimportant at physiological frequencies, but during HFOV they are critical factors in determining the system's efficiency. Obviously if either of these parameters are too large, some of ventilator's work is wasted on gas compression and overheating may result. The dimensions of tubes connecting the ventilator to the patient (including the endotracheal tube) are major contributors to ventilator resistance.
- Gas compression at high frequencies may mean that the volume leaving the ventilator is less than that reaching the alveoli.
- Gas moving at high velocity may entrain particulate material. Lubricants used in piston or rotating valve pumps can be a source of such material.

- The volume of fresh gas delivered to the upper airway during HFOV can result in very large tracheal minute ventilation. If the gas is not properly conditioned, the potential exists for severe dehydration of the upper airways. Current humidification systems have not been tested and verified experimentally.
- Accurate measurement of P_{AW}, V_t, and Fr during HFOV is exacting and sometimes difficult.
- High-compliance and inappropriate internal diameter of tubing used in connections can influence the measurements.
- Placement of pressure transducers in the ventilator circuitry can also lead to erroneous readings. The poor response of pressure sensors at 20 Hz or higher frequencies can also be problematic.
- Rapidly moving parts in HFOV can present serious risk of injury to either operator or patient. Excessive noise and component failure is also associated with these devices.
- Lack of proper alarms to monitor airway pressure can endanger the patient.
- Calibration, precision and linearity of pneumotachographs at high frequencies can be problematic.

3.9 Closing remarks

In this chapter, mechanical ventilators and some of their important features were discussed. Different techniques used in commercial ventilators for compressing air were investigated. High frequency ventilators and the mechanisms of gas transport into the human respiratory system were addressed. Some of the most common technical problems associated with high frequency ventilators were also mentioned.

Chapter four will describe in detail the mechanical design and development of the RVV. Mathematical modeling of the ventilator leading to the computation of delivered flow will then be presented. The chapter will end with a description of some of the major components used in the construction of the RVV.

4

RVV: Mechanical Design

The mechanical design of the pressure chamber is a major innovative aspect of the RVV. In this chapter the mechanical setup and construction of some of the components of the RVV will be described. The layout of the ventilator will be given, and the functioning of the drive circuit (pressure chamber), a crucial element of the ventilator will be explained. The resistance to the flow passing by a rotating vane will be mathematically modeled. Following this, a model of the pressure chamber will be derived. It will be shown how the flow generated by the vane is determined without having to use a pneumotachograph. The chapter will close with a description of some other components of the RVV.

4.1 RVV overview

The mechanical construction of the RVV is a major factor in its performance. Figure 4-1 gives an overview of the ventilator, and shows the layout of the components. These will be described in more details in coming sections. The pressure chamber and the other components of the RVV are secured in a box made of Plexiglas of dimensions 50L, 35W and 36H cm (see section 4.5). Its compactness makes the ventilator portable.

However the principal reason for using Plexiglas, as opposed to other materials, is that it is a convenient material for prototyping a design. Operations like reshaping, tapering and cutting are done easily. Keeping the material clean is also easy. A final design would almost certainly use stainless steel or some other appropriate material (see chapter 9).

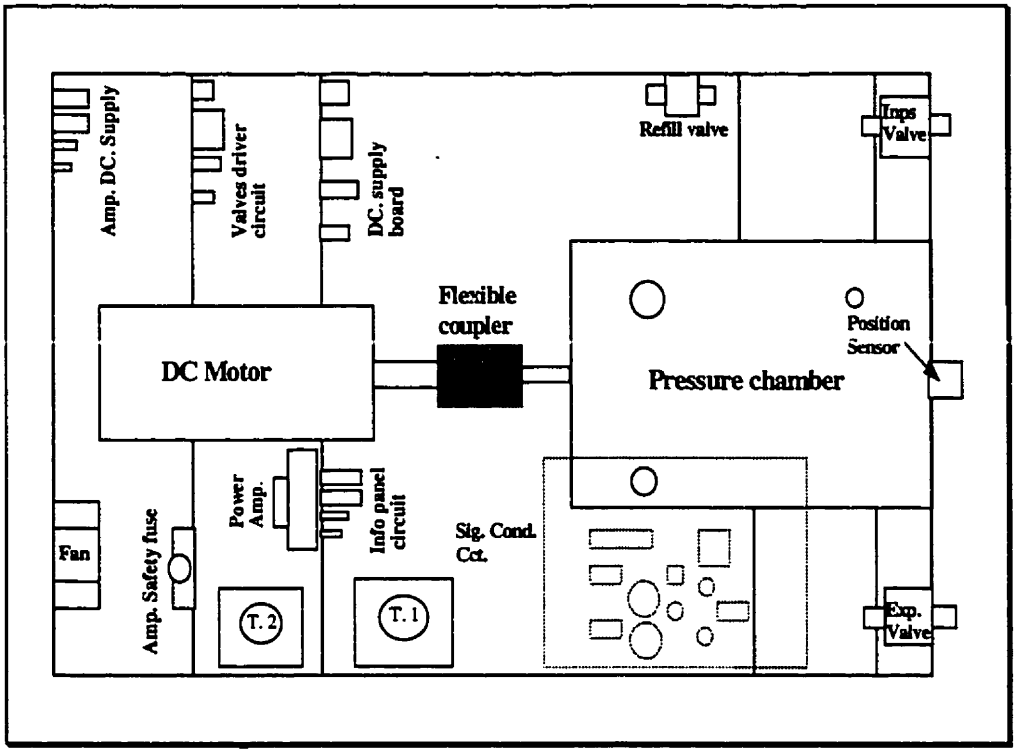

Figure 4-1: Overview of the RVV

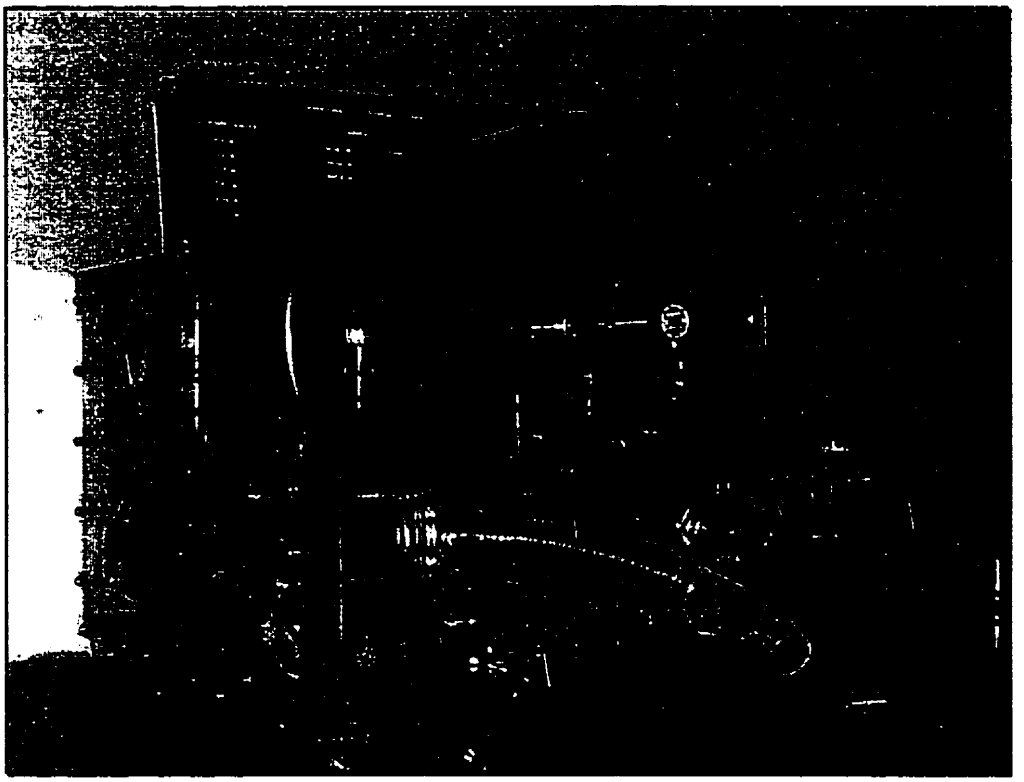

Figure 4-2: RVV, front view

4.1.1. RVV design

4.1.1.1 Overall design

We have designed a new type of mechanical ventilator (the RVV) that will overcome the obstacles mentioned in the preceding chapter, while at the same time allowing for a wide range of ventilatory modes to be applied. The RVV is under full computer control for maximum flexibility so that it can apply broadband perturbations in flow to the respiratory system. Equally importantly, estimation of the mechanical impedance of a ventilated load follows naturally from the RVV's unique design. This is achieved without the need to interpose pressure and flow transducers between the endotracheal tube and the ventilator tubing.

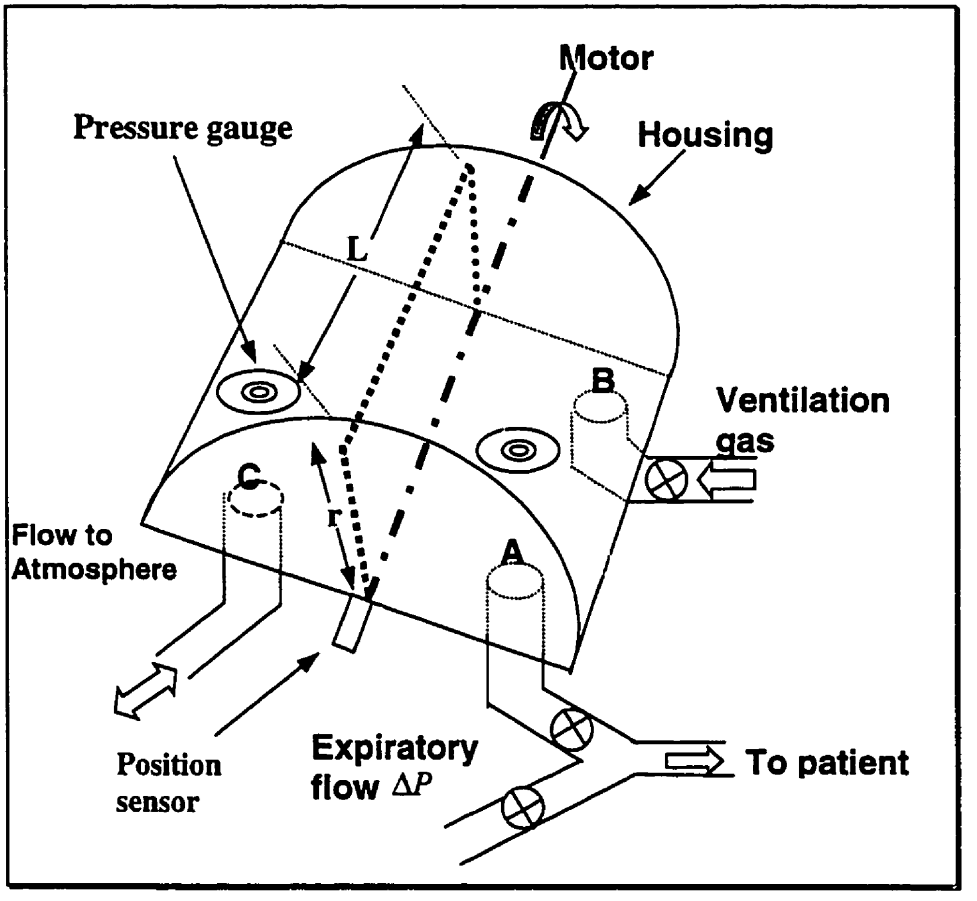

Figure 4-3: RVV drive mechanism (pressurizing chamber)

To create air pressure to force flow out of the RVV, a rotating vane is driven in a closed half-cylindrical housing (inside radius r, length l) enclosed on both ends and on the bottom by a flat plate (Figure 4-3 and Figure 4-4). The vane's dimensions are such that it has a very fine clearance (~ 50 microns) with respect to the cylindrical housing as it rotates through its allowable range, displacing up to 2 liters or more of gas. The vane is driven by an electric torque motor. The vane's supporting rod passes through the end plates via two sealed bearings. On one end, it is connected to the motor via a direct coupler and on the other, it is attached to the position sensor.

The housing to the right of the vane contains two valves, each with an open diameter of about 2 cm. These valves are labeled A and B in Figure 4-3. Valve A connects the housing directly to the patient via a relatively short segment of flexible but not compliant tubing. Thus, when A is open and B is closed, gas is forced into the patient as the vane sweeps in a clockwise direction. Conversely, when A is closed and B is open, fresh gas is drawn into the housing as the vane sweeps in a counter clockwise direction. At the same time, another valve allows the patient to exhale to atmosphere. In the floor of the housing to the left of the vane is another hole, also about 1 cm in diameter, which connects to the atmosphere.

The housing of the chamber was made from commercially available Plexiglas tubing, wall thickness is ¼ inch. The vane was also made of ¼ inch thickness Plexiglas. These components were prepared and machined at the Physics Machine Workshop, Department of Physics, McGill University, where an advanced numerically controlled lathe was used.

At the heart of the ventilator control is a Pentium computer. Feedback is used to control the position of motor's shaft, which in turn is monitored by a rotational variable differential transformer (RVDT) sampled via an analog-to-digital converter (ADC). The computer calculates the control signal and outputs it to the servomotor through a digital-to-analog converter (DAC) and power amplifier (Figure 4-5). Pressures on either side of the vane are also monitored. The computer control of the motor plant is flexible. Depending on the requirements of a given load, the control parameters can be adjusted to obtain optimal system performance (bandwidth, overshoots, response time etc.).

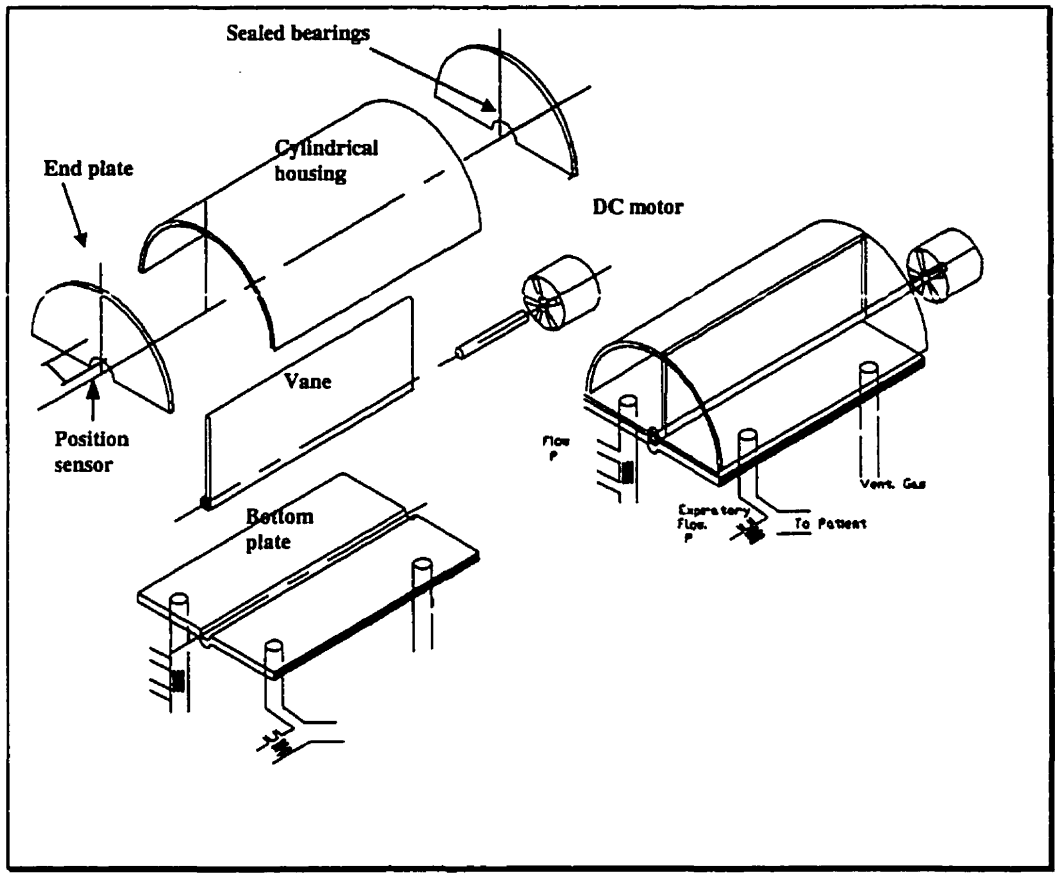

Figure 4-4: Pressure chamber overview with associated components

The ventilation and/or perturbation flow waveforms can easily take different characteristics within the capability of the device. The waveforms merely need to be specified in software and exported to the ventilator drive. This design allows ventilation by controlling the vane movement to generate a conventional ventilator waveform at the airways.

As a safety feature, an expandable information display panel has been built which uses real time key signals to continuously monitor and indicate the state of some important components such as power supplies, valves and other parameters involved in the operation of the RVV (see section 4.6). The panel also uses an integrated circuit line driver and a series of LEDs to give a display signal proportional to volume or pressure at the RVV's out-port. Finally, for compactness and portability, a support box has been

designed which houses the vane housing and all associated electronics as well as the valves. Part of its design includes positioning of the drive motor, which has to be done very accurately with respect to the vane, to avoid creation of any mechanical friction or transational distortion. With the exception of the signal from the vane position sensor, all other signals are collected via an amplifier/conditioner box (see chapter 6).

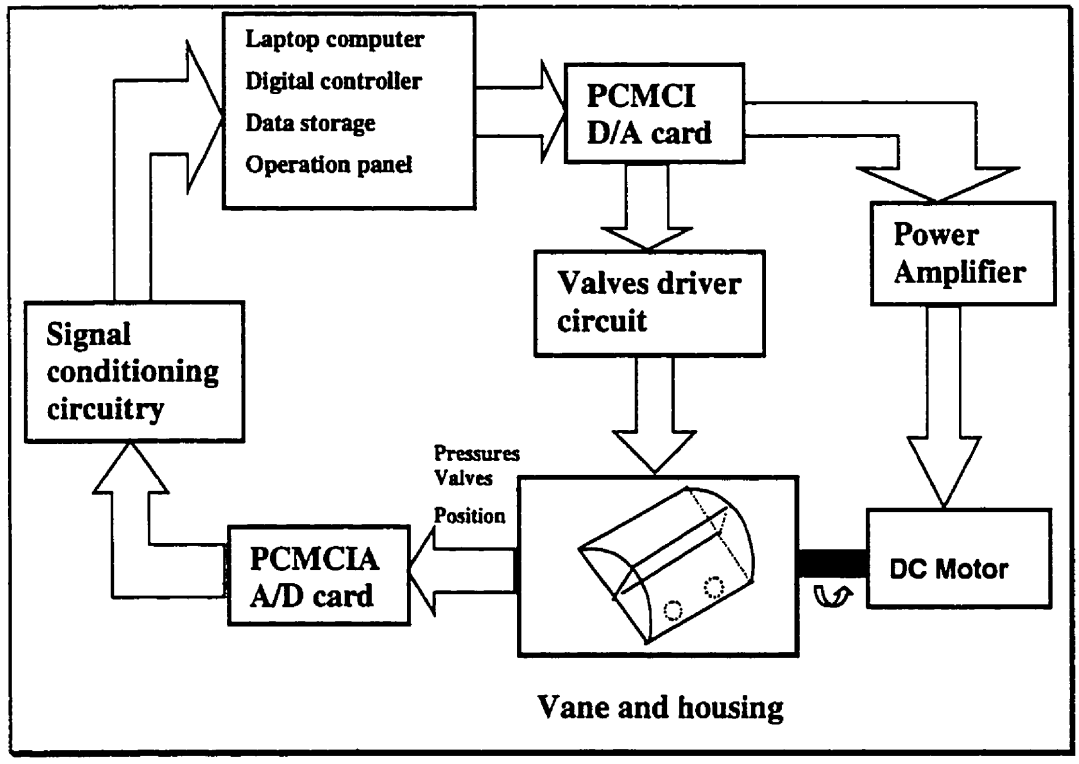

Figure 4-5: schematic diagram of RVV closed loop control. Note the position of the computer within the loop

4.1.2. Calculation of Resistance to Back-Flow

4.1.2.1 Theoretical resistance

As mentioned in section 4.1.1, a distinct feature of the ventilator is its air compression mechanism that uses a rotary vane in a closed housing. The clearance of the vane with respect to the surrounding housing directly influences the amount of flow or pressure created in the ventilator. For this reason it is important to establish the flow resistance

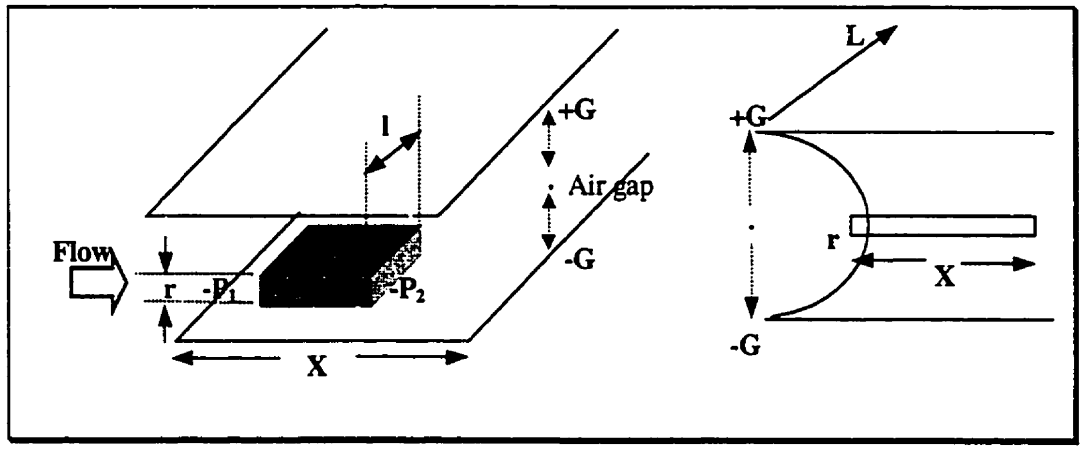

Figure 4-6: Steady flow of a rectangular system of fluid between two physical barriers

between the vane and the housing. To do this, consider an infinitesimal rectangular system incompressible fluid of thickness r as shown in Figure 4-6. Assuming a steady laminar flow, and a Newtonian liquid, we can apply Newton's viscosity law to establish the forces acting on the system. In the direction of flow the forces sum to zero (the forces from hydrostatic pressure variation cancel at the top and bottom surfaces.) Thus,

$$\Delta PLr = -2\mu \frac{dv}{dr} LX \qquad (4.1)$$

where

μ is the air viscosity

v is the flow velocity

X is the thickness of the vane

$\Delta P = P_1 - P_2$

Since dv/dr does not vary with X,

$$\frac{\Delta \mathrm{Pr}\, dr}{2\mu X} = dv \tag{4. 2}$$

Integrating both sides one obtains,

$$v = \frac{\Delta \mathrm{Pr}^2}{4\mu X} + C \tag{4. 3}$$

where C is the constant of integration. At the air-gap boundary, $r = G$, flow velocity, v, is zero. Substituting for r and v in Equation (4. 3) one obtains, after simplification,

$$C = -\frac{\Delta P G^2}{4\mu X} \tag{4. 4}$$

Hence, the velocity profile can now be written as

$$v(r) = \frac{\Delta P}{4\mu X}\left(r^2 - G^2\right) \tag{4. 5}$$

Note that the profile $v(r)$ is parabolic. The total flow $\dot{V}$ can be expressed as

$$\dot{V} = \int_{-G}^{+G} v(r)Ld(r) = 2\int_{0}^{G} v(r)Ld(r) = 2\int_{0}^{G} \frac{\Delta PL}{4\mu X}(r^2 - G^2)d(r) = \frac{\Delta PL}{2\mu X}\left[\frac{G^3}{3} - G^3\right]$$

$$\dot{V} = \frac{\Delta P L G^3}{3\mu X} \tag{4. 6}$$

where L is the length of the vane. Finally the flow resistance, $\Re$, is

$$\Re = \frac{\Delta P}{\dot{V}} = \frac{3\Delta P \mu X}{\Delta P L G^3} \tag{4. 7}$$

$$\Re = \frac{3\mu X}{L G^3} \tag{4. 8}$$

Equation (4. 8) signifies that for $\Re$ to be as large as possible X has to be as large as possible (i.e. thick vane) while L and G must remain as small as possible. The RVV housing was built using prefabricated cylindrical stock. Since the radius of the cylinder is fixed, only its length, L, and the gap (G) could be tailored to control $\Re$. Substituting for the parameters in Equation 4.8 and aiming for $\Re$ to be at least ten times greater than human respiratory resistance yields an air gap of 0.12 mm. The vane was prepared and machined at the Physics Machine Workshop, Department of Physics, McGill University, where an advanced numerically controlled lathe was used.

4.1.3. Mathematical model of the ventilator

4.1.3.1 Theoretical Flow estimation

Figure 4-7 represents the ventilator with two pressure chambers P_{RC} and P_{LC} on the right and the left sides of the vane. V_R and V_L are the geometric volumes of the right and left chambers, respectively. The corresponding compressed gas volumes are V_{RC} and V_{LC}.

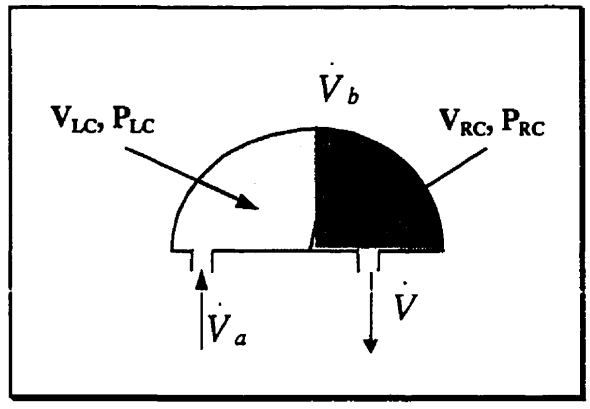

Figure 4-7: RVV pressure chamber

$$V_R = \frac{r^2 l}{2}\theta \qquad (4.9)$$

$$V_L = \frac{r^2 l}{2}(\pi - \theta) \qquad (4.10)$$

where:

θ = Position of the vane

The ventilator can be considered as made up of two independent chambers separated by the vane. For the left chamber (Figure 4-8) we have:

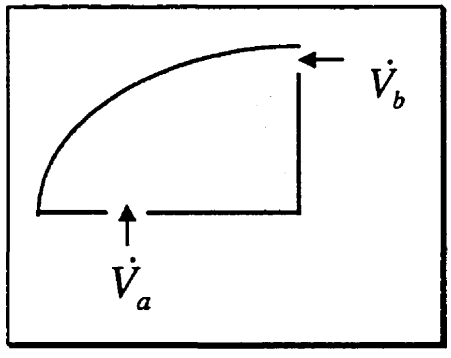

Figure 4-8: Left chamber

$$\dot{V}_b + \dot{V}_a = \dot{V}_{LC} \qquad (4.11)$$

Where:

$\dot{V}_b$ is the back flow from the right chamber

$\dot{V}_a$ is the flow into the left chamber from the atmosphere

and $\dot{V}_{LC}$ is the net flow into the left chamber. The resistance R_a of the opening to flow $\dot{V}_a$ (opening C in Figure 4.3) is given by

$$\dot{V}_a = \frac{-P_{LC}}{R_a} \tag{4. 12}$$

For the right chamber (Figure 4-9) we can write

$$-\dot{V} - \dot{V}_b = \dot{V}_{RC} \tag{4. 13}$$

where:

$\dot{V}$ is the net generated flow (i.e., patient flow)

$\dot{V}_{RC}$ is the flow into the right chamber

As the vane moves, the pressure and the compressed volume of gas in either chamber will change. Assuming isothermal conditions, by applying the continuity law to the ventilator, we can write:

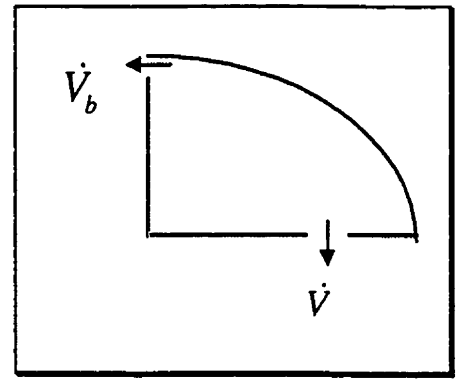

Figure 4-9: Right chamber

$$\dot{V} = \dot{V}_a - \frac{d}{dt}(V_{RC} + V_{LC}) = \dot{V}_a - \left(\dot{V}_{RC} + \dot{V}_{LC}\right) \tag{4. 14}$$

The compressed gas volumes V_{RC} and V_{LC} on either side of the vane are given by:

$$V_{RC} = V_R \frac{P_{RC}}{P_a} = \frac{r^2 l\theta}{2} \frac{P_{RC}}{P_a} \tag{4. 15}$$

$$V_{LC} = V_L \frac{P_{LC}}{P_a} = \frac{r^2 l(\pi - \theta)}{2} \frac{P_{LC}}{P_a} \tag{4. 16}$$

Substituting for V_{RC}, V_{LC} and R_a from Equations 4.15, 4.16 and 4.12 into Equation 4.14 we then find the generated flow $\dot{V}$ to be:

$$\dot{V} = \frac{-P_{LC}}{R_a} - \frac{d}{dt}\left(\frac{r^2 l\dot{\theta}}{2}P_{RC} + \frac{r^2 l(\pi-\theta)}{2}P_{LC}\right)$$

$$= \frac{-P_{LC}}{R_a} + \frac{d}{dt}\left(\frac{r^2 l\theta}{2}(P_{LC}-P_{RC}) - \frac{r^2 l\theta}{2}P_{LC}\right) \qquad 4.17)$$

Differentiating 6, P_{LC} and P_{RC} in equation 4.18 with respect to time yields:

$$\dot{V} = \frac{-P_{LC}}{R_a} + \frac{r^2 l\dot{\theta}}{2}(P_{LC}-P_{RC}) + \frac{r^2 l\theta}{2}\left(\dot{P}_{LC}-\dot{P}_{RC}\right) - \frac{r^2 l\pi}{2}\dot{P}_{LC} \qquad (4.18)$$

The above Equation will be used to compute the flow generated by RVV. However, we will see in chapter 8 how $\dot{V}_a$ (Equation 4.12) will be characterized and substituted for, in Equation 4.18. Furthermore the validity of this equation will also be extensively tested.

4.2 DC Motor

The dc motor used with the RVV was taken from an old PDP7 computer tape reel. Since no technical specifications for the device were available, for the purpose of identification of relevant parameters and subsequent modeling of its dynamic performance, tests had to be performed in the lab to measure armature resistance, inductance, rotor mass and torque (see chapter six).

4.3 Shaft coupling

The vane-supporting rod is connected to the motor shaft via a flexible direct coupler (Morton's Manufacturing, Ohio, USA) with 15 degrees freedom of movement in all directions. It is made of hardened aluminum, with incorporated setscrews for installation.

4.4 Valves

The inspiratory and expiratory valves used in the ventilator are shown in Figure 4-10 and Figure 4-11. They are 2-way normally closed, direct lift, pilot assisted diaphragm valves. They have orifice diameters of 3/4 and 5/8 inches respectively and they are made by Honeywell Inc. Skinner Valve, 95 Edgewood Avenue, New Britain, CT 06051. They both operate at 12V dc and have 22 Watts power consumption. Figures 4-10 and 4-11 show the mechanical and electrical components of one such valve, respectively. The refilling valve is an Asco Red Hat type of ¼ inch orifice diameter by Ascoelectric limited, Brantford, Ontario, Canada. It also operates at 12 V dc but has much lower power consumption.

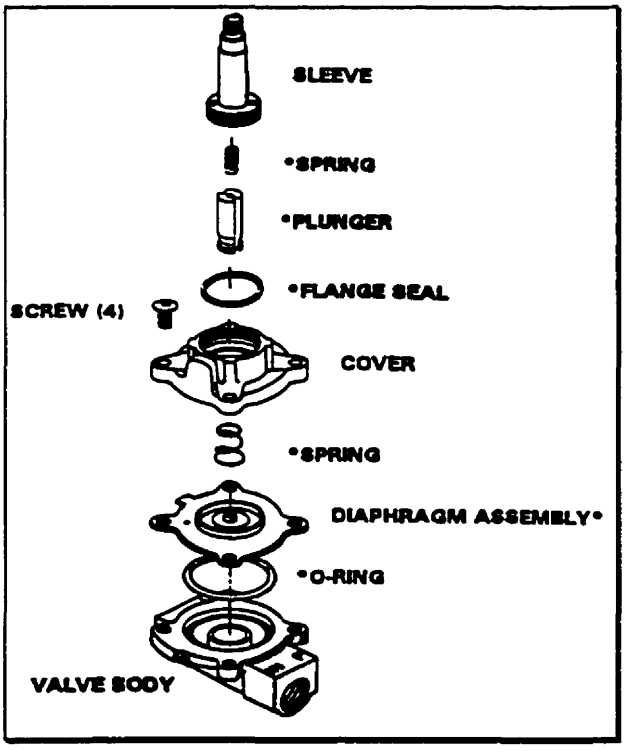

Figure 4-10: Honeywell solenoid valve assembly

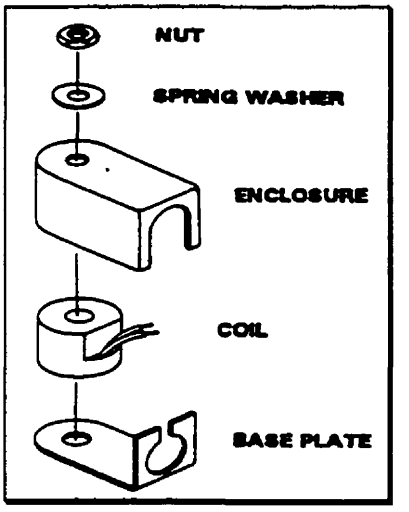

Figure 4-11: Solenoid assembly

4.5 Compartmentalized support box

With the exception of the operational display panel, all other components are housed in a support box (Figure 4-12). It is made of Plexiglas and was machined and assembled in the workshop at the Meakins-Christie Laboratories. Its compact design makes the ventilator portable and, with installation of appropriate connector terminals on the box, the Laptop computer is easily connected to the device. Two power supply transformers and the signal conditioning circuitry are installed in the bottom section. The dc supply boards, power amplifier, valve driver and the rest of the electronic boards are mounted vertically on either side of the Motor. The valves are located as shown in Figure 4-1. An air ventilation dc fan installed on the rear end of the box eliminates the heat produced by the electrical components and provides adequate air circulation for safe thermal conditions.

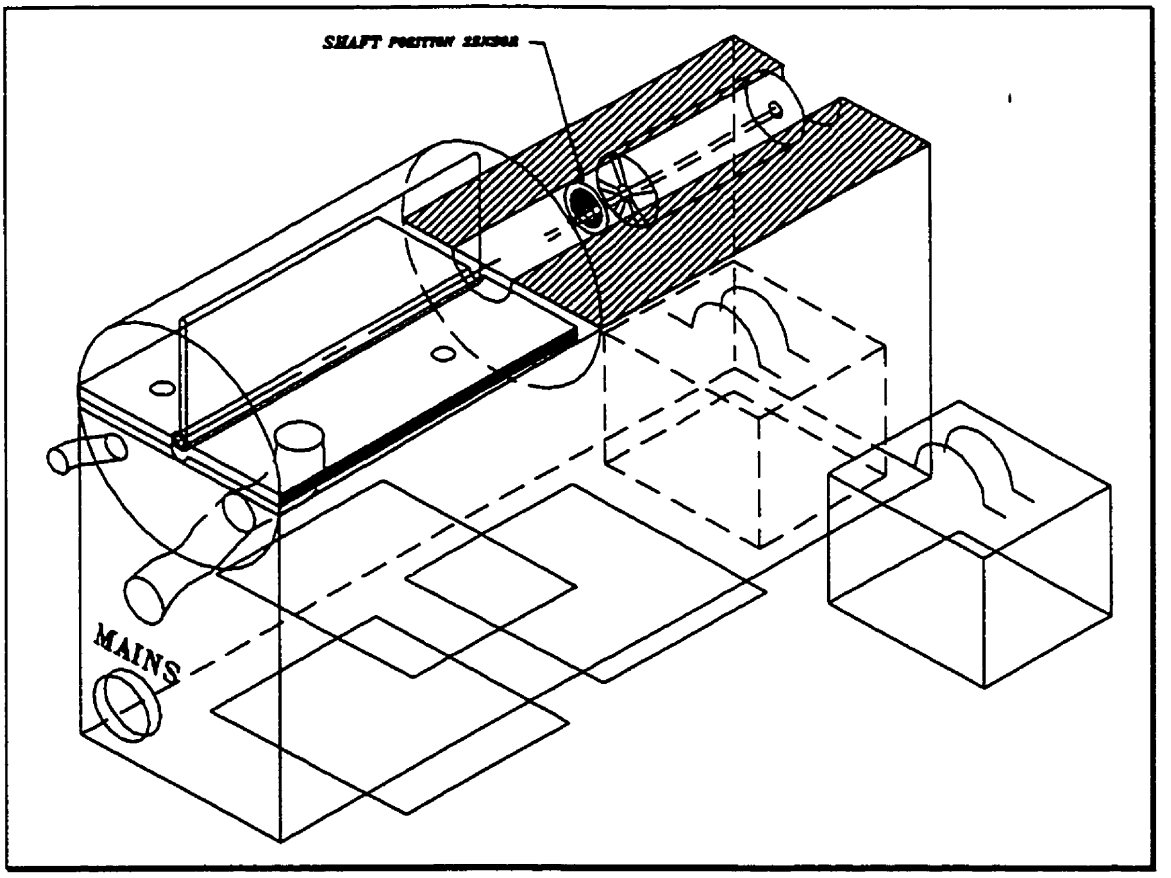

Figure 4-12: The support box. Note the pressure chamber housing is integrated into the box

4.6 Electronic board installation

With the exception of the operational display panel, all other electronic boards are installed in the support box. Figure 4-13 gives the layout of the display panel that is made of a small box containing the connector that receives the information signals through a flexible cable. There are a series of LEDs used to display operational information. The signal cable is flexible and permits easy displacement as well as movement of the panel for better positioning and viewing.

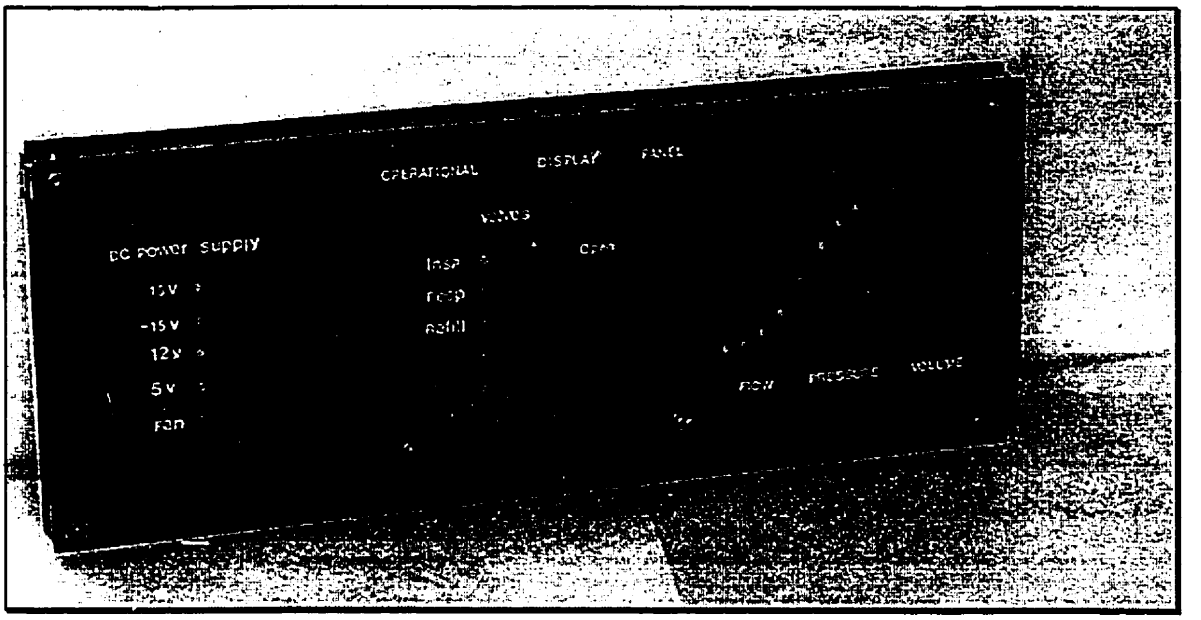

Figure 4-13: Information display panel

4.7 Position sensor

The device that measures the position of the vane is a rotational variable differential transformer (RVDT) (Lucas Control System Products, Schaevitz Sensors, 1000 Lucas way, Hampton, Virginia, 23666, USA) which has been installed at the tip-end of the vane. To make sure that the sensor is coupled directly to the vane, with no loading on its shaft, it is housed in a small cylindrical holder, made of Plexiglas, that is mounted on the end plate (see Figure 4-1 and Figure 4-2). Care has been taken to insure

perfect and torsion free insertion of the sensor shaft into the vane shaft. A setscrew is used to keep the coupling in place.

4.8 Closing remarks

The current chapter gave an overview of the RVV. The principal of gas compression based on the use of a rotating vane was discussed. A detailed mechanical design of the ventilator with its mathematical model was also presented. Flow computation from the geometry of the design was developed and some of the components used in the construction of the RVV were introduced.

Chapter five will give a complete treatment of the electronics setup of the RVV. Starting with an assessment of the power amplifier for the motor, it goes on to explain the data acquisition circuit, pressure sensors and all other supporting electronics required for the correct functioning of the RVV.

5

RVV: Electronics setup

Electronics design and construction was a major component of the RVV development. The power amplifier, data acquisition circuitry, power supplies, valve drivers, information display panel, and position and pressure sensors will be discussed in this chapter. Special attention will be given to the acquisition system, and in particular the more recent D/A and A/D boards which use personal computer memory card international association (PCMCIA) technology.

5.1 The Power amplifier

5.1.1. Assessment of power requirements

Before making the selection of a power amplifier, a power assessment had to be carried out in order to estimate the power required to drive the linear dc motor. If sinusoidal motion is considered, the amount of energy necessary to overcome the mechanical inertia of the moving mass, the "Inertial" power, can be stated as

$$E = \frac{1}{2}mv^2 = \frac{1}{2}mA^2\omega^2\cos^2(\omega t) \tag{5.1}$$

where E is the translational energy, m is the total moving mass, ω is radial frequency and A is the amplitude. The inertial power (P) is thus given by

$$P = \left|\frac{dE}{dt}\right| = mA^2\omega^3\left|\cos(\omega t)\sin(\omega t)\right| \tag{5.2}$$

Equation (5.2) gives the maximum value of P at $\omega t = (2n+1)\pi/4$ where n is an integer. For a given frequency, the maximum power is then given by

$$P = \frac{1}{2}mA^2\omega^3 \tag{5.3}$$

or

$$A = \sqrt{\frac{2P_{amplifier}}{m\omega^3}} \tag{5.4}$$

Equation (5.4) gives a relationship between amplitude and frequency for given amplifier power. The evaluation of this equation for various readily available integrated power amplifiers from different manufacturers led to a final selection. The integrated amplifier currently in use, the PA12 (120W), is manufactured by Apex Microtechnology, Az, USA. Its amplitude response is shown in Figure 5-1 by the dashed line. This choice is based on appropriate amplitude bandwidth and perturbation signals of at least 50 Hz. It gives an output of ± 24 V and a current limit of 10A. However, it is worth noting that, in practice, part of the amplifier power is lost in electrical heat production and/or friction. Furthermore, Figure 5-1 indicates the frequency response with all the losses neglected. Since the mass inertia consumes a major part of the power, the amplitude-frequency relationship still gives a good estimation of power required from the amplifier.

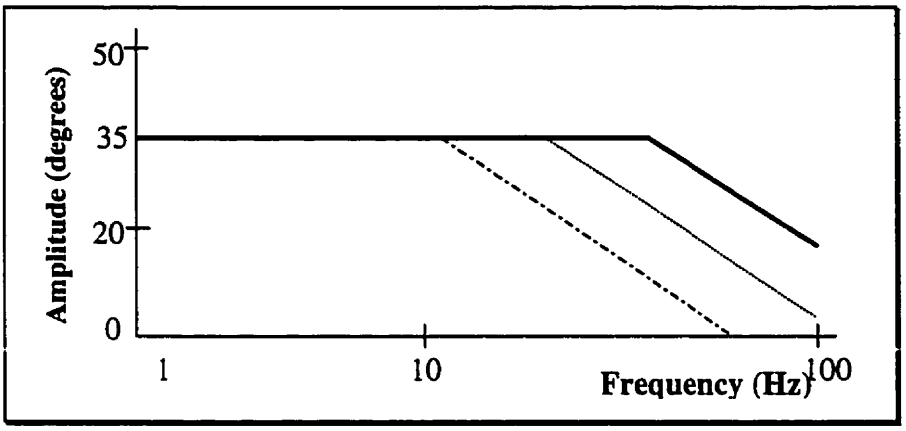

Figure 5-1: Amplitude-frequency relationship for different amplifier powers

5.2 Power supply for the amplifier

5.2.1. Power supply

Figure 5-2 shows the power supply used to supply dc excitation voltages for the power amplifier. As can be seen, it is unregulated since maximum efficiency is required. Furthermore, no stabilization is required because the power amplifier has its own compensation feedback. The source of the dc supply is a *Hammond* transformer rated at 25V/125VA (center tapped). The nominal output voltage of the supply circuit is

$$V_{supply} = \pm\left(\frac{25V \cdot \sqrt{2}}{2} - 0.7V\right) = \pm 16.8V \tag{5.5}$$

This voltage is valid with maximum load (i.e. when maximal current is drawn). The capacitor configuration filter is designed to maintain the 60 Hz ripple on the supply below 2.5 V_{pp}. Capacitance values have been chosen according to:

$$C = \frac{1}{2f}\frac{I}{V_{ripple}} = \frac{1}{2.60Hz}\frac{9.3A}{2.5V} = 3100\mu F \tag{5.6}$$

I is the current set by the current limit circuit of the amplifier and f is the frequency of the public mains, 60 Hz, in Canada.

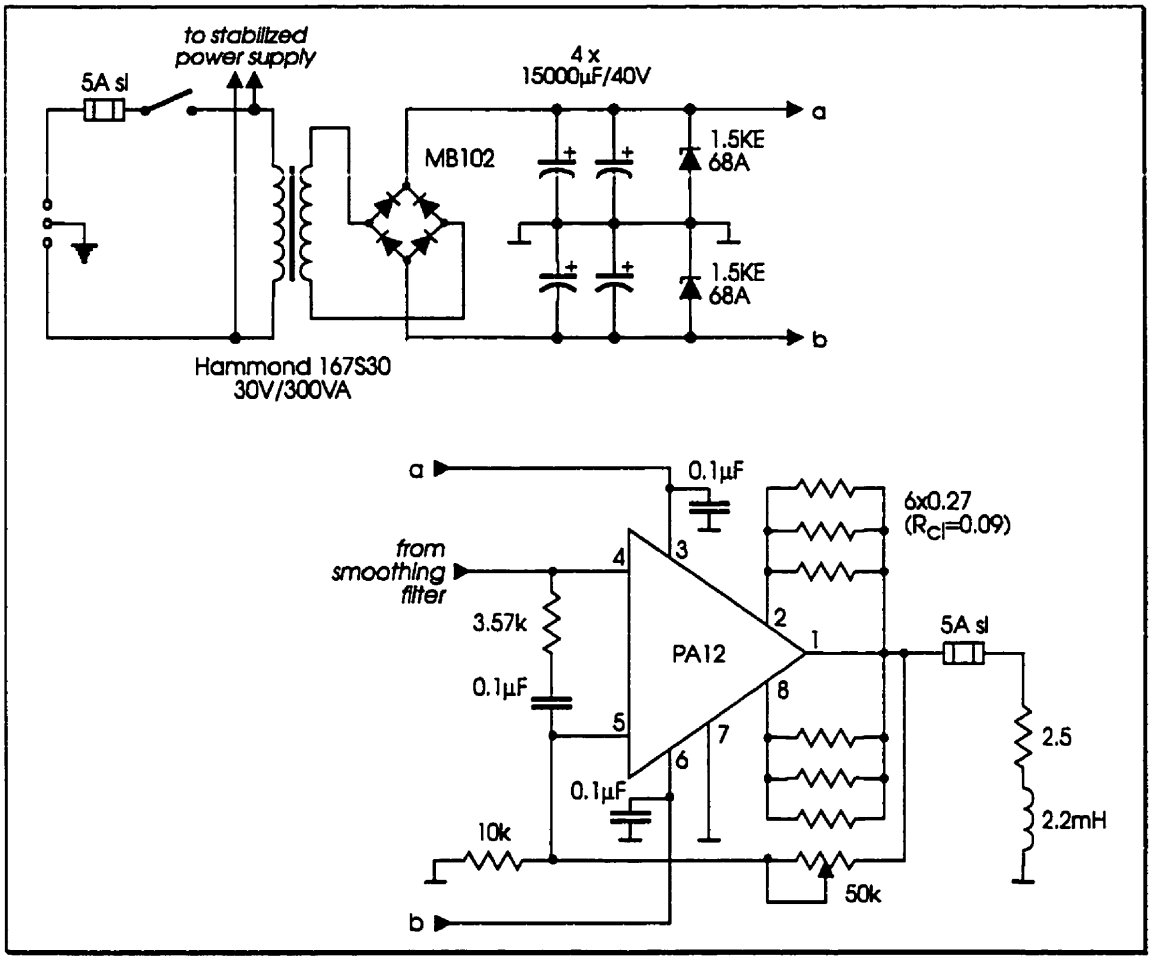

Figure 5-2: Top: power supply, Bottom: power amplifier

5.2.1.1 Current limiting and thermal considerations

For a purely resistive load, when the current is maximal, the voltage drop in the amplifier is minimal. In the case of an imaginary or reactive load, maximal current is drawn when output voltage crosses zero. The power dissipated within the power amplifier depends on the nature of the load, and is considerably higher in the case of reactive loads. To protect the semiconductor of the power amplifier from overloading, without limiting the current to unnecessarily low values, the PA12 permits the use of a foldover current

limiting circuit which, depending on the nature of the load, adapts to different current limits. The minimum and foldover current limits were thus set to 6.5A and 9.3A, respectively, which are well within the safe operating limits. However, for further protection of the amplifier, a quick blow fuse also isolates the load. An important consideration in the design of the heat sink for the amplifier is safe and efficient removal of the heat generated within the op-amp semiconductor junction. The junction temperature of the PA12 must not exceed 200°C. Maximal power dissipation takes place around 54 watts and is calculated as follows

$$P_{dissipation} = 2V_s I_q + 0.5V_s I_l = 53.3W \tag{5.7}$$

This is when output voltage is almost half the supply voltage V_s, output current I_l is 5 A and I_q, the amplifier quiescent current, is 50 mA. The junction-to-case resistance of the op-amp is 1.4°C.W^{-1} (given by the manufacturer). The maximum thermal resistance, which is permitted to exist between case and air, assuming 30°C ambient temperature, is given by

$$R_{thermal} = \frac{200^o C - 30^o C}{53.3W} - 1.4^o C.W^{-1} = 1.68^o C.W \tag{5.8}$$

To maintain the thermal-case-to-air resistance of the setup below that of Equation (5.8), the op-amp was mounted on an appropriate heatsink and a dc ventilator was installed in the back of the supporting box to maintain an efficient air drag.

5.2.1.2 Power amplifier stability

When amplifier gain is low, the feedback section of the amplifier must have a higher gain. In effect, this is a high open-loop gain with respect to the amplifier itself and can cause instabilities. To prevent this, a compensating RC-network was inserted between the non-inverting and inverting inputs of the op-amp. The corner frequency of this

network was set to be at 450 Hz. It should be noted that the gain of the power amplifier is adjustable and in the present application it is set to 2.

5.3 Data acquisition

5.3.1. Data acquisition circuitry

Figure 5-3 gives an overview of the data acquisition concept. The RVV is capable of collecting data from up to 8 or 16 channels, depending on whether differential or

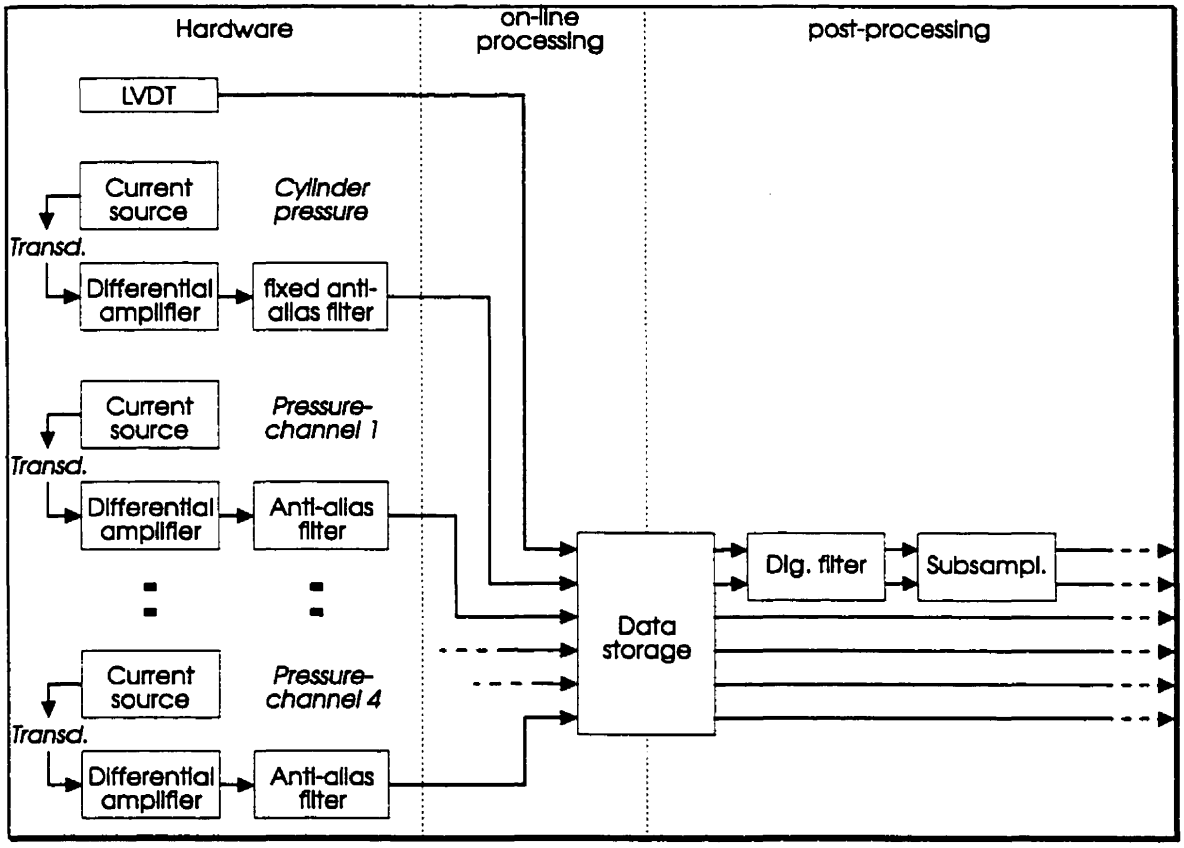

Figure 5-3: Data acquisition circuit

single-ended inputs are used. In the present configuration, pressures on both sides of the vane and vane position have to be recorded. The outflow (patient-flow) is then computed very precisely from these three signals. However, the vane position is used within the motor control algorithm, and hence must be sampled at the control-sampling rate of 1

kHz. Input signals are anti-aliasing filtered with a cutoff of 200 Hz, in order to satisfy the sampling theorem at the control-sampling rate (i.e., minimum rate of 500 Hz). The data are then stored and any digital filtering or subsampling takes place subsequently. The channels on the conditioner box are designed for use with the *Fujikura* FPM-02PG piezoresitive bridge pressure transducer (see 5.3.2), although they can be readily adapted for other types of transducer or input signals.

5.3.2. Optimized current source for resistive bridge sensors

The *Fujikura* FPM-02PG type, is shown in Figure 5-4. Table 5-1 gives an excerpt from the data sheet for this transducer. The excitation of this sensor is by constant current. In practice, it is very sensitive to small changes in the driving current. Figure 5-5 shows the constant current source that was employed. It is a standard op-amp current source with a precision 2.5 V reference element at the non-inverting input. However, to eliminate the thermal drift caused by self and mutual heating of the components, thermal optimization of the current source is also implemented.

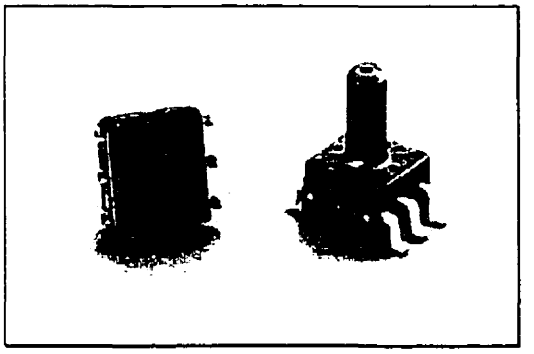

Figure 5-4: *Jujikura* FPM-02PG solid state pressure sensor

Table 5-1: Properties of the *Fujikura* FPM-02PG

Pressure range	± 2 psi/13.8 kPa
Output range (FS)	± 80 - 130 mV
Bridge resistance	5.4 ± 0.6 kΩ
Excitation	1.5 mA
Zero offset	± 10 mV
Comp. temp. range	0 - 50 °C
Output temp. error	± 1.5 %FS (0 - 50 °C)

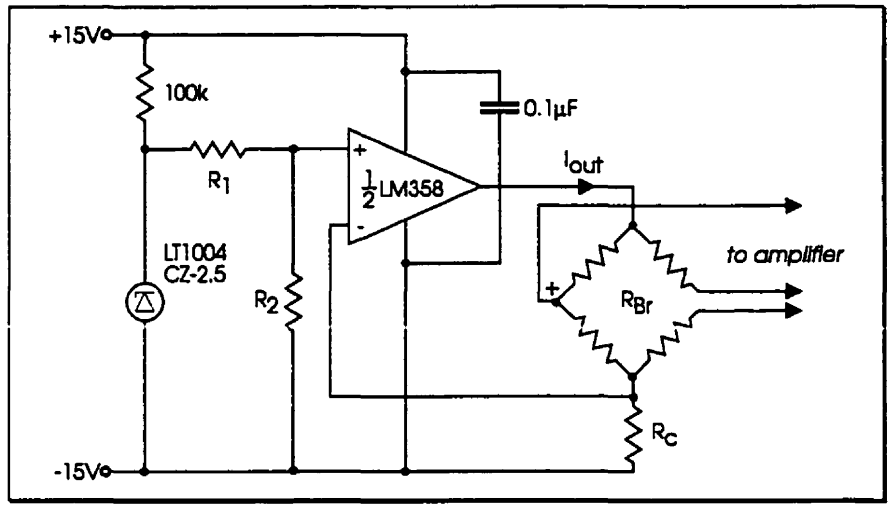

Figure 5-5: Constant current source used to excite the pressure sensors

5.3.3. The pressure channels

Before digitization of the pressure transducer output signals, they must be compensated for any offset present, amplified and band-limited. The pressure channels, each contain an offset-trim potentiometer and a differential amplifier whose gain can be adjusted. The amplified signal is then fed through a 6-pole Bessel anti-aliasing filter with adjustable cutoff frequency.

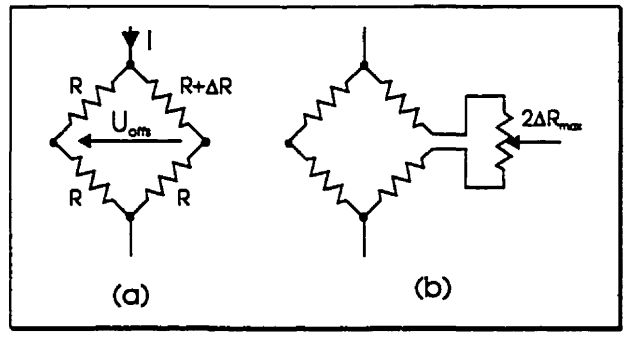

Figure 5-6: (a) asymmetric bridge, (b) offset compensation

5.3.3.1 Offset compensation

To design a compensation circuit to correct for the zero offset of the pressure transducers, first an estimate of the bridge asymmetry was obtained. Figure 5-6(a) shows the model of the bridge, consisting of three resistors of value R and one resistor of value $R+\Delta R$. The offset voltage is given by

$$U_{offs} = \frac{R\Delta R}{(4R+\Delta R)} I \,. \tag{5.9}$$

Solving for ΔR, gives

$$\Delta R = \frac{4RU_{offs}}{RI - U_{offs}} \approx 4\frac{U_{offs}}{I}. \tag{5.10}$$

With a maximal $U_{offs} = \pm 10\,\text{mV}$ and an excitation of $I = 1.5\,\text{mA}$, the bridge asymmetry is found to be no greater than $\Delta R_{max} = \pm 26.7\Omega$. The offset compensation is then achieved by insertion of a potentiometer of at least $2\Delta R_{max}$ between the two open pins of the transducer as shown in Figure 5-6(b). The value of the potentiometer chosen for the RVV is 100Ω.

5.3.3.2 Differential amplifiers

In order to achieve good resolution after digitization, signal amplification that prevents clipping of the signals is necessary. Within the signal conditioning circuitry of the RVV, a standard differential amplifier of integrated circuit type IN101 (*Burr*

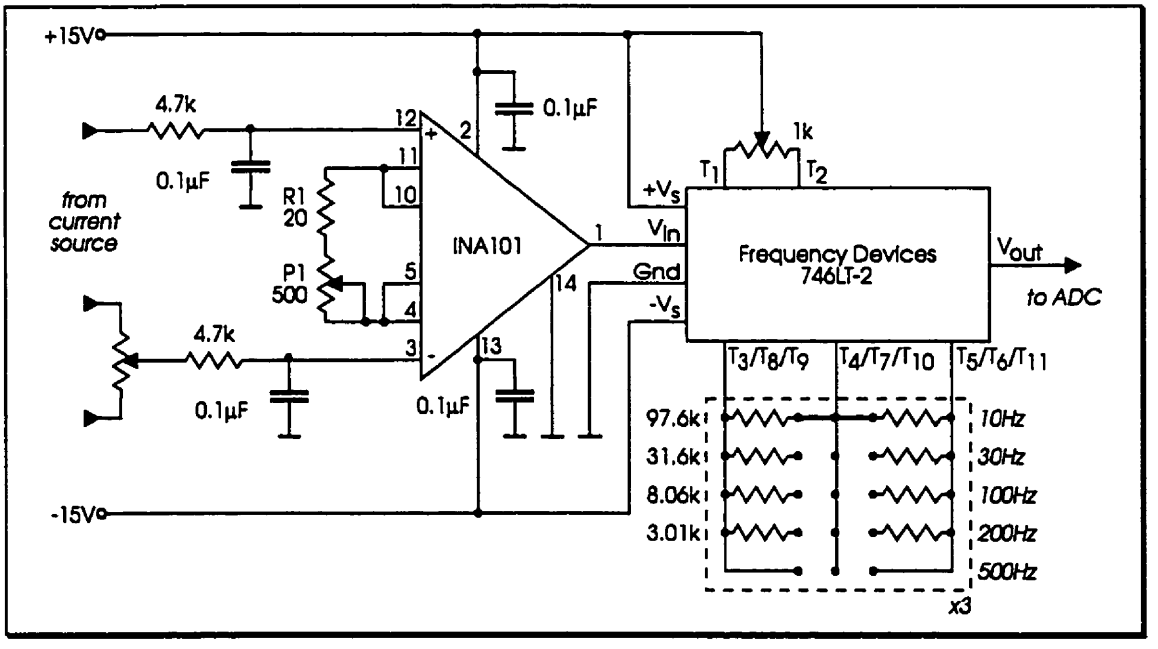

Figure 5-7: Differential amplifier and anti-aliasing filter with only one resistor bank shown

-*Brown*) is used. To be able to achieve a good amplification range for all possible pressure values from the *Fujikura* sensor, a gain range of 100 to 2000 is required. This is in conjunction with the input span of the A/D board which is software programmable, and is chosen to be at ±5 V. Figure 5-7 shows a schematic of the differential amplifier and the anti-aliasing filter for one pressure channel. The gain of the integrated differential amplifier INA101 is computed from the equation

$$G = 1 + \frac{40k\Omega}{R_G}. \tag{5.11}$$

R_G is the resistor which determines the gain of the amplifier and is equivalent to the sum of R_1 and P_1.

5.3.3.3 Anti-aliasing filters

Sampling data involves measuring a continuous function at discrete time intervals. The sampling rate has to be sufficiently so that the samples can describe the high frequency information in the signal and at the same time will not generate redundant and highly correlated samples that increases the labor and cost of analysis for no additional information. Sampling a signal that contains power at frequencies higher than half the sampling rate leads to a phenomenon known as aliasing. The high frequency components in the signal appear in the sampled data at lower frequencies and hence distort the information. One way of preventing aliasing, is to band limit the signal to a value that does not exceed that of the sampling frequency. The RVV uses a resistive-tunable 6-pole Bessel filter (*Frequency Devices* -746LT-2) to band limit the signals before digitization. Table 5-2 gives an

Table 5-2: Specifications of the Frequency Device 746LT-2

Number of poles	6
Cutoff frequency range	1-500
Supply voltage	± 12 to ± 18 V
Dynamic range	± 10 V
Gain	0 dB
Output offset	± 5 mV

overview of the characteristics of this filter. Figure 5-7 shows one such filter within the data conditioning circuit. By the use of six resistors of equal value, arranged in 3 lots of two, the cutoff frequency of the filters is selected. The values of such resistors are chosen according to an equation given in the manufacturer data sheet. The RVV uses filters with corner frequencies adjustable to 10, 30, 100, 200 and 500 Hz. With the above corner frequencies, suppression of mains noise at 60 Hz can easily be achieved.

5.3.4. Signal conditioning within the control loop

As will be explained in chapter 6, the position of the vane is used as the feedback variable within the control algorithm of the RVV. A Rotational Variable Differential Transformer (RVDT) is used to measure the position. The output span of the device is ± 5 V for a rotational displacement of ± 40 degrees, which yields a sensitivity of 125 mV/degree. The output signal of the sensor is read with an A/D board with a gain of 1 to maximize the resolution of the position signal after digitization. The RVDT output signal is also band-filtered with the –3 dB point at 500 Hz (see 5.4 for more details). With a sampling rate of 1 kHz, prevention of aliasing is guaranteed without any further signal conditioning.

5.3.5. Analog-to-digital converter board

Analogue to digital conversion of the data is carried out through a type II slots compliant personal computer memory card international association (PCMCIA) card from ComputerBoards, Inc. 2 Commerce Park Blvd. Middleboro, MA 02346, USA. A detailed specification of the card is given in Table 5-3. It is installed in a Laptop computer. Analog signals are routed to the A/D via an 8:1 differential multiplexer controlled by a register on its main board. The analog input range is fully programmable in both bipolar and unipolar ranges. An on-board pacer clock and external pacer inputs as well as software polling may trigger A/D conversions. Transfers may be via software polling or interrupt service. A FIFO (first in first out) buffer provides buffering between the A/D circuit and the PCMCIA bus. Eight digital I/O lines (8 in or out, or, 4 in 4 out) provide a means of sensing and controlling discrete events. However, in the present

application the I/O lines of the D/A board are used instead. The A/D chip always runs at full speed. The A/D converter and sample & hold circuit captures and digitizes a signal in 10 microseconds ($10\,\mu S$). The conversion of the A/D remains constant under all conditions and at all throughput rates.

Table 5-3: PCMCIA type 2 analog-to-digital board data specification

Analog Input Specification	
PCM-DAS16D/12	8 Differential A/D channels
Input resolutions	12-bits (1 in 4096)
Input ranges	±(10,5,2.5,1.25)V,0-10V, 0-5V, 0-2.5V, 0-1.25V
Range selection	Software programmable
Max sample rate	100 kHz
Sample rate set by	Internal or external clock
Internal clock frequency	1 MHz or 10 MHz
Input Impedance	Greater than 10 MΩ
Power consumption	
+5V quiescent	65mA typ, 90mA max
+5V active	75mA typ, 110 mA max
Form factor	
PCMCIA	Type II compliant
Digital I/O	
Configuration	8 HC family bits in two 4-bit ports independently set as input or output.

When, for example a sample rate of 20 kHz is requested, the A/D converter still converts each sample in $10\,\mu S$. The 20 kHz rate comes from the fact that conversions are initiated every $50\,\mu S$. This converter provides a resolution of 1/4095 parts of full scale. The accuracy is specified as smallest reading or Least Significant Bit (LSB). The board is accurate to +/- 1 LSB and depending on the input range selected this can vary from

4.88×10^{-3} to 1.22×10^{-3} V. Throughout the operation of the RVV, the gain on the A/D is set to ±5 V. This gives a resolution of 2.44×10^{-3} V.

5.3.5.1 Connecting Signals to the Analog Inputs

The PCM-DASD/12 has 8 differential inputs. This type of input requires three connections to complete the input circuit. These are Signal High, Signal Low, and Low Level Ground. The analog measurement is made between Signal High and Signal Low. The measurement is the difference between the two. Signal Low may not be fully independent of low-level ground. There must be some reference between the two such that the difference between Signal Low and Low Level Ground does not exceed the Common Mode Range of the input circuit. (i.e. the voltage range over which a difference between the Signal Low and Low Level Ground have no impact on the A/D measurement of the signal). This is ± 10V. However, Figure 5-9 shows the correct connection of a differential input when the signal source has three signals. Figure 5-8 on the other hand, shows a situation when the signal source has only two signals and the source is floating relative to ground. The 10 KΩ resistor between the signal low and low-level ground provides a reference for the A/D circuit. Without the resistor in place, the signal may float outside the cumulative signal range

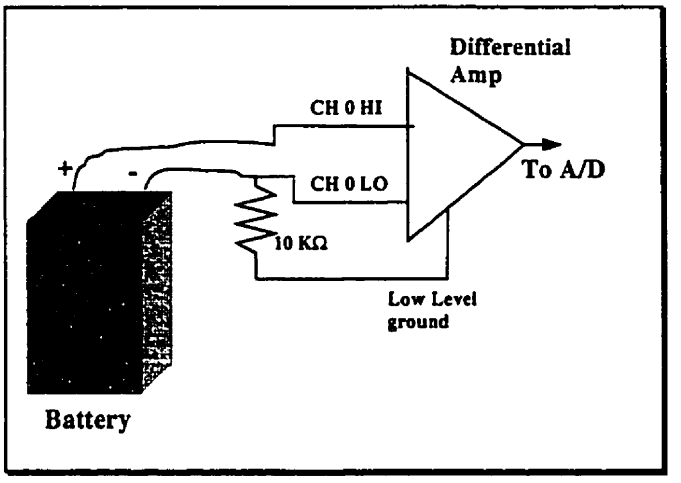

Figure 5-8: Two signals with floating source

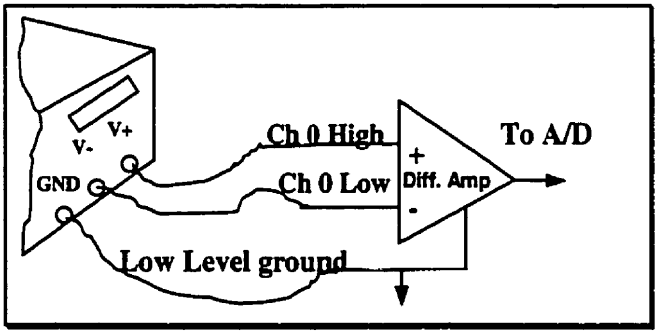

Figure 5-9: A differential input with three signals

(CSR), yielding full scale positive or negative readings. This can be the case when the Laptop computer is running on battery power, so the computer can be floating with respect to earth.

5.3.5.2 Digital-to-analog converter board

The RVV communication with the outside world takes place through a digital to analog (D/A) converter board of PCMCIA slot 2 type. It is a PCM-DAC02 from ComputerBoards, Inc. 2 Commerce Park Blvd. Middleboro, MA 02346, USA. At the heart of the board is a pair of 12-bit digital-to-analog converters. Signals are generated by the D/A via a register on the main board. Eight bi-directional digital I/O lines provide a means of sensing and controlling discrete events. In addition, there is 1 interrupt input, and a digital ground. A chassis ground is in the cable shield and clips to either side of the 15-pin connector. Table 5-4 gives further technical details for the board. An overview of the 15-pin I/O connector is provided in Figure 5-10. There are four possible output voltage ranges. Each D/A channel may be controlled independently, meaning that each DAC may have a different range. The output range is controlled by software. The available ranges, LSB step size and corresponding codes are given in Table 5-5.

Table 5-4: Digital to analog board data specification

General Specifications	
Model PCM-DAC02	PCM-DAC02 12-bit D/A outputs
Channels	8, 12-bit D/A outputs
Output ranges	± 10V, ± 5V, 0-10V, 0-5V
Output current	5 mA min
Setting time	150 μS
Supply current	45 mA typ, 90 mA max
Form factor	
PCMCIA	Type II compliant
Digital I/O	
Configuration	8-bits in two 4-bit ports

Table 5-5: Voltage gain ranges of D/A board with their corresponding digital codes

Range	LSB Step Size	0 Code	2048 Code	4095 Code
0 to 5 V	0.00122 V	0 V	2.5006 V	5 V
0 to 10 V	0.00244 V	0 V	5.0012V	10 V
±5 V	0.00244 V	-5 V	0 V	+5 V
± 10 V	0.00488 V	-10 V	0 V	+ 10 V

The PCM-DAC02 analog outputs are single ended. There is an analog ground for each analog output channel. In the case when multiple channels are connected, one must make sure that pin 1 is the ground for channel 0, while pin 3 is the ground for channel 1. It is very important that there is no measurable potential between the grounds at pins 1, 3,7 and chassis ground (Figure 5-10). In addition, there must not be any potentials between signal ground and chassis ground on the computer. In our application, with a Laptop computer working on battery power, the computer will be floating with respect to earth ground. Care has to be taken to meet the requirements for the correct differential input (see section 5.3.5.1). However if the Laptop is on the charger unit or connected to the mains, the computer may be grounded.

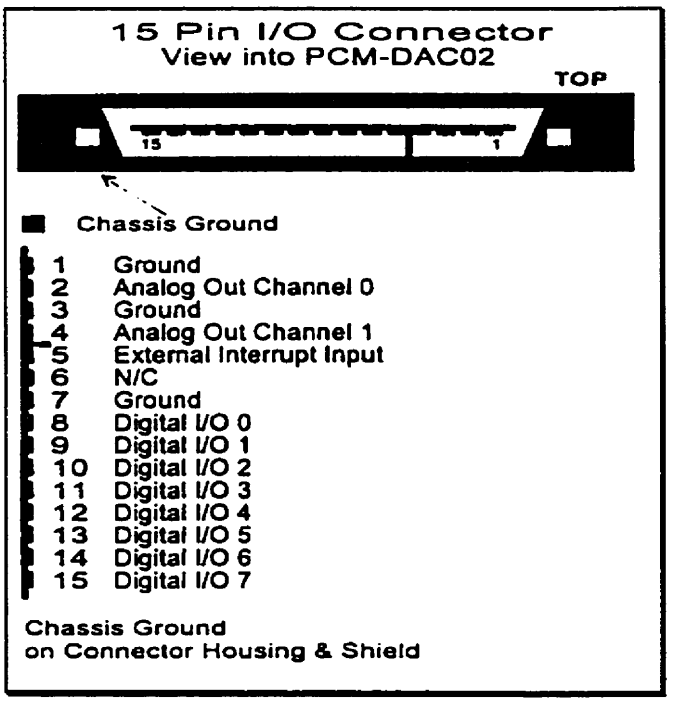

Figure 5-10: Digital to analog 15 pins input-output connector

It is important that whenever the Laptop is grounded, the signals should be connected in a way so that there is no potential between PC ground and signal ground. If there is a potential, it will be added to the signal. For example, if the D/A is supplying

3.5 volts and there is a potential of –1.5V between the PC and the amplifier ground, the amplifier under control will read 2.0V instead of 3.5V. It is also very important that the digital signals should not grounded to the analog ground. The maximum current supplied by the analog outputs is 2.5mA. Therefore the minimum resistance, or maximum load, which the output may drive is 2K Ohms. Loads greater than this will cause the analog output to droop, meaning that a code of 4095 will not be able to generate a voltage of 5V, but one that is somewhat less. As mentioned in section 5.3.5.2, the D/A has also an interrupt line. In the present configuration the controller output is sent out to the amplifier through channel 1 of the D/A board. It is programmed to work in bipolar ±5 V and thus the output high, and ground, are the same at a code of 2048. I/O lines 1 to 4 in different bit combinations are used to activate or deactivate the respiratory, supply and expiratory valves. A register controls the direction of digital I/O lines and is set via software. At power on or reset the digital lines default to input.

5.3.6. PCMCIA board installation

At the heart of the control loop of the ventilator is a Laptop computer that receives data from the ventilator through the A/D board and sends data to the ventilator via a D/A board. Unlike the older Industry Standard Association (ISA) technologies, PCMCIA is recent and demands certain procedures, with respect to installation, calibration and ultimate proper functioning. There are specific steps for installing PCMCIA boards in computers and they have to be followed exactly. For the computer to be able to talk to A/D and D/A boards, the PCMCIA slots first have to be initialized and configured . This is carried out through a piece of software universally known as *Card and Socket Services* (CSS). By adding a few lines to the computer AUTOEXEC.BAT file, every time the computer is booted up, CSS will also be automatically loaded and installed. Once this is done, the cards can be inserted into or removed from the slots without any power down. If CSS is successfully installed, every time a card is inserted or removed the Laptop will emit beep, and there is usually an icon present that indicates the presence of the boards. The boards can then be installed, tested and/or calibrated through a piece of software usually provided by the manufacturers. It has to be noted that with PCMCIA cards there

are no switches to set and all the installation steps including address setting, interrupt level and triggering type are programmable. Furthermore, CSS is a terminate-and-stay-resident program (TSR) and takes up about 71 kbytes of conventional memory which can be installed DEVICEHIGH.

5.4 Position sensor

To measure the angular displacement of the vane a *Rotary Variable Differential Transformer* (RVDT) model R30D is used (Figure 5-11). It is a dc operated non-contacting rotary transducer. Integrated signal conditioning enables the sensor to operate from a bipolar ±15 V dc source with a high level dc output that is proportional to the full range of the device. It has been factory calibrated for operation to ±40 degrees. The R30D provides a constant scale factor of 125 mVdc/degree. Within this range, linearity is better than ± 0.5 percent of full-scale displacement. Nonlinearity error of less than ±0.25% FS is achieved while maintaining thermal performance over 18°C to 75°C. The dc excitation is internally converted to an AC carrier signal, which excites the transducer primary coil. An integrated demodulator amplifier and filter convert the differential secondary output into a smooth, high level, dc output signal (Figure 5-12), that is linear with the shaft angle position. Resolution is essentially infinite, enabling measurements to a fraction of a degree. The –3 dB response of the sensor is at 500 Hz.

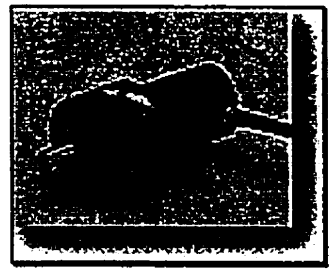

Figure 5-11: RVDT Position Sensor

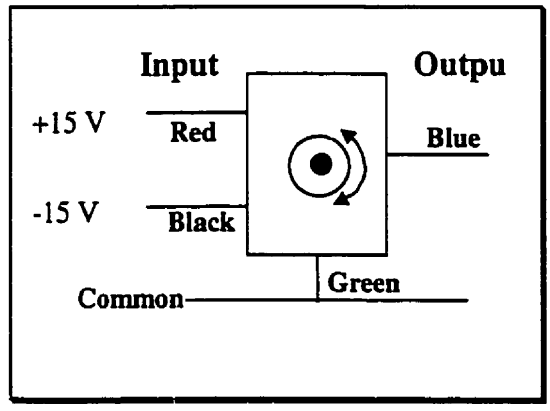

Figure 5-12: RVDT electrical connections

5.5 Power supplies

With the exception of the power amplifier, which has its own power supply on a separate board, all other DC supplies are generated on one board. However, to prevent cross talk between the power amplifier and the data acquisition circuitry, a separate stabilized power supply was built for the signal conditioning hardware. A separate transformer and a ground line were also used to generate stabilized ± 15 V supplies for the RVDT position sensor. In all, the ventilator uses regulated dc supplies of +5V, +15 V which feed the LEDs information display panel, +12 V for the air drag fan, a non-regulated +25 V for the valve driver board, and finally, a ± 15 V for the excitation of the position sensor. Figure 5-13 shows a typical circuit diagram used for stabilizing the power supplies, where integrated voltage regulators and filters have been used to achieve stabilization.

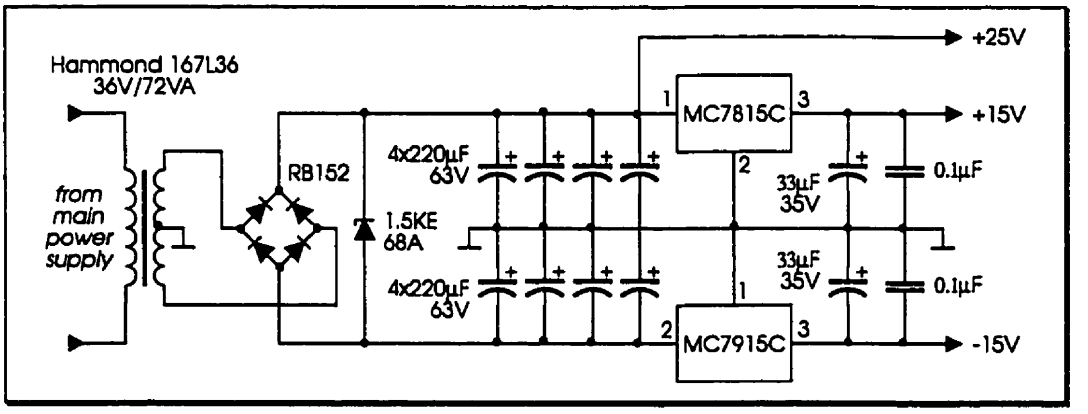

Figure 5-13: Stabilized power supply

5.6 Valve drivers

As described in section 4.4., there are three solenoid vales used in the ventilator, all driven by the digital I/O lines of the D/A board. To protect this board, a buffer amplifier is necessary, to switch the inductive load that the valves present. Figure 5-14 shows the circuit diagram of one such amplifier used in the ventilator. An unregulated 15 V dc supply provides the excitation power. The opening thresholds of the valves are around +5 V, so that the 15 V supply is sufficient to insure fast operation of the valves.

Steady state power consumption of the inspiratory and the expiratory valves is fairly high, therefore a proper sized heat sink had to be designed to safely and efficiently remove the heat generated within the power transistor that delivers the current to the valves. This is shown as Q_2 in Figure 5-14. This amplifier design works very satisfactorily and, in particular, the static power dissipation of the valves does not present any problems.

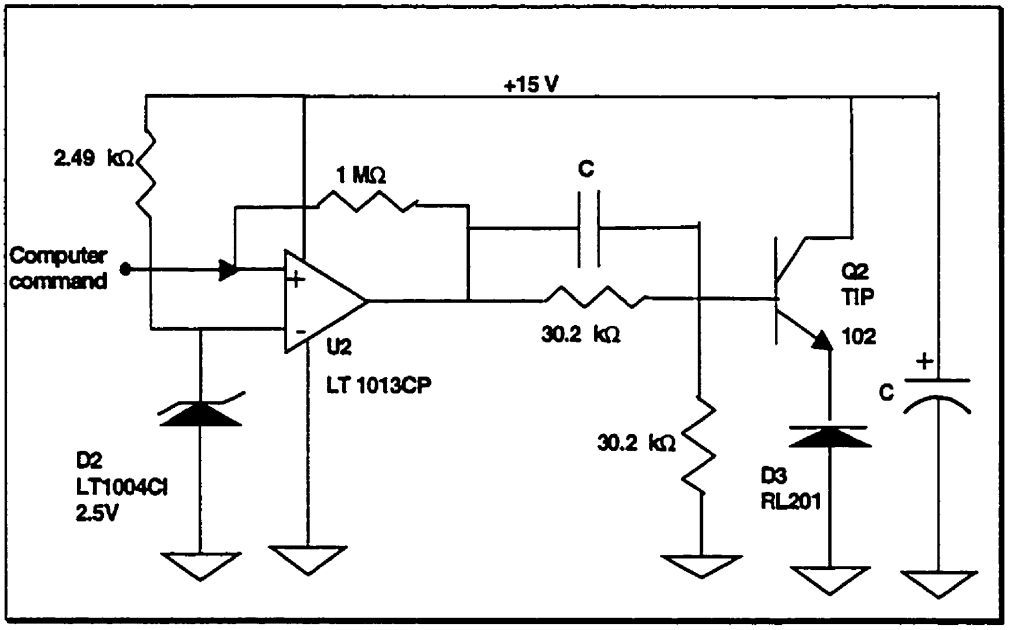

Figure 5-14: Amplifier driver for the valves

5.7 Information display panel

As shown in Figure 5-15, some critical signals are conditioned and prepared electronically, and then displayed on a panel that uses an integrated circuit line driver and LEDs. At the same time, the panel also acts as a display platform for the self-testing mechanisms incorporated within the electronics of the ventilator, every time the device is switched on and/or remains functional. It uses computer updates to display the status of the valves. DC power supplies are also constantly monitored and displayed. The vane position or pressure signals in the ventilator can also be displayed in real time on the information panel. Figure 5-15 gives the layout of the panel. To protect the sources of the

signals arriving at the panel, they pass through a buffer that operates in open collector mode. However, the vane position and the pressure signals are fed into an integrated circuit line driver display, *LM3914N* which enables a proportional analog display of the signals using the LEDs.

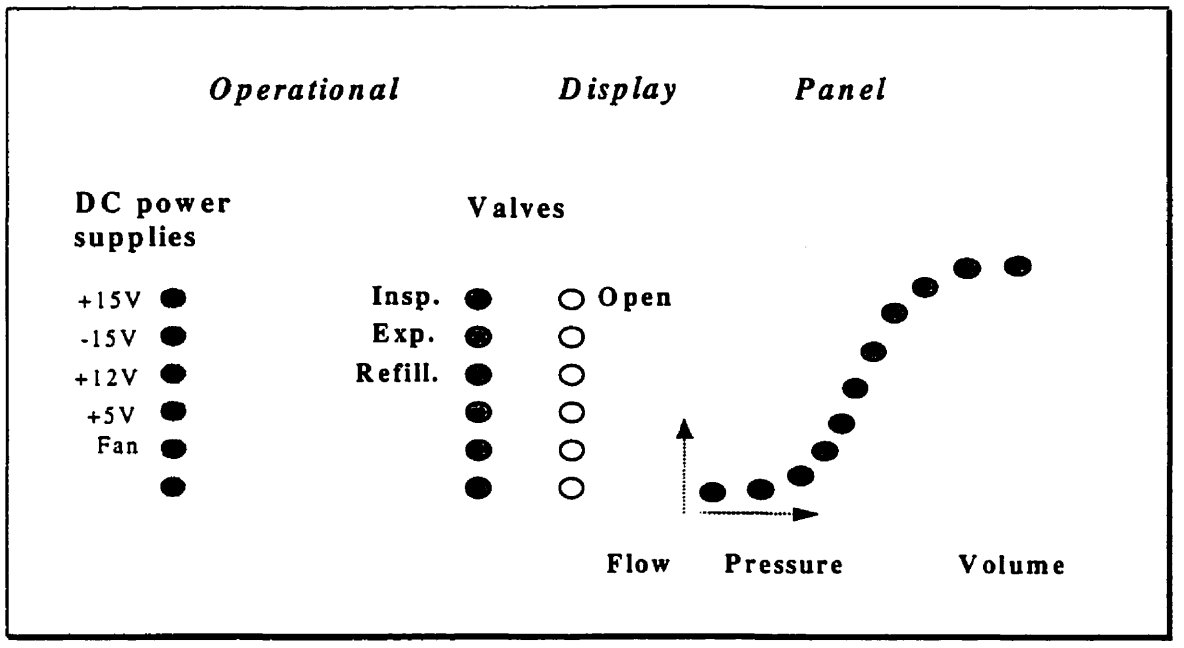

Figure 5-15: layout of the information display panel

5.8 Air circulation fan

To ensure efficient and safe working of the electronics of the RVV, a dc fan has been installed on the back of the support box as shown in Figure 4-1, the main objective being proper dissipation of the heat generated by the electronics and electrical components. In particular, the power amplifier needs a degree of air drag to maintain the junction temperature of the solid state integrated circuit within safe limits. The air ventilator is powered by a dc +12 V supply fed from the dc power board.

5.9 Closing remarks

In the present chapter, the electronic setup of the RVV was presented. The design, construction and the use of some components such as power amplifier, power supplies, data acquisition, signal conditioning, A/D, D/A, position and pressure sensors were explained. Some of the potential problems in the use of PCMCIA technology were also highlighted.

In the next chapter, the control aspects of the ventilator will be examined and a detailed study of the dynamics of the plant including nonlinearities presented. A real time controller has been designed and extensive system simulations are used to test its performance with some of the tools available in the domain of automation and control engineering. The chapter closes with the steps taken to optimize and implement the RVV controller.

6

RVV: System control analysis

Computation of flow from the RVV depends on the position of the vane. Good plant control is therefore essential to achieve precision of delivered flow. This chapter discusses the RVV dynamics and the overall plant model based on linear system theory. The open loop behavior of the system is evaluated and used to design a controller that yields satisfactory performance when controlling the position of the vane. A nonlinear model of the plant is then simulated. The controller is implemented in the RVV and its parameters are further optimized. Finally the RVV controller performance is evaluated.

6.1 RVV System Analysis and Control

Discrete control algorithms can be designed in two ways:

1) by designing a continuous-time controller and transferring it into a discrete realization.
2) by formulating the plant in discrete form, i.e., *in z-domain*, and developing the controller in the same domain

In present application the sampling rates are relatively high with respect to the low system bandwidth of 0-10 Hz, therefore the first approach is preferred. Moreover it has the advantages of being simpler to incorporate nonlinearities. A full model of the control system consists of both the hardware (ADC, DAC, antialiasing filter, power amplifier, plant and the position sensing RVDT) and software (controller and adder) portions of the controller as illustrated in Figure 4-5.

6.2 Linear Model Development

6.2.1. Plant model

The geometry of the motor together with its electrical circuit is displayed in Figure 6-1. It consists of a resistance R and an inductance L of the coil windings. The induced voltage in the coil as the rotor moves is represented by U_{ind}.

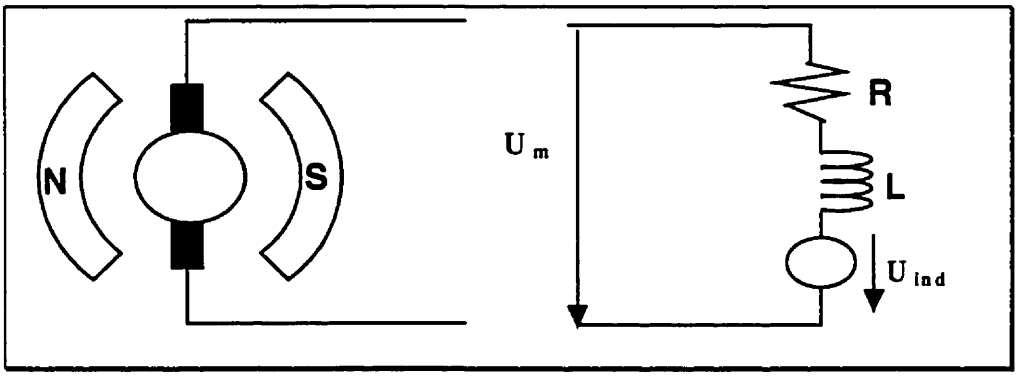

Figure 6-1: Sketch of the plant, motor electrical system

The applied voltage U_m is the input to the circuit and can be written as

$$U_m = Ri + L\frac{di}{dt} + U_{ind} = Ri + L\frac{di}{dt} + M\dot{\theta} \tag{6.1}$$

where i is the current in the coil, and M is the motor constant that relates induced voltage to shaft speed. M can be measured as the torque-to-current ratio, since it relates the

torque generated by the motor to the current through the coil. Newton's laws govern the linear dynamics of the motor, thus:

$$J\ddot{\theta} + D\dot{\theta} + AP_{chamber} = iM \tag{6.2}$$

where

J - Total moment of inertia of the moving masses including coil attachments and vane.

D - Viscous friction torque of the motor and vane supporting rod bearings.

θ - Vane position with the dot denoting the time derivative.

A - Vane surface area.

$P_{chamber}$ - Pressure in the right chamber.

r - Radius of the Vane.

In the frequency (s) domain, Equations 6.1 and 6.2 are Laplace-transformed to give

$$Um - Ms\theta = (R + Ls)I \tag{6.3}$$

and

$$(Js^2 + Ds)\theta + AP_{chamber} = MI \tag{6.4}$$

Solving Equations 6.3 and 6.4 explicitly for θ, the linear plant model in the Laplace domain is obtained as

$$\theta = \frac{M}{s(JLs^2 + (DL + JR)s + M^2 + DR)}U_m - \frac{A(R + Ls)}{s(JLs^2 + (JR + DL)s + M^2 + DR)}P_{chamber} \tag{6.5}$$

Equation 6.5 characterizes the dynamics of the system. The first term represents the motor with no load (i.e. motor Transfer Function, MTF) and the second term is the disturbance transfer function (DTF). Figure 6-2 shows the structure of the plant given by Equations 6.3 and 6.4.

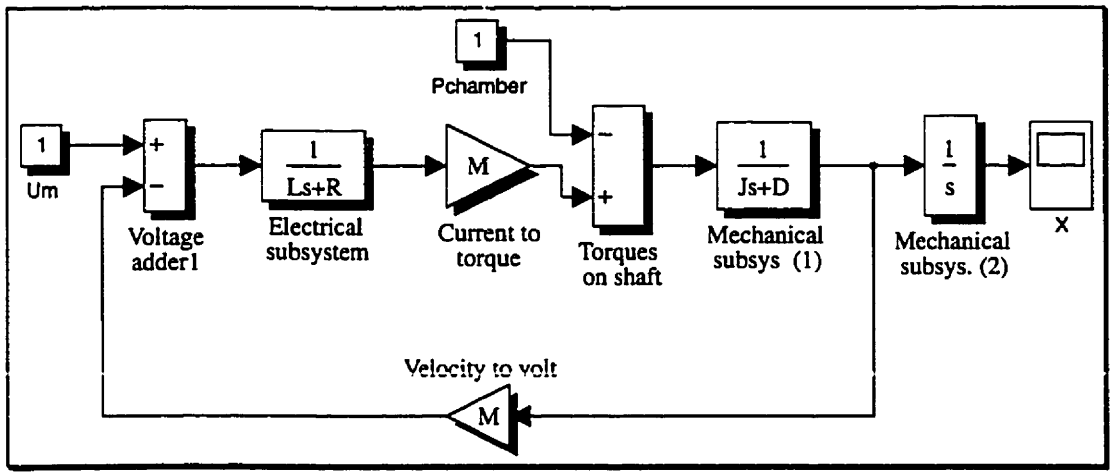

Figure 6-2: Block diagram of the linear plant

6.2.1.1 Parameter values

Since there was no data available for the motor, the parameter values were determined experimentally. The results are given in Table 6-1. To measure *M* the motor was connected to a DC power-supply. Known torque-loads were applied to the shaft and resulting motor current was measured. *M* was calculated by dividing the torque by the current. A digital voltmeter was used to measure *R* across the armature. *L* was determined by measuring the impedance of the winding while keeping the rotor stationary. All masses were measured using an electronic weighing scale. Dynamic friction was computed by evaluating the difference between the total motor torque (*Mi* for a given current) and the net torque produced at the shaft. For additional information see (Electro-Craft 1980).

Table 6-1: Parameter Values

Parameter	Measured value	Unit
Inductance *L*	14.3×10^{-3}	H
Resistance *R*	6.3	Ω
Moving mass	0.502	Kg
Motor constant *M*	14	N/A
Dynamic friction	0.65	Kg/s
Vane area	17.8×10^{3}	mm^2

6.2.2. Dynamic analysis of the plant

To analyze the dynamics of the plant, the roots of its characteristic polynomial (i.e. poles) must be computed. These are given by the common denominator in Equation 6.5. The plant has 3 poles, one at zero and the other two at:

$$\lambda_{2/3} = \frac{1}{2}\left[\left(\frac{D}{J}+\frac{R}{L}\right) \pm \sqrt{\left(\frac{D}{J}+\frac{R}{L}\right)^2 - 4\left(\frac{D}{J}\frac{R}{L} - \frac{M^2}{JL}\right)}\right] \tag{6.6}$$

Substituting for the measured parameters R, L, M, J and D in Equation 6.6, the poles are found to be

$$\begin{aligned} \lambda_3 &= -1187 - j4137.95 \; s^{-1} \\ \lambda_2 &= -1187 + j4137.95 \; s^{-1} \\ \lambda_1 &= \pm 0 \; s^{-1} \end{aligned} \tag{6.7}$$

These three poles influence the dynamics of the motor. λ_1 represents the integration relation between velocity and position and is parameter invariant. The influence of λ_2 and λ_3 become significant when frequencies approach 685 Hz, but this far exceeds the range of interest of the RVV. Furthermore, the nonlinear limitations of the system will attenuate its response to the point that these poles will never have any influence.

To gain insight into the system behavior in general, a sensitivity index α, of the form described by Equation 6.8, was computed to compare the changes of the position of the poles to the changes of R, L, M and moving mass (m). It was established that the most sensitive plant parameters were R and m, both of which were measured very precisely.

$$\alpha_p = \frac{\frac{\delta\lambda_n}{\lambda_n}}{\frac{\delta_p}{p}} = \frac{p}{\lambda_n}\frac{\delta\lambda_n}{\delta_p} \tag{6.8}$$

p and λ in Equation 6.8 represent parameter and pole of the plant, respectively. In this case, the dominant pole at zero governs the dynamics of the linear motor. This signifies that the plant has integral behavior. Since, the only variable to be measured is 6 the need for more elaborate modeling and control of the system in state space is not necessary. Due to the simplicity of the system, using feedback control in the Laplace domain is satisfactory.

6.2.3. PID controllers

When it comes to linear systems with a single feedback loop (as opposed to a state space controller with multiple feedback loops), the following three types of controllers are commonly used

- Proportional-derivative (PD) control
- Proportional-integrative (PI) control
- Proportional-integrative-derivative (PID) control

Their corresponding mathematical representations in the Laplace domain are given by:

$$F_{PD}(s) = G_c\frac{1+T_n s}{1+T_d s} \tag{6.9}$$

$$F_{PI}(s) = G_c\frac{1+T_n s}{s} \tag{6.10}$$

$$F_{PID}(s) = G_c\frac{(1+T_{n1}s)(1+T_{n2}s)}{s(1+T_d s)} \tag{6.11}$$

where G_c is the controller gain. T_n and T_d denote numerator and denominator time-constants respectively. It is worth noting that the parameters of the (*PD*) and (*PID*) controllers given above, are specifically for practical implementation since they include denominator time-constants (T_d) to cushion the problems introduced by noise passing through the derivative block.

6.2.4. Controller design

6.2.4.1 Open loop analysis

The open loop transfer function (F_{open}) consists of controller, power amplifier, and position sensing device (RVDT), all connected in series without closing the feedback loop as indicted in Figure 6-3. To optimize the controller parameters an appropriate software package (e.g., *Matlab*, The MathWorks Inc., Natick MA) was used. It permits the use of interactive graphical methods such as Bode plots and the root locus to obtain more details and insights about the system dynamics very quickly. Bode plots give the amplitude and phase of the system for all frequencies and a given set of parameters. The root locus, on the other hand, gives the trace of the positions of the poles of the closed loop system as the controller gain is varied from zero (i.e. open loop) to infinity. The control model used in linear feedback closed loop simulations of the plant is shown in Figure 6-4.

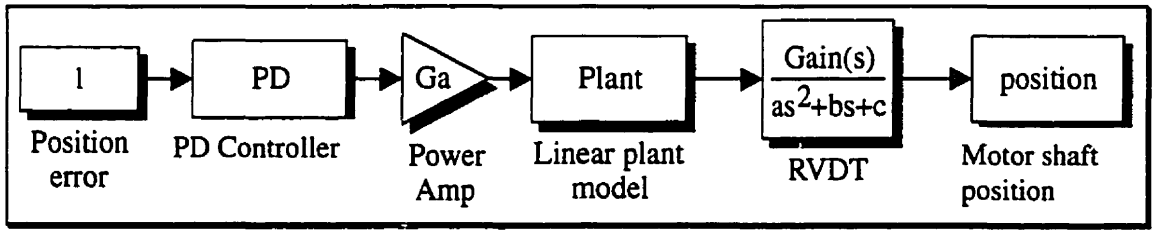

Figure 6-3: Open loop transfer function

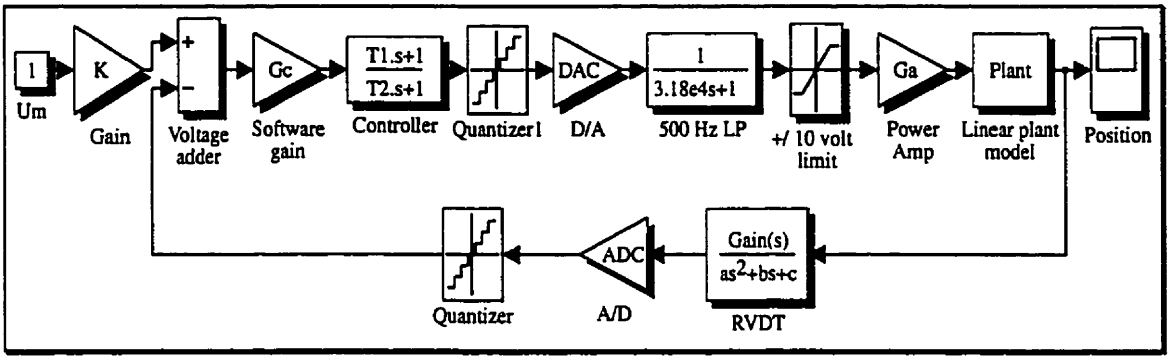

Figure 6-4: Control model used in linear feedback closed loop simulations

Figure 6-5, the root locus, shows the location of all the poles (denoted by "×") of the open loop plant. Note the existence of the dominating pole at zero due to $\lambda_1 = \pm 0$ as computed by Equation 6.7. The frequency response (Bode plot) of the plant is shown in Figure 6-6, and indicates an integrative behavior as the output signal attenuates at a rate of 20 dB/decade.

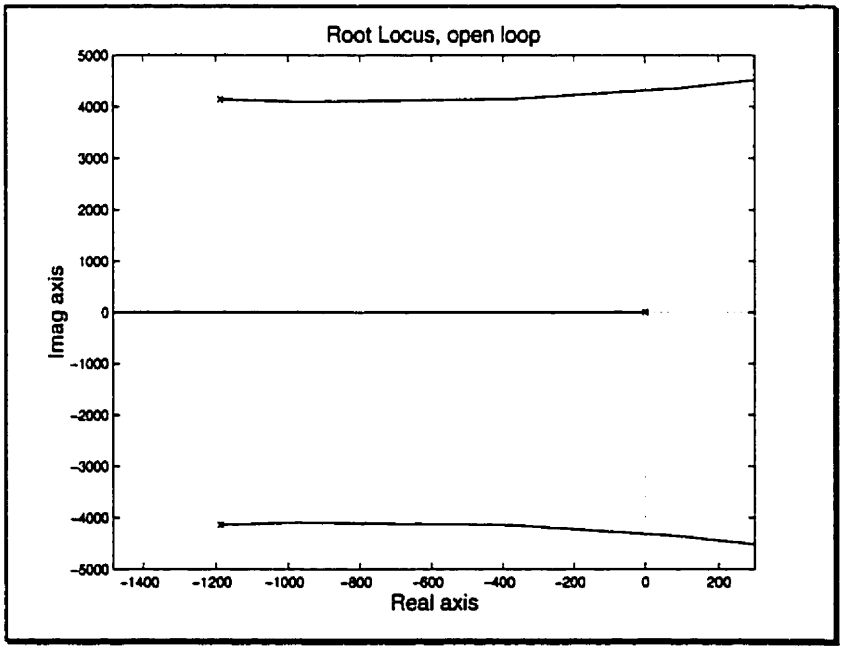

Figure 6-5: Plant open loop root locus

However, if the plant input-output signals are compared and their difference fed to a unity gain controller, we obtain the plant performance under closed loop feedback control. Figure 6-7 and Figure 6-8 show the root locus and frequency response of the

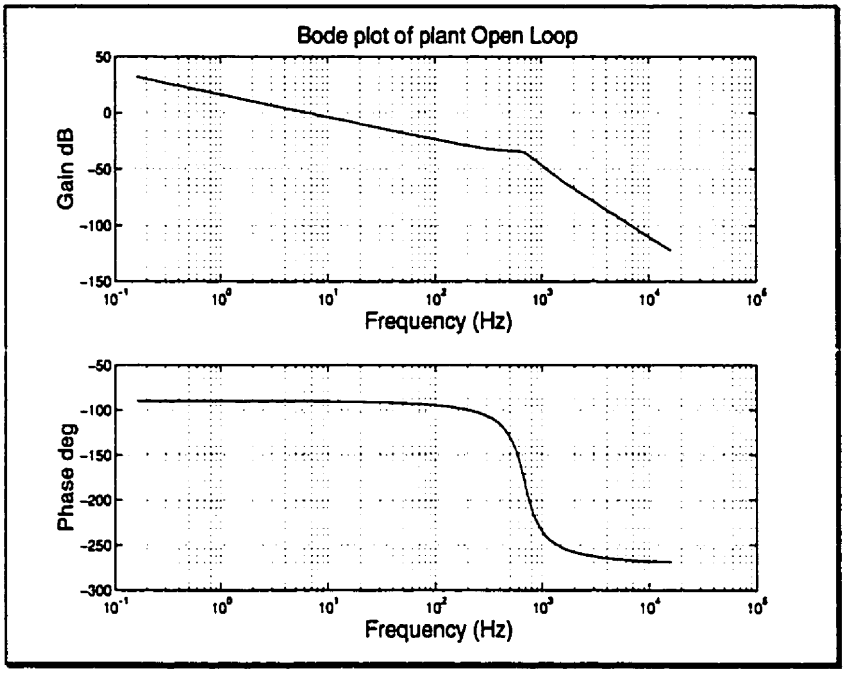

Figure 6-6: Plant open loop frequency response

system, respectively. It can be seen that closed loop control immediately improves the plant behavior by moving the dominant pole further to the left on the real axis. In particular, a marked improvement in system bandwidth is observed

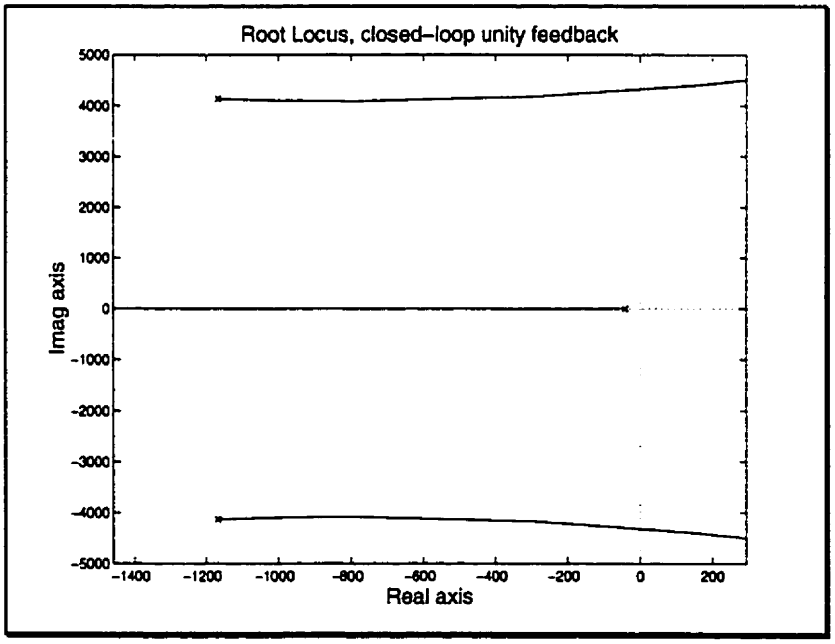

Figure 6-7: Bode plot, closed loop unity gain feedback

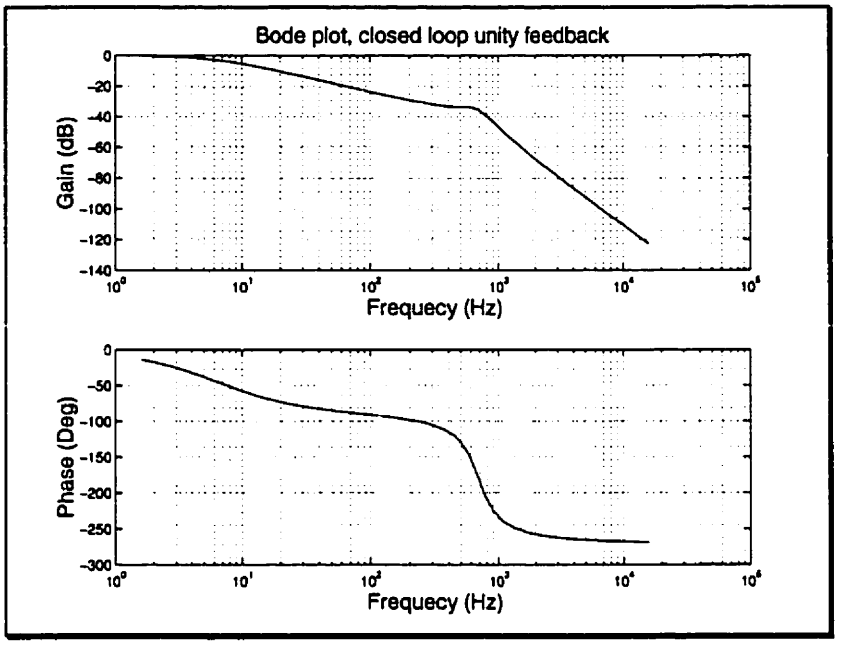

Figure 6-8: Root locus, closed loop unity gain feedback

6.2.5. Proportional-Derivative compensation

The controller should compensate for the effects of poles at zero and other dominant poles in F_{open}. To eliminate the steady state error, integration is desirable, i.e. a pole at zero. On the other hand, to increase the bandwidth of the plant with the dominant pole, a controller whose gain increases with frequency at frequencies above the pole must be used. This can be achieved using derivative control. Proportional control does not guarantee zero steady state error, and can introduce oscillations (overshoots) whose elimination is made at the cost of bandwidth reduction. However, since the plant in case already has a pole at zero, a *PD* controller is preferred. It must be noted that the power amplifier and position sensor have flat frequency responses to 80 kHz and 500 Hz, respectively, and so they do not introduce any additional dominant poles. Hence, only the single dominant pole of F_{open} must be compensated for Ideal *PD* and *PID* controllers are problematic because they amplify noise through derivative action. Therefore practical implementations of these controllers usually have an additional small denominator time-constant that cushions noise effects. In effect, real *PD* controllers shift poles further to

the left of the complex plane rather than canceling them. Consequently, a real *PD* controller of the following form was chosen:

$$F_{PD}(s) = G_c \frac{(1+T_1 s)}{(1+T_2 s)} \tag{6.12}$$

It gives an open loop transfer function with a single pole at zero and compensates for the non-zero pole of the plant. G_c is the controller gain, T_1 and T_2 are derivative and smoothing time-constants, respectively. This controller introduces a pole at $1/T_2$ and a zero at $1/T_1$ to the system. The degree of smoothing is a function of magnitude of T_2. However, after compensation the pole at $1/T_2$ is likely to be the dominant pole of the system, therefore a trade-off between smoothing and bandwidth should be considered.

6.2.5.1 Choice of controller parameters

In theory compensation of the plant dominant pole should be fairly easy once the plant has been modeled successfully and accurately. By simply selecting an appropriate derivative or zero time constant the dominant pole can be compensated for. In practice, the task is more difficult since model parameters are only known within a certain tolerance. Consequently, it is not possible to place the zero exactly at the pole, but only close to the point where it is expected to be. This discrepancy can yield a very different root locus and system behavior. The RVV controller parameters were chosen to yield a system bandwidth of at least 10 Hz and a fast step response with no overshoot. On this basis, the controller was determined to be

$$F_{controller} = 2.5\frac{1+0.15s}{1+0.08s}. \tag{6.13}$$

Figures 6-9 to 6-11 show the root locus, frequency response, and step response of the closed-loop compensated plant, respectively. As Figure 6-10 shows, the *PD* controller has

improved the plant bandwidth considerably, and the step response is also fast and has no overshoots or oscillations (Figure 6-11).

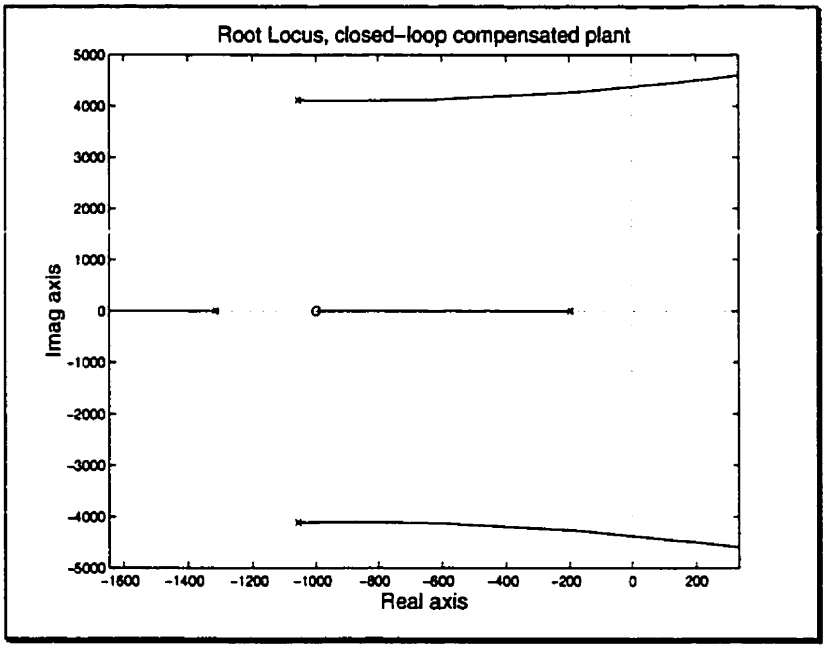

Figure 6-9: Root locus closed loop compensated plant, PD controller

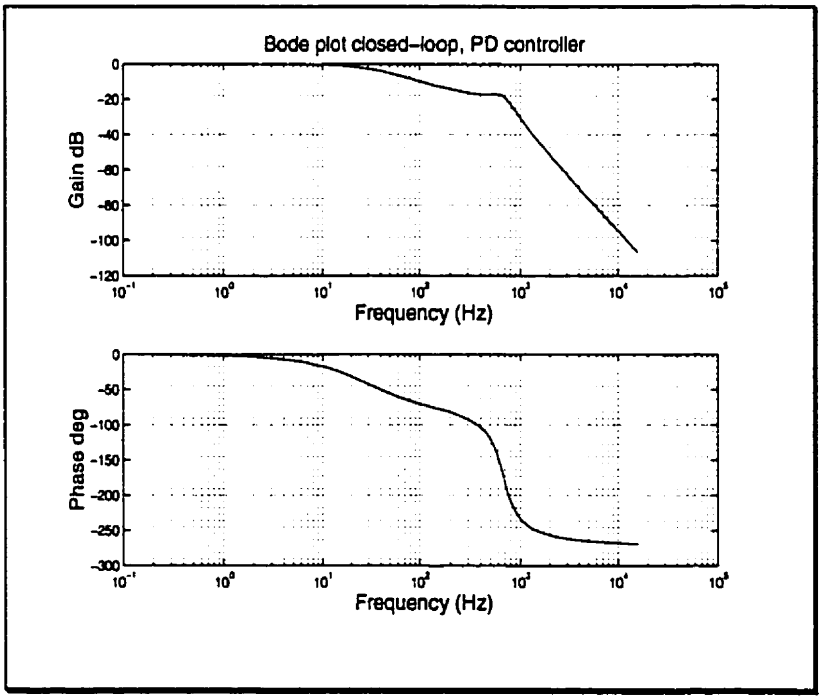

Figure 6-10: Bode plot, closed loop feedback, PD controller

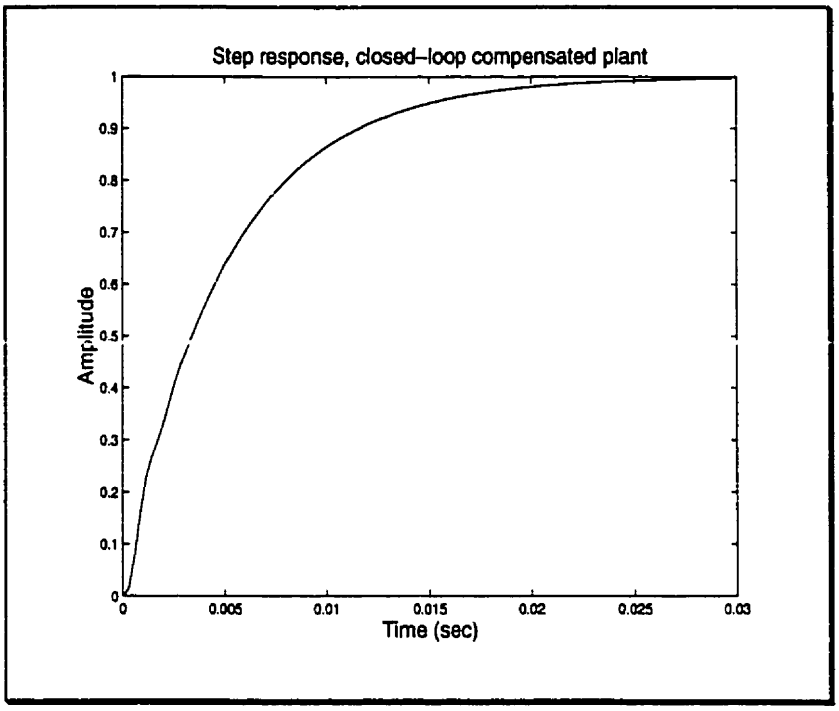

Figure 6-11: Closed loop, step response, PD controller

6.2.5.2 Operation under load

Under the circumstances considered so far, the integrator in the open loop will give zero static error for a step input. However, this is not the case when a subject is attached to the ventilator. Air compression inside the chamber also adds to the sum of forces before the integrator (see Figure 6-2) thus, the system can only be in steady state if there is no input to the integrator, that is, when the velocity signal $\dot{x}$ is zero. For the steady state situation, rewrite the plant model of Equation 6.5 as

$$-\frac{AR}{DR+C^2}P_{chamber}+G_cG_a\frac{C}{DR+C^2}e=0, \tag{6.14}$$

where e is the error and G_a and G_c are the amplifier and controller gains, respectively. The above holds true for $P_{chamber}\neq 0$ if $e\neq 0$. What this means is that pressurizing the

chamber leads to a static error. Note that the amplitude of the error is inversely proportional to the controller gain G_c.

To compensate for a load disturbance of this nature, a second control loop can be employed that compensates only for the impact of the disturbance. Figure 6-12 shows how one such controller can be implemented. In Figure 6-12 F_{dc}, the transfer function, should ideally be designed so that $F_{dc}F_1 = -1$ or

$$F_{dc} = -F_1^{-1} \tag{6.15}$$

However, it is important to verify if the effect of pressurization of the chamber will produce any significant error before implementing the additional controller discussed above. Moreover, the inversion of F_1 will usually include differentiation that is noise sensitive and should be avoided where possible. The maximum pressure envisaged for the chamber is approximately 3 kPa (30 cmH_2O). The force exerted on the vane shaft by a chamber pressure of 3 kPa is well below that of any dry friction force (≈ 0.89 N), and the error in the vane position is negligible. It was therefore decided not to implement the disturbance compensation as described by Equation 6.15

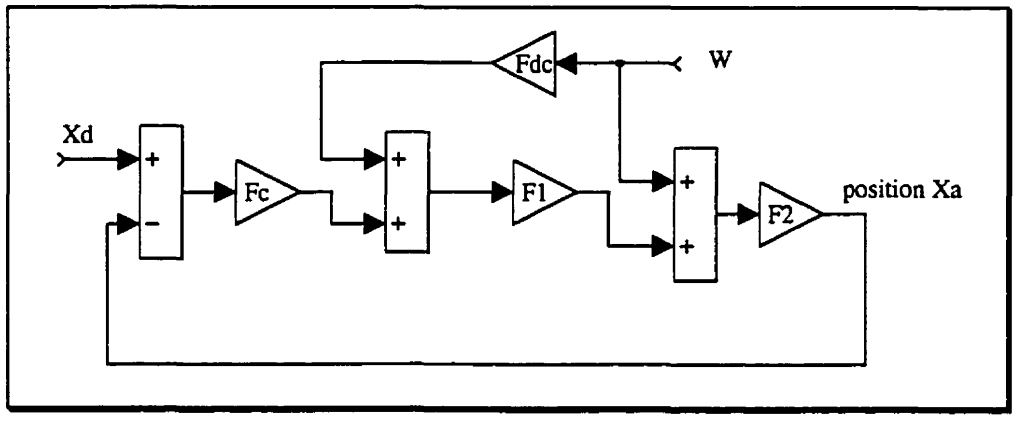

Figure 6-12: Disturbance compensation

6.3 The Nonlinear plant

6.3.1. Nonlinearities

Nonlinearities are significant and alter the system response; hence, they can not be neglected. Dry friction effects the motor response and may increase the steady state error

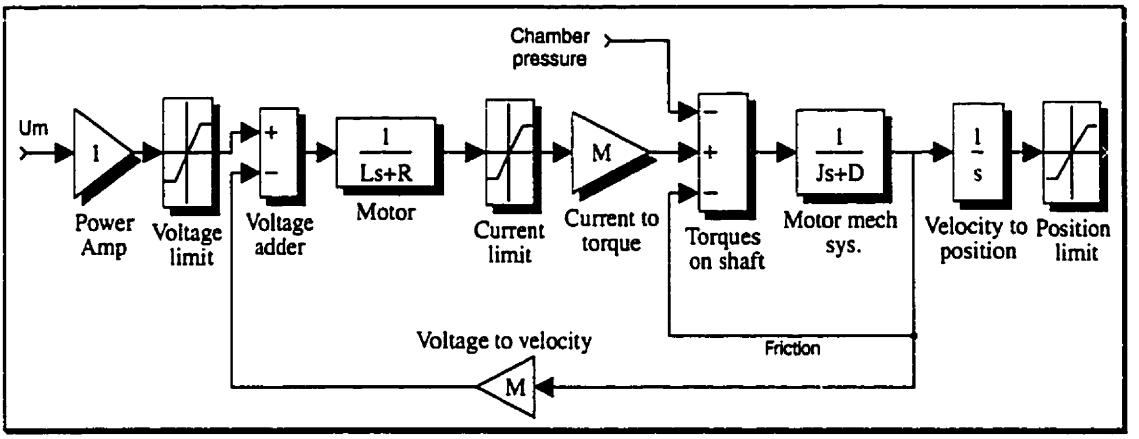

Figure 6-13: Model of the plant and the power amplifier

by acting on the input of the integrator. In order to include the effects of friction in the nonlinear simulation, Equation 6.16 was implemented in a *Matlab* function block:

$$F_{applied} = F_{sum} - F_{dyn} \qquad \left|\dot{x}\right| > \varepsilon$$

and (6.16)

$$F_{applied} = F_{sum} - \min(F_{sum}, F_{stat}) \qquad \left|\dot{x}\right| \le \varepsilon$$

$F_{applied}$ is the net force applied on the motor shaft that includes the effects of dry friction. F_{sum} is the sum of the forces before friction is accounted for, F_{dyn} and F_{stat} are the dynamic and static friction forces, respectively and ε is a small threshold of velocity (Figure 6-13). The friction forces were measured by using a torquemeter and found to be

1.3 N for the static and 0.98 N for the dynamic case with slight variations depending on the position of the vane.

Mechanical hard limits of the vane are another obvious nonlinearity present in the system. Also the power amplifier can only provide output voltages up to a few volts below its supply voltage. Higher inputs will yield a clipped output signal. Current limiting is used to prevent destruction of the semiconductor through power dissipation. Both the current and voltage limitation were taken into account in the model of the plant shown in Figure 6-14. However, a *PD* controller can saturate the amplifier very quickly due to amplification of sudden output errors by its derivative term. It was therefore expected that the T_d would have to be reduced to optimize the PD controller for the nonlinear plant. Also, in the presence of dry friction the step response tends to be dampened and have less overshoot. This means that the gain of the controller has to be increased. A full model of the control system consists of hardware, (A/D, D/A, smoothing filter, power amplifier, plant and RVDT) and software (controller and adder) as shown Figure 6-14. Quantizations are due to A/D and D/A converters. The amplifier voltage and A/D limits exceed the ranges of their respective inputs and therefore do not need any voltage limiting. The results of the closed loop nonlinear simulations indicated a marked drop in the bandwidth compared with that of the linear plant. However in the case of the nonlinear plant, the closed loop performance using the lead-lag compensator was superior to the simple proportional controller. Since compensating for the plant nonlinearities can

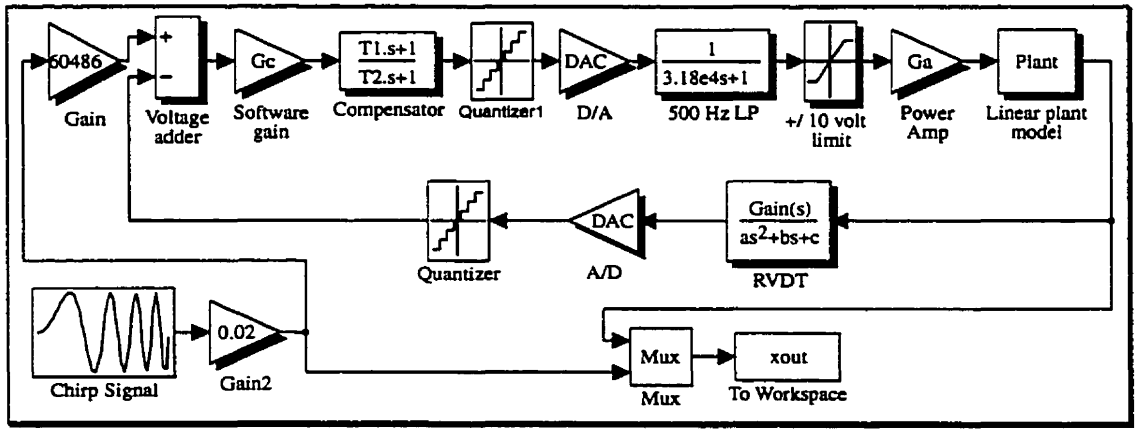

Figure 6-14: Full model of control system used in simulations

be a difficult task, the performance of the *PD*-controller was evaluated to establish if any further efforts were needed to modify its characteristics.

Figure 6-15 illustrates the system response to a chirp signal of 1-100 Hz sampled at 400 Hz with an amplitude of 0.5×10^{-2} (note only a portion of the signal is shown). Although, the controller at this stage was not fully tuned, system output follows the input signal reasonably well with slight discrepancies in amplitudes. The parameters chosen for the controller based on linear theory proved to be a suitable starting point for the final optimization that was carried out on the real system.

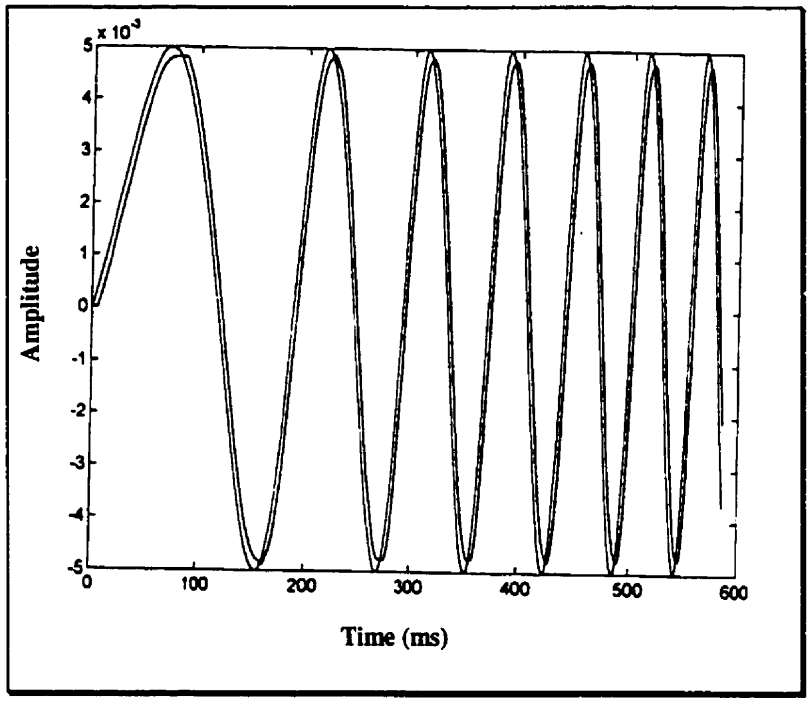

Figure 6-15: System response to a chirp input signal

6.4 Discrete realization

To be able to implement the continuous time control algorithms thus far developed in the software, it must be transformed into a discrete time formulation. Since the sampling rate of 1 kHz is much greater than the system bandwidth, a simple discrete realization of the continuous time controller of Equation 6.13 yields satisfactory results

and therefore there is no need for controller design in the Z-domain. Equation 6.9 for the PD algorithm can be written as

$$(1+T_d s)U_c = G_c(1+T_n s)e \tag{6.14}$$

where U_c is the controller output and e is the error signal. The above equation transformed into the time domain gives

$$U_c + T_d \frac{dU_c}{dt} = G_c\left(e + T_n \frac{d_e}{d_t}\right) \tag{6.15}$$

If the derivative term is now replaced by a finite difference we obtain

$$U_{c,k} + T_d \frac{U_{c,k} - U_{C,k-1}}{T_s} = G_c\left(e_k + T_n \frac{e_k - e_{k-1}}{T_s}\right) \tag{6.16}$$

where $e_k = e(kT_s)$, T_s is the sampling interval and G_c is the controller gain. Equation 6.16 can be rearranged to give the recursive PD-controller in discrete time form, thus

$$U_{c,k} = \frac{G_c(T_s + T_n)}{T_s + T_d} e_k - \frac{G_c T_n}{T_s + T_d} e_{k-1} + \frac{T_d}{T_s + T_d} U_{c,k-1} \tag{6.17}$$

In the z-domain this controller is described by

$$U_c(z) = G_c \frac{(T_s + T_n)z - T_n}{T_s + T_d)z - T_d} e(z) \tag{6.18}$$

The above controller was implemented in software in 32-bit fixed-point arithmetic. The most significant 24 bits are used for the integral part, while the last eight least significant bits are for the decimal part. Since the controller output is reduced to 12-bit format for D/A conversion, a precision of $2^{-8}=3.9\times10^{-3}$ for the decimal part would give satisfactory results.

6.5 Implementing and tuning the controller

Having designed and simulated the controller we are now finally in a position to implement and tune it in the RVV. Recall that the design objectives are to achieve a bandwidth of at least 10 Hz and a fast step response with minimal overshoot. This level of performance must be achieved under worst-case operating conditions, namely when the RVV is subjected to maximum load. Hence tuning was performed with the outlet valve closed The frequency response was determined by a stochastic technique using white noise to excite the RVV. Figure 6-16 shows an example of the input signal and the resulting system response. Figure 6-17 shows the amplitude content (probability density function) and frequency content (power spectrum) characteristics of said signals. The

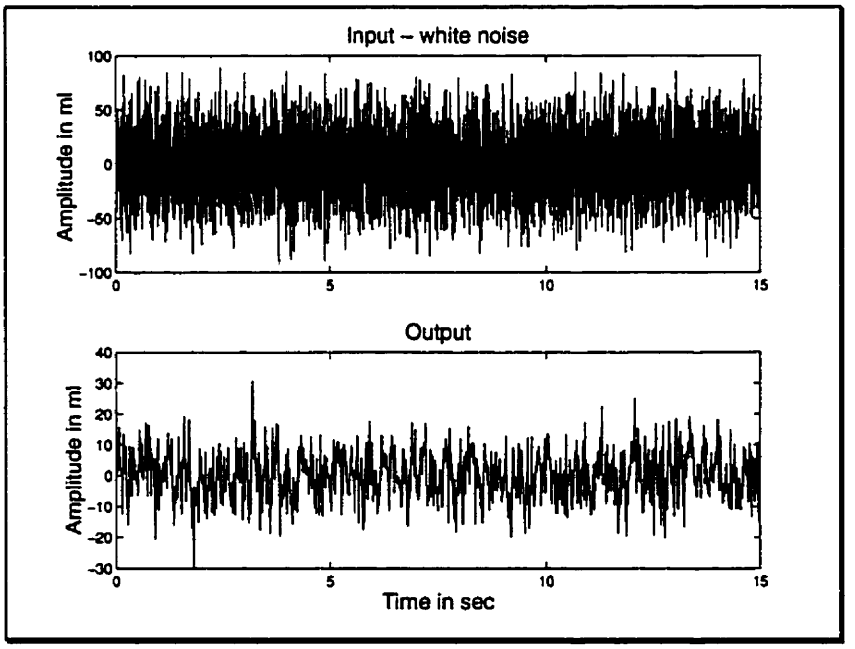

Figure 6-16: Example of Input -output signals, loaded ventilator

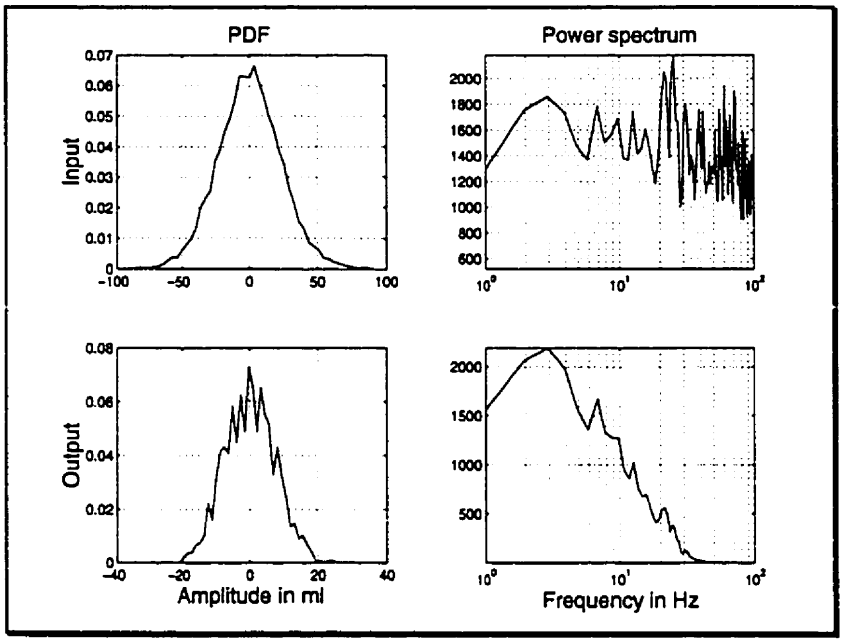

Figure 6-17: Amplitude and frequency content of input-output signals, loaded ventilator

total air volume of the RVV pressure chamber is 3.0L of which the displaceable air under the vane control is 1.363L. The vane position sensor (RVDT) has a linear span of ± 40 degrees, so that 1 ml gives a 5.8×10^{-2} degree amplitude.

Figure 6-18 gives the frequency response of the plant when subjected to the input signal of Figure 6-16. The optimization of the response was based on the nonlinear plant and the actions anticipated in section 6.3.1. The parameters of the controllers were adjusted so that a flat bandwidth up to the –3 dB point at 17 Hz for a perturbation amplitude of about 140 *ml* was obtained. For higher amplitudes, the limitations of the power amplifier through voltage limiting will affect the response, of course. Note that the coherence squared function (Figure 6-18) between the input and output indicates that the system is essentially linear up to a frequency of about 50 Hz. The near-unity coherence indicates the presence of noise and/or slight nonlinearity. Furthermore, the step response of the system for various step amplitudes showed no overshoot and the measured static error never exceeded 0.5% of the step amplitude. Finally, the controller values of Equation 6.19 were implemented. As anticipated, when compared to the optimized

system under linear conditions an increase in gain and a decrease in time constants was observed.

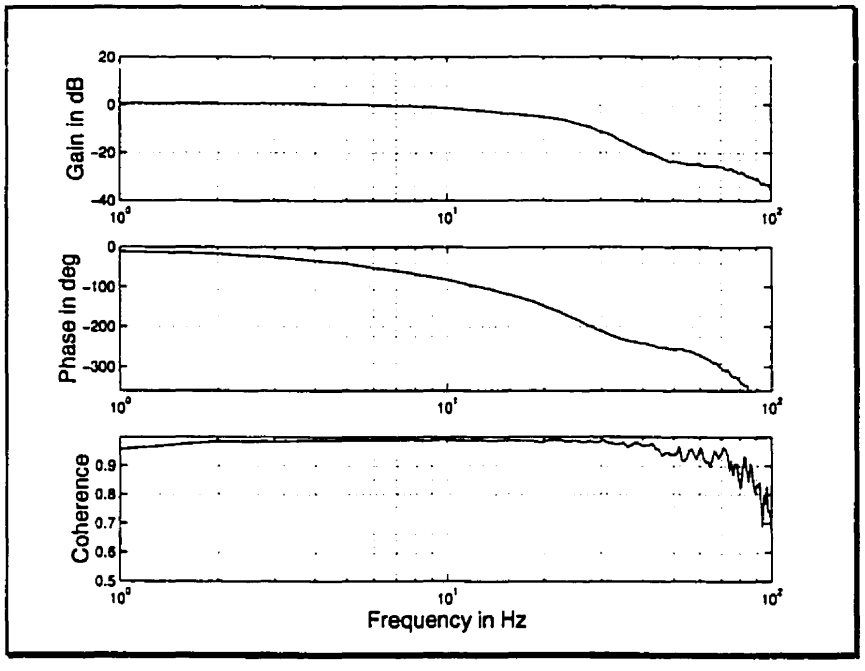

Figure 6-18: Frequency response gain and phase margin, coherence squared function, loaded ventilator

$$G_c = 6.8 \quad \text{(Controller gain)}$$
$$T_1 = 0.1 \text{ ms} \quad \text{(Integrator time constant)} \qquad (6.19)$$
$$T_2 = 0.01 \text{ ms} \quad \text{(Differentiator time constant)}$$

The variance of a signal is a measure of how much the signal differs from its mean value. The percentage variance-accounted-for (%VAF) is a convenient measure of the similarity between two signals. It is based on the ratio of the variance of the residuals ($Y_{experimental} - Y_{reference}$) to the variance of the reference signal, i.e.,

$$\%VAF = 100\left[1 - \frac{\sum_{1}^{n}(Y_{experimental} - Y_{reference})^2}{\sum_{1}^{n}(Y_{reference}{}^2)}\right] \tag{6.20}$$

where n is the number of data points. A perfect match between signals yields a %VAF of 100.

Figure 6-19 gives the impulse response function (IRF) of the system. In this case %VAF can be used to validate the controller performance. $Y_{reference}$ is taken to be the measured system output while $Y_{experimental}$ is the output predicted using the estimated IRF. A %VAF value of less than 100 could be attributed to the presence of noise or an inadequate model. The %VAF between the measured system output and the predicted output, based on the identified IRF, is 98.3 indicating an essentially noise free, linear system.

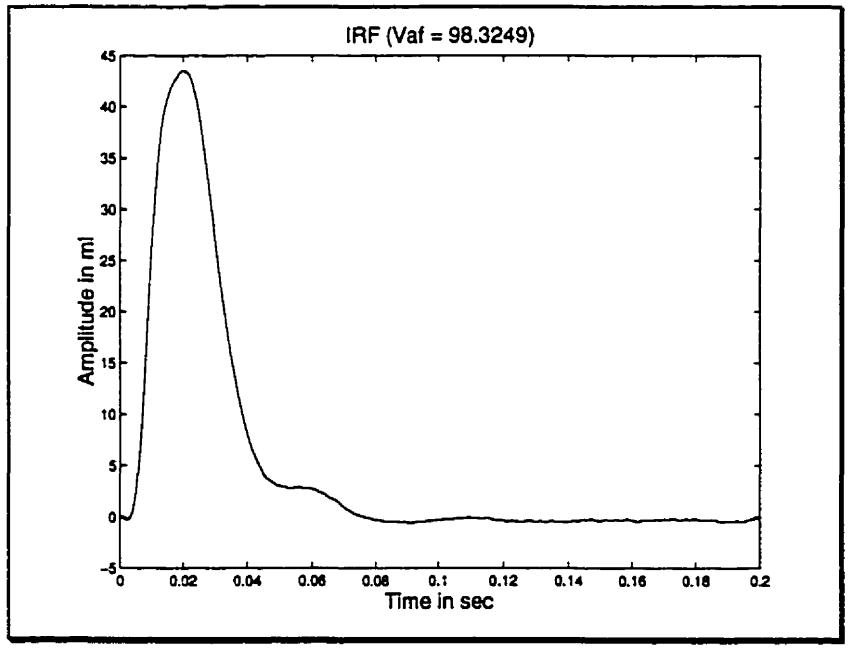

Figure 6-19: Impulse response function of the loaded ventilator

6.6 Closing remarks

This chapter covered the RVV dynamic analysis in open loop and obtained the plant model. Using the model based on linear system control theory, a *PD* controller was designed and tested. Nonlinearities of the system were then considered. The controller was implemented and optimization was performed. Finally, controller performance was evaluated.

The next chapter focuses on the software code that drives the RVV. First an overview of the program is given and some of the features that have been developed will be discussed. The choices for programming language, hardware and operating system requirements are explained next. The Menu System and the concept of user interaction through dialog boxes developed for this work are then introduced. Some of the functions which are directly involved in control and data acquisition are discussed in detail. The concept of the hardware interrupt service routine used in the control of the RVV and the method for data storage are also covered.

7

RVV: Software Design

This chapter describes the computer program that operates the RVV. It starts off by giving an overview of the software and its main features. Among other things, it addresses the issues of hardware requirements, choice of programming language and calibration of the pressure sensors. The chapter then focuses on real time control, acquisition and storage of data.

7.1.1. Overview

The RVV program is based on a menu system whose main items can have up to 15 selections, displayed as a drop down list when the main item is selected. *Hot key* combinations, using characters, function keys, and the *ALT SHIFT*, and *CTRL* keys can be assigned to main menu items or sub menu options that designate an action. The menu system is also easily managed and driven by a mouse. The function responsible for driving the RVV and data acquisition does certain tasks. It must attend to feedback position control of the vane at precise time intervals, at all times, since this is responsible for the ventilation of the subject. In other words the RVV control algorithm must have priority over all other computing jobs. Furthermore, valve configurations for opening and

closing sequences together with data acquisition must also be precisely timed. A technique based on the hardware interrupt concept has been utilized to realize the above requirements robustly. In this method, the precision timing of an event is achieved using a procedure called an Interrupt Service Routine (ISR). This routine is called upon every time a hardware interrupt (i.e. interrupt 0) is issued. Since it has priority over all other interrupts, the processor immediately responds to this call and executes the contents of the ISR. Precision timing of the ISR is based on a hardware signal derived from the timer chip on the computer motherboard, which is the source of timing references for the operating system. This concept will be discussed in detail in the coming sections.

V_t, F_r and I/E for the ventilation waveform signal are configurable in a controlled and easy fashion. The program is also capable of saving the experimental data in a standard format. The design of the code is based on a modular approach and attempts have been made to maintain easy flow and readability of the code. Almost every task is defined within a self-contained function for clarity and easy debugging purposes. The number of Global Variables is kept to minimum and care has been taken to keep the variables Local where possible.

Figure 7-1 shows the program's GUI at start-up. The graphics board is configured and the menu is drawn. The A/D and D/A boards are then re-set. However, prior to this, the valves are configured to safe mode and the vane is positioned to mid range before D/A inputs are disconnected from the power amplifier through a computer-controlled relay switch. The program runs the menu in graphics mode permanently (see 7.2.2).

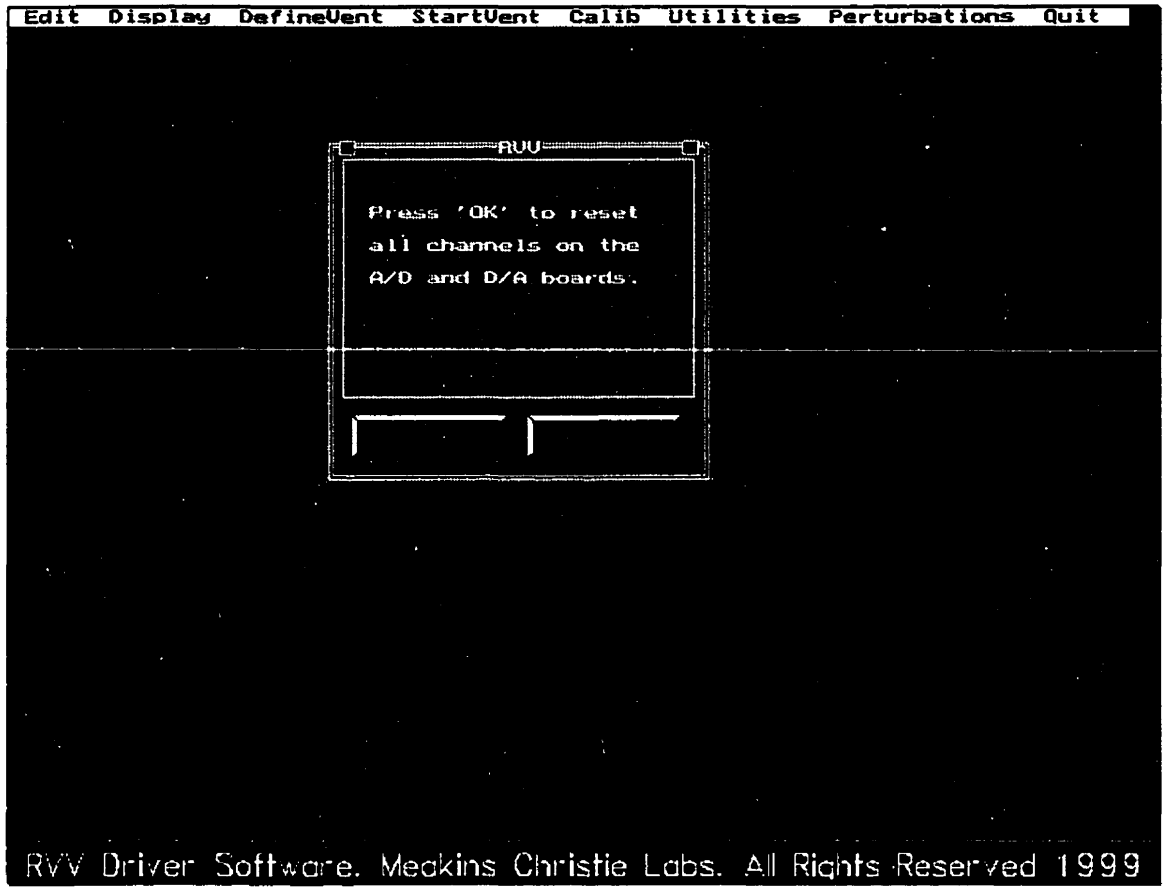

Figure 7-1: RVV main graphic user interface at the start up

Figure 7-2 gives a very simple overview of the structure of the code. The program starts off with a series of initializations of parameters including those of the menu, servo position controller, interrupt service routine and the settings for ventilation. The main program function initializes the graphics adapter and the mouse. It then creates and draws the menu and status bar, and resets all the hardware including the A/D channels and all the I/O lines on the D/A board. The program then checks for menu events and processes them as they are acknowledged. However, a built in mechanism makes sure that, with the exception of designated hot keys for the main menu items and the F10 function key, all other non destructive reads from the keyboard buffer are removed. The user is always asked for a hardware initialization before functions become available.

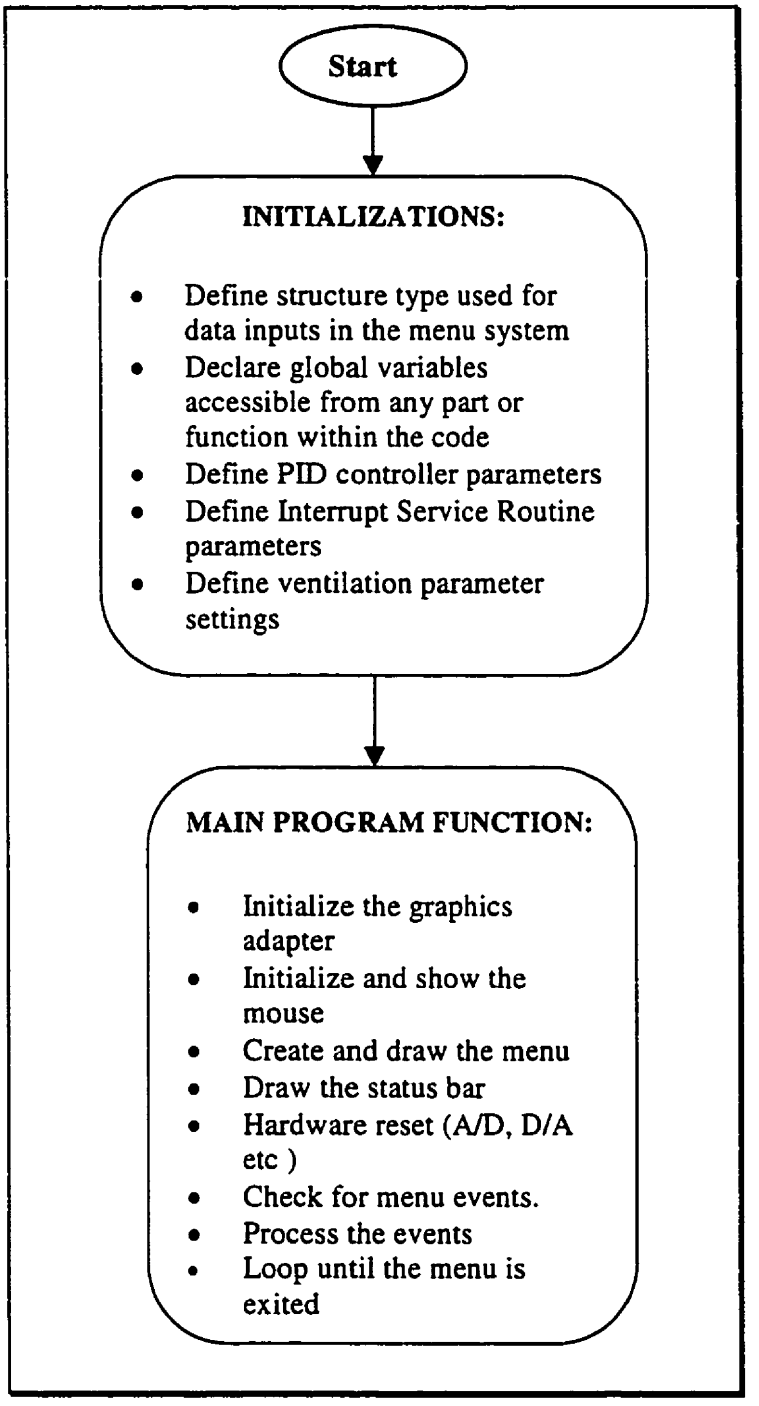

Figure 7-2: RVV simplified main program flow-chart

7.1.2. User interaction

An important aspect of the software design is the provision of easy and intuitive mechanisms for user interaction. The user can interact with the program at various levels and stages. This mainly takes place through specific dialog boxes where inputs (i.e. data fields) are automatically boundary and type checked to avoid stalling of the operating system. This also makes sure that unsafe parameter values are rejected. Figure 7-3 shows one such dialog box where parameters for the ventilation volume waveform are configured. Editing of the fields is achieved with a mouse and or some designated hot keys.

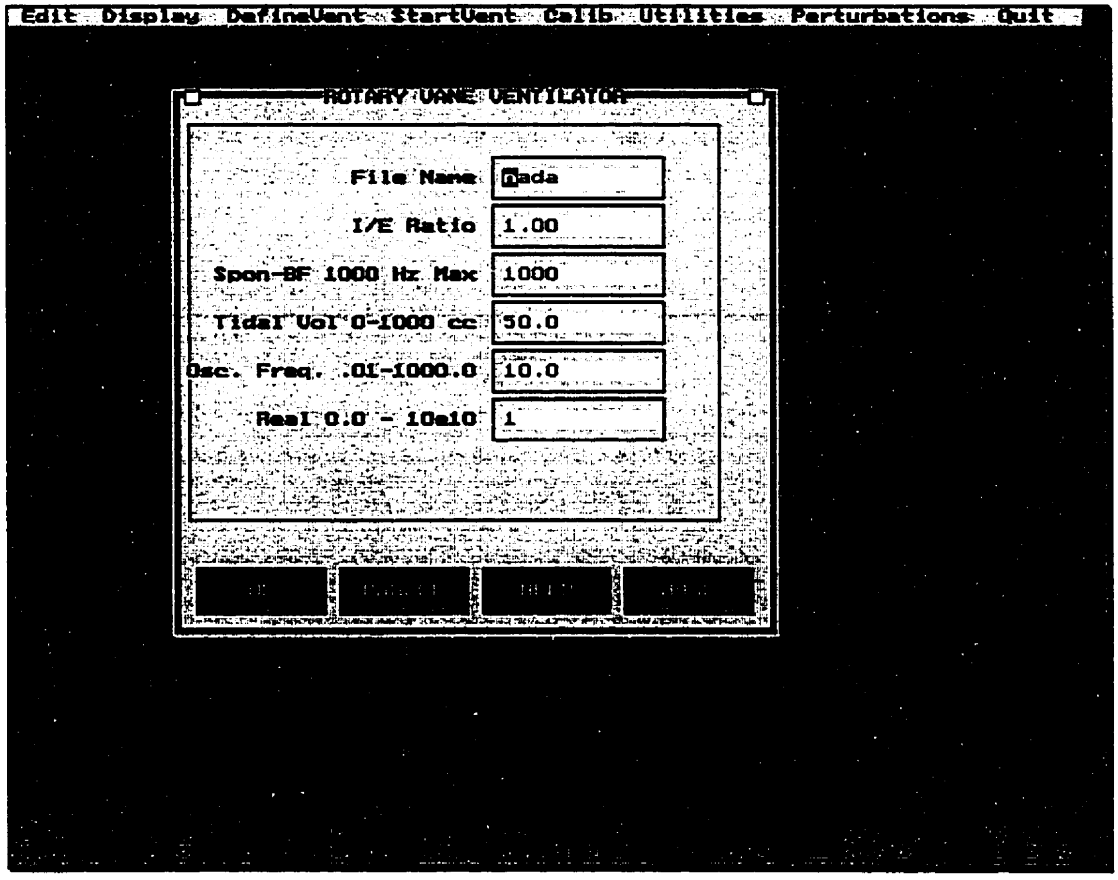

Figure 7-3: An example of program interaction dialog box where user defines ventilation parameters

7.1.3. Programming language and operating system

The programming language used to write the software was C/C++, and the development environment was *Turbo C* (TC) version 3.2 of *Borland International Inc.*, Scots Valley CA. C/C++ is a high-level programming language. In part it resembles other procedural languages, such as Pascal, Basic, Fortran and Ada. When using a procedural language, one writes explicit directions for a computer about the steps it is to perform. The programmer must understand the meaning of the data, the steps being performed, and the results. A high-level language frees the programmer from having to determine the locations of data in main storage. These details are provided by a compiler, which translates a program from source code in the high-level language to machine instructions. The C language is relatively simple and orderly with a distinctive appearance. For some types of work, it has substantial advantages over other languages. C compilers can be made to run on small computers. The language is also designed so that the compiler can translate the high-level code into efficient machine instructions. It is system independent and requires no operating system services. It also provides flexible data structures and a wealth of detailed data manipulations. These characteristics have made C attractive for microcomputers and for applications such as user interfaces, communications, control systems, operating systems, computer-aided design and so on.

For IBM compatible personal computers, there are two window operating systems available, *Microsoft Windows*, and *OS/2*. They offer the advantages of multitasking and unlimited memory accesses. *Disk Operating System* (DOS), on the other hand, limits the use of memory to 640 Kbytes with the biggest individual data structure not exceeding 64 Kb. The former type is designed for multitasking applications where the emphasis is on sharing of computer resources rather than direct hardware access and control. Real time applications, on the other hand, are more easily programmed in DOS. The RVV needs fast control of certain parameters at the hardware level, and the timing of some events has to be precise. DOS was therefore chosen to be the operating system for the RVV. However, certain characteristics of window based programs, such as a GUI and intuitive operations, have also been incorporated for easy use of the software.

7.1.4. Hardware requirements

To make the ventilator compact and portable, it was decided to implement the software on a 90 MHz Pentium IBM compatible Laptop computer. PCMCIA technology A/D and D/A boards of type 2 for data acquisition and control are used. Data collection and data output to the controller is possible simultaneously, and although the A/D board has no direct memory access (DMA) controller facility for storage of acquired data without engagement of the CPU, fast data acquisition and storage is still possible. A PC type mouse facilitates convenient operation of the program. The RVV uses a single supply cable for connection to the mains for all its power requirements.

7.2 Realization

7.2.1. Main Program

The design of the code is modular. The actual main program is short and on loading it declares and defines a series of global variables that hold their scope throughout the main program function. They are accessible from anywhere within the code. Their numbers are kept to a minimum to save memory since they remain resident for the duration of the main function. The following is a list of various components whose relevant variables are declared as global:

- Real time graphics and displays
- User input dialog box fields and initialization values
- Menu structure type
- Data acquisition (A/D, D/A boards)
- PID Controller
- The Interrupt Service Routine (ISR)

Once the declaration of the variables is done, the graphics adapter is initialized, the mouse is initialized and appears on the screen, and a menu is drawn. The status bar at the bottom of the screen appears next. At this stage the user is asked if a hardware reset is required. Upon positive response to this request the output on D/A channel 1 is reset to

zero and all input output lines (I/Os) that control the valves are also grounded. The A/D is reset and the data on the operational display panel are updated. The program now enters a Do Loop which captures all mouse and keyboard events and passes them to appropriate processing functions for execution.

7.2.2. Menu system

In order to create a central platform where the user will have a simple way to select between different paths in the program, it was decided to develop a menu system in graphics mode. This also avoids constant switching between text and graphics display in DOS, which can be irritating. To set up the menu, its structure must be first created and initialized to defaults. Adding individual menu items to the structure then creates a complete customized menu system. Figure 7-4 shows a menu where item "Displays" has its own sub items with their designated hot keys for activation. When the mouse pointer is used, a menu function can be selected by clicking on the main menu item and dragging the selection cursor down the dropped window until the desired item is highlighted. The function is then selected by releasing the mouse button. If the keyboard is used, function key F10 is pressed to select the menu bar. Arrow keys are then used to select the desired menu items. Pressing "ESC" key closes the menu.

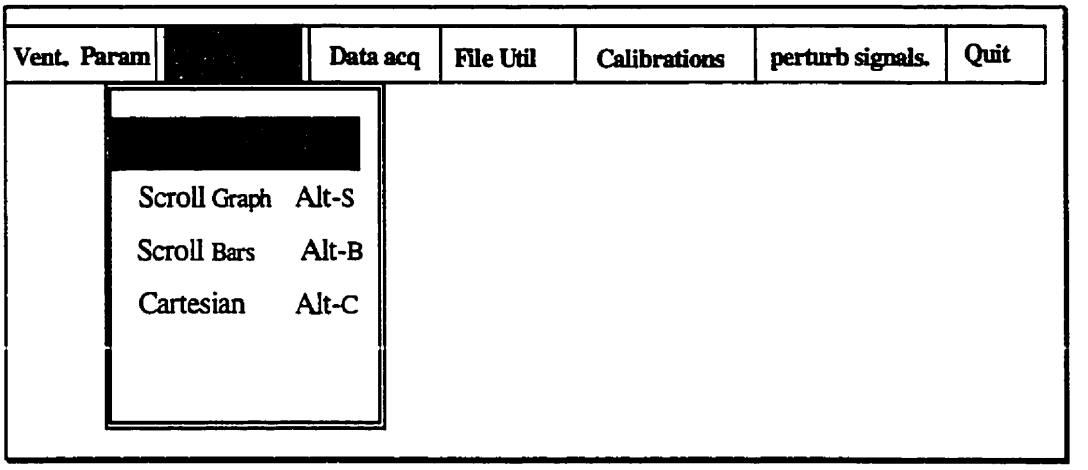

Figure 7-4: A simplified overview of RVV program menu

7.2.3. Function modules

The following is a list of all functions that are called upon from the main menu, sub menu and or within other functions. Some of them will be discussed in full detail in the coming sections.

- **int *datacq* (void)**: Responsible for driving the ventilator and data acquisition
- **int *dobargraph* (void)**: Selects the type of graphical display
- **int *generaldialogprocessproc* (int I, char *fn)** : Processes the data field inputs to the program via dialogboxes
- **void *generaldialogcloseproc* (int I, char *fn)** : Closes a dialogbox once it is no longer needed
- **int *dogeneraldialogbox* (void)** : Presents a dialogbox to the user according to the function in use
- **int *quityesproc* (void)** : Closes the menu system and releases all internal memories in a controlled manor.
- **void *initthemenu* (menutype *am)** : Initializes the menu at program startup
- **void *announcement* (void)** : Makes an announcement to the user if hardware reset is required
- **int *boardsetup* (void)** : Resets and initializes all the relevant hardware signals at startup or when the corresponding menu item is pressed.

- **int *calposition* (void)** : Calibrates the A/D channel on which the position of the vane is read
- **int *channelcal* (void)** : Calibrates all or any A/D channels as requested by the user.
- **int *footingstatus* (void)** : Draws the status bar on the bottom of the screen
- **int *fileoperation*** (void) : Changes the format of data file from ASCII to Binary and vice versa
- **int *filedisplay* (void)** : Displays the contents of the data file
- **int *changedirectory* (void)** : Changes the current working directory
- **int *setbordercolor* (void)** : Selects a border as well as background color for the central platform menu environment
- **void set_*border* (int)** : Places a border round the menu
- **int *changedrive* (void)** : Changes the current working drive
- **int signal (void):** Reads the perturbation signal into memory
- **realtype *getdataout* (int)** : Sends the controller output to the D/A board
- **void *interrupt* int_8253_routine(void)** : Sets the vector for a new interrupt service routine
- **void *interrupt* (*old_vector) (void)** : Gets DOS timer interrupt vector
- **void *clearundertitle* (void)** : Clears twenty four lines of text and data from the screen in graphics mood
- **void *ClearScreen* (void)** : DOS routine to clear text from the screen
- **void *GetCursor* (int *x, int *y)** : DOS routine to get the cursor position
- **void *MoveCursor* (int x, int y)** : DOS routine to position and move cursor

7.3 Setup and autocalibration

7.3.1. Hardware initialization

At startup, the program asks the user if a hardware initialization and setup is required. The entire procedure is incorporated in the function *boardsetup*. During this procedure, the error handling routine is initiated to make for safe return to the main

program every time an error occurs. The I/O lines on the D/A board are configured for output and data value 64 is sent out to set the first four least significant bits to zero to close all the valves. The display panel is now updated and the output of the D/A board is set to zero to avoid any unwanted input to the power amplifier so as not to drive the vane uncontrollably. At this point a computer controlled safety relay is activated which closes the contact between the power amplifier and the motor. The vane is now driven to the center point or zero position. The safety relay is deactivated and finally all background operations on A/D and D/A are explicitly stopped and the control is handed back to the menu system. Figure 7-5 gives the flowchart of these operations.

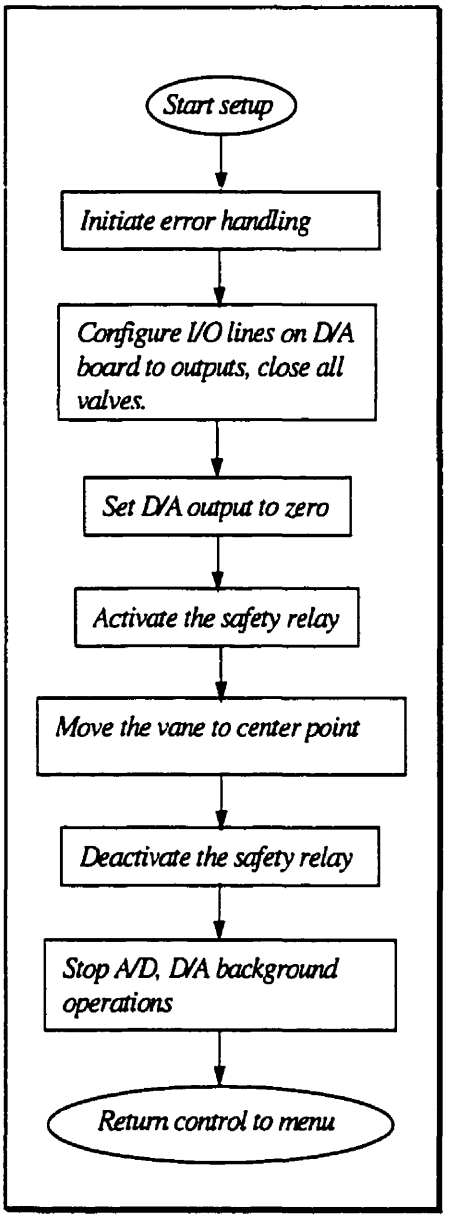

Figure 7-5: Hardware setup and initialization at program's startup

7.3.2. Position and pressure channel calibration

The program does both position channel and pressure channel calibration. Function *calposition* is called to calibrate the position channel. It starts off by dynamically allocating memory for an array to be used for calculating the mean value of up to 600 data points. The power amplifier safety relay is then activated and, by applying a constant voltage to the motor, the vane is driven to both end positions, designated by X_{min} and X_{max}. The position sensor output is read and an average of 600 data points is acquired. Volume displacement resolution is then calculated by:

$$m = \frac{1363}{4095}\left[\frac{ml}{bit}\right] \qquad (7.1)$$

where volume displacement of the vane from one end to the other is 1363 ml. The value of m is used to convert and transform the acquired position data into ml units. The function finishes by deactivating the safety relay and returning the allocated memory to the heap. Figure 7-6 gives a flow chart of this function. It should be noted that the position calibration routine can be called as frequently as desired from within the menu. Similarly, function *channelcal* can calibrate up to four pressure channels. When called, it requires a channel number from the user and then requests the pressure transducer to be subjected first to atmospheric then to a known constant pressure. 500 samples are taken in each case. An average of these samples is then used to calibrate the sensor. Future voltage readings of the transducer are converted to pressure units using these calibration values.

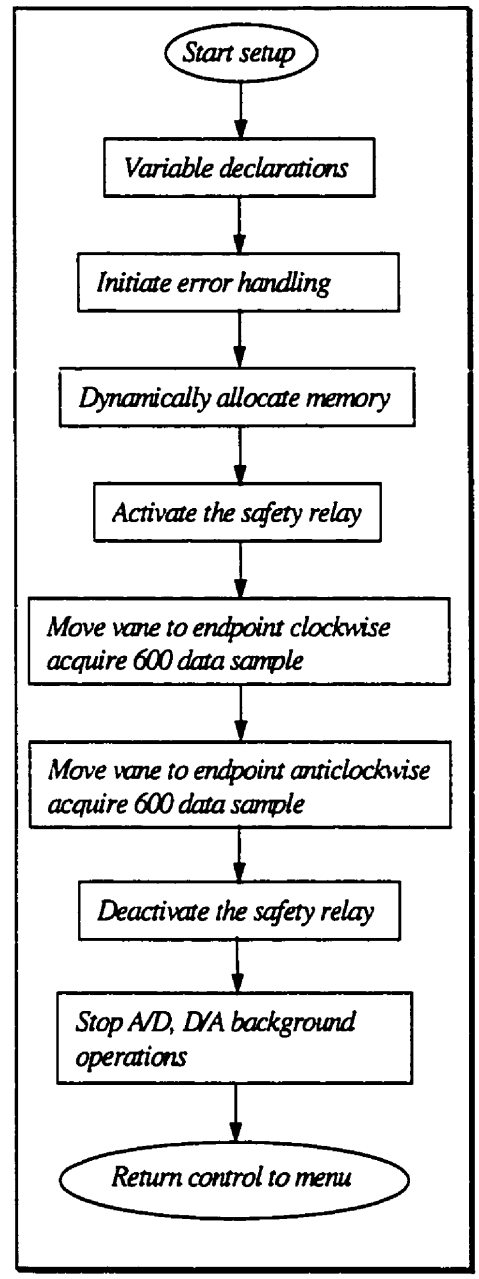

Figure 7-6: Position channel auto calibration flow chart

7.4 Data acquisition function

The major function that controls and acquires data is called *Datacq*. Figure 7-7 gives the flow chart of this function. The code starts with variable declarations. It takes the name given in the user dialogbox for data storage. The program appends an index to the name and increments the index for subsequent filenames. However, the user can change the filename for every acquisition if required. A series of other initializations are

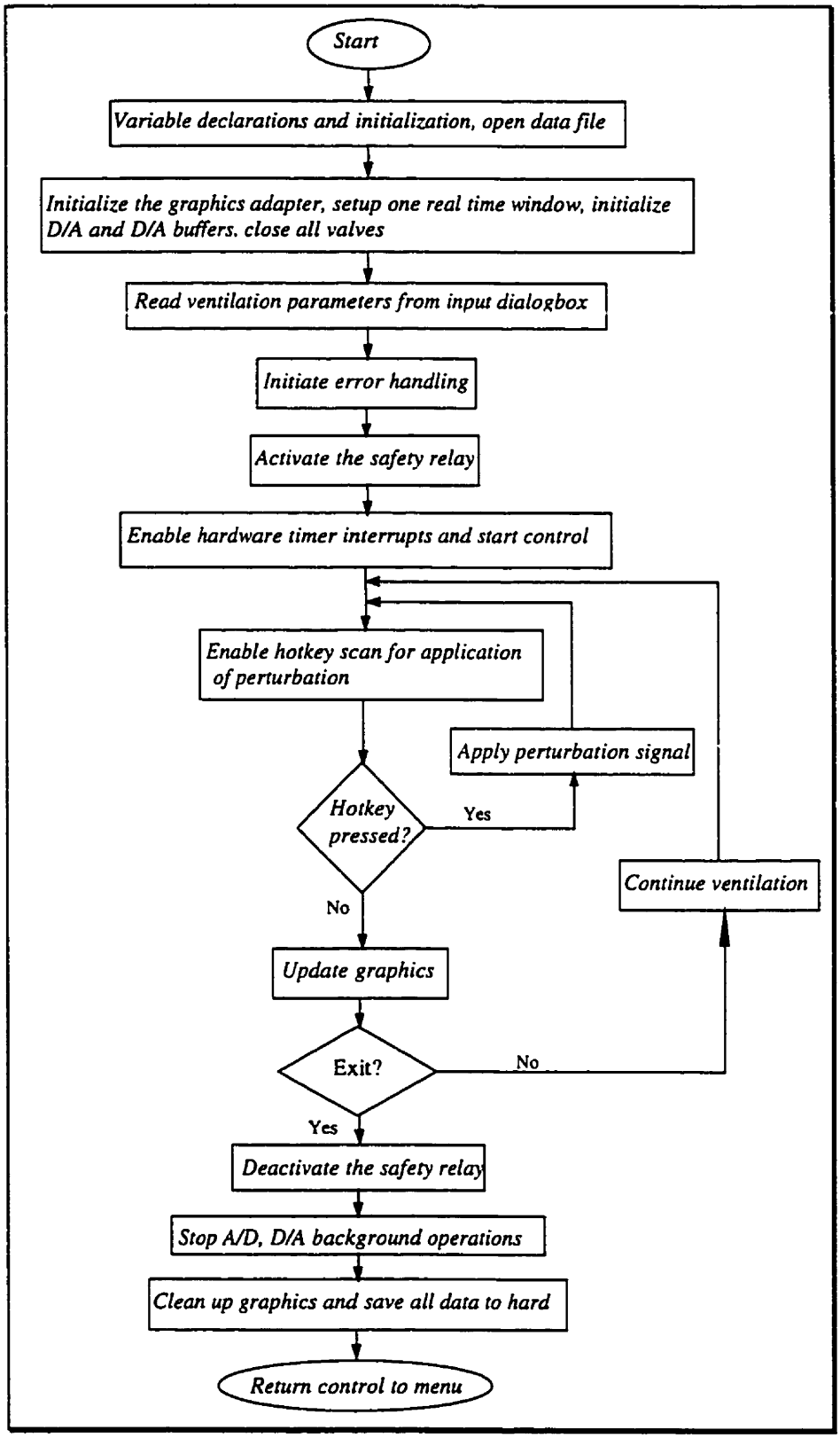

Figure 7-7: RVV control and data acquisition flow chart

carried out next as shown in Figure 7-7. The parameters defined for ventilation by the user are read and, after initiation of an error handling code, the safety relay that permits the movement of the vane by the motor is activated. At this point, the hardware driven interrupt is enabled and the control of the motor starts (see section 7.4.2). The ventilation waveform is constantly fed to the power amplifier to be delivered to the vane. A loop also simultaneously scans the keyboard and checks if the user wishes to apply a volume perturbation by pressing "ESC" key. If this hot key is pressed, the perturbation signal previously defined and loaded into memory is applied to the vane. The program stops when another specific hotkey "SPACEBAR" is pressed. The safety relay is deactivated, background A/D and D/A operations stop and the data previously saved in random access memory (RAM) are transferred to the hard disk (see section 7.4.3). Finally, the program control is given back to the menu system.

7.4.1. Perturbation signals

A perturbation signal consists of a file containing a sequence of real numbers describing the time structure of the signal. RVV software can read files of specified binary or ASCII format not exceeding 15000 points or 64 Kbytes in size and sampled at 1 kHz. Thus, duration of the perturbation signal is limited to 15 seconds. Presently, the software can accommodate signal files written in either *Matlab* or *Anadat* (RHT-Infodat, Montreal, Quebec) format.

7.4.2. Interrupt service routine (ISR)

As previously mentioned, the position control of the vane must have priority over all other administrative tasks within the software. Furthermore, the valve sequences must also be timed precisely. One way to achieve this in a robust fashion is to use a hardware interrupt routine, where at a precise time interval, the normal flow of program execution is interrupted and a specific routine (ISR) is called upon to carry out some user defined tasks. Once the ISR is executed, the instruction pointer is returned to the main program at the point where it was prior to occurrence of the interrupt. In an IBM PC compatible computer there are a number of possible interrupt sources which are assigned various

levels of priority (this is set within the hardware). For example, the 8253 Timer/Counter (which drives the DOS time and date function) is at level 0, the RS232 serial ports 0 and 2 (COM1: and COM3:) are at level 4 and ports 1 and 3 are at level 3. An 8259 PIC (Programmable Interrupt Controller) controls which interrupt level is enabled at any time and arbitrates between the different priorities. However, in the present application to designate the highest interrupt priority to motor control and data collection, Timer 0 of the 8253 chip is connected to hardware interrupt 0, which has the highest priority. The Timer is programmed so that a 1.193 MHz oscillator clock pulse counts 1193 cycles before issuing another interrupt. This gives a controller sampling rate of 1 kHz. Figure 7-8 shows the flow chart of the code within the ISR. On entering the routine, the valve sequence is configured and sent out to the corresponding driver board via I/O lines on the D/A board. In normal ventilation mode, the relative timing of the valves is a function of the respiratory cycle time as well as the inspiratory to expiratory ratio (I/E) as specified by the user. When a perturbation signal is applied, the valve configuration changes according to the protocol specified by the signal. Next, the vane position value is read and compared with that of the desired position. A new controller value is calculated according to the PI control algorithm and applied to the motor. Before leaving the ISR, all data channels are stored to a file on RAM disk and DOS time keeping is restored.

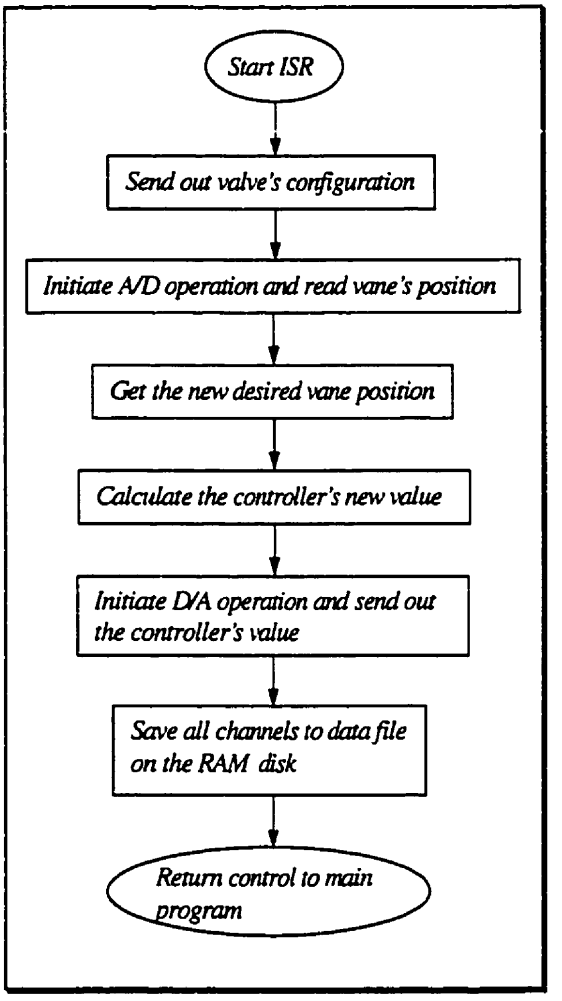

Figure 7-8: Interrupt service routine (ISR) software structure

Programming a hardware interrupt routine is not easy because debugging the code is difficult. Furthermore, one has to take great care when activating and deactivating an ISR since the ISR process could itself encounter an interrupt, in which case the procedure will not be completed with unpredictable consequences.

7.4.3. Data storage

The simplest type of file to use is a standard DOS file on a hard disk. The advantage of hard disk files is that they can be very large. The file size is only limited by the amount of free space on the disk. However, they have the disadvantage of being somewhat slow, and in certain cases during an ongoing data acquisition process, speed and/or interrupt priority conflicts make the use of a hard disk for immediate data storage problematic. Alternatively, data can be stored in RAM and transferred to the hard disk once data acquisition has been terminated. A major restriction in DOS is the size of any individual data structure, which has to be contained in a single segment in RAM and so must be limited to 64 Kbytes. Clearly this can be a problem when it comes to acquiring data for long periods of time at a high sampling rate. There are some complex programming techniques that can solve this problem, such as the dynamic memory allocation technique where the heap memory is allocated dynamically and released when there is no need for it. One can also use third party application packages, which permit the use of extended or expanded memory under DOS.

The RVV uses a very simple but effective technique to solve the memory problem for on line control and data storage. The idea is based on the use of a RAM or virtual disk. A Ram disk is not really a disk. It is a piece of code (device driver) that comes with DOS and that sets aside some of the computer's memory and makes it appear to DOS as a disk drive. At computer boot up, the CONFIG.SYS file calls on RAMDRIVE.SYS to install the required RAM disk. Once installed on the computer, it appears exactly as if one has another very fast hard disk drive. Furthermore, DOS commands work exactly the same on the RAM disk as on the hard disk. For example one can COPY, DEL, MKDIR, CD just as it is done on a hard disk. Naturally, the only restriction to the size of a single contiguous data file on a RAM disk is the actual total size of available memory in the

computer. In the Laptop computer used with the RVV this is limited to 15.5 Mbytes. The entire contents of the RAM disk are saved to the hard disk every time *Datacq* function terminates.

7.5 Utility functions

This is a module within the RVV program that includes miscellaneous routines for general-purpose file keeping as well as customizing the parameters of the GUI. One of the routines embedded in the utilities makes it possible for the user to change, delete, or add overlays and/or a status bar to the main program's operating platform. There is also a function which permits periodic examination of the physical alignment of the contacts between the position sensor shaft and the vane with respect to the reference index signal of the sensor. By driving the vane to the index reference point in closed loop control mode, one can observe the accuracy and or changes in the sensor output, as well as any physical misalignment which might have occurred. The design of the software is such that any further ideas concerning new functions for the ventilator or on line processes of data can be easily integrated into the program.

7.6 Closing remarks

In this chapter the RVV program features were presented. The tasks that the software has to perform were explained. The concept of the menu system as well as the choice of programming language, hardware and operating system platform were described. Details about some of the functions, such as control and data acquisition, ISR and RAM disk data storage were given.

In the next chapter, a demonstration of the RVV flow computation capability is presented. Measured flow is compared to that computed by the algorithm developed in section 4.1.3. Finally, the mechanical impedance of a ventilated load is measured.

8

RVV: Validation

For the RVV to measure respiratory impedance it has to compute the patient flow $\dot{V}$ (i.e. the flow that leaves the pressure chamber through opening A in Figure 4-3). Equation 4.18 shows how $\dot{V}$ is computed as a function of the position of the vane, pressures on either side of the vane and the flow $\dot{V}_a$ that leaves the ventilator to atmosphere through the opening (in/outlet) labeled C in Figure 4-3. To quantify $\dot{V}_a$, the pressure-flow characterization of opening C has to be carried out. This chapter describes how this was done, and how the accuracy of $\dot{V}$ computation by the RVV was assessed.

A further set of tests is described where an impedance load was connected to the RVV and subjected to a broad-band $\dot{V}$ waveform. Load impedance was computed from the driving pressure signal (i.e. P_{RC} in Figure 4-3) and $\dot{V}$.

8.1 Characterization of the flow through opening C ($\dot{V}_a$)

We want the opening C to have a measurable ΔP at the flows to be encountered. We therefore adjusted the flow resistance of opening C by placing aluminum meshes in the passage of the flow of the flow Figure 8-1. The experimental setup is shown in Figure 8-1. A blower generated flow, which passed through a rotameter for some indication of its magnitude before entering the pressure chamber. Flow was measured accurately by a calibrated pneumotachograph while a *Fujikura* solid state type pressure transducer

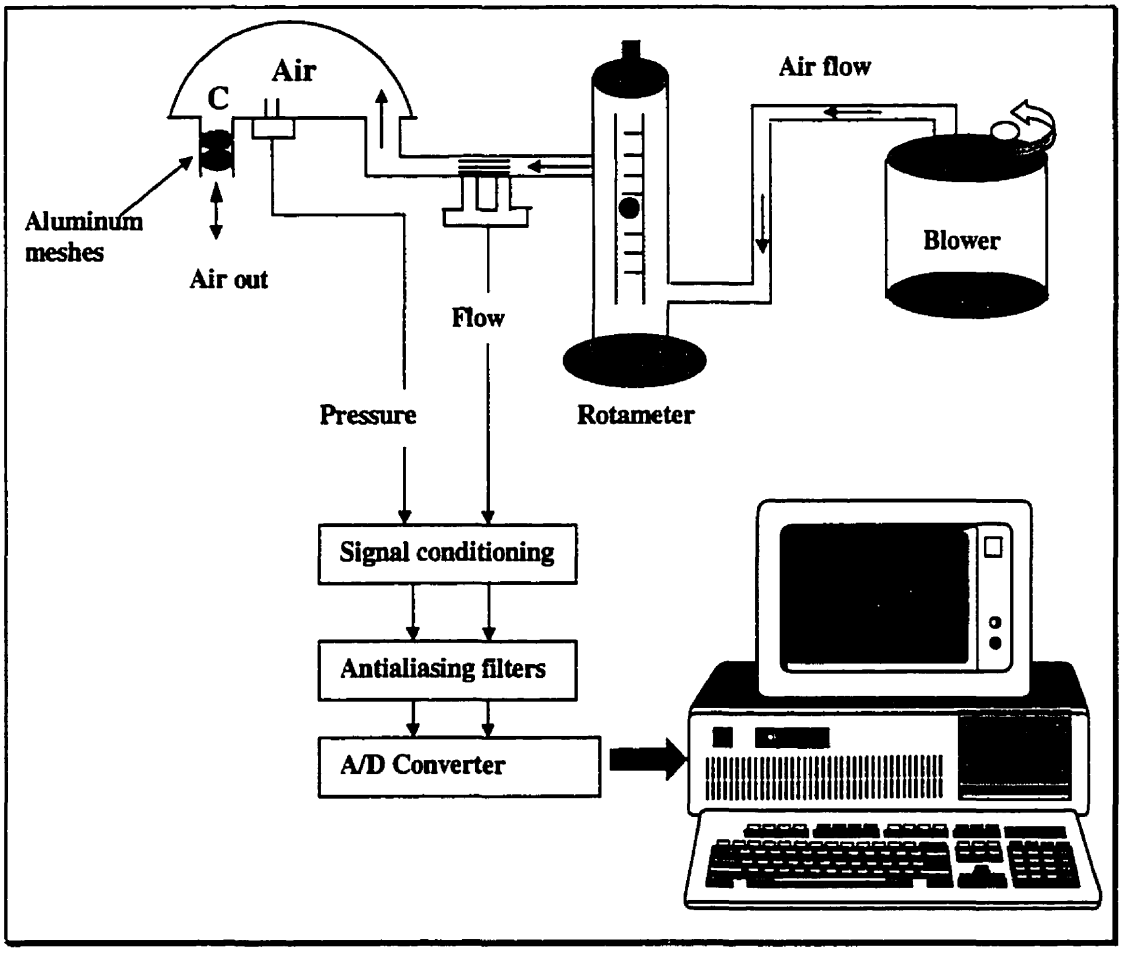

Figure 8-1: Experimental setup for characterization of opening C

measured the pressure in the chamber. Note that although in the experimental setup the vane had been removed, this did not affect the pressure-flow relationship of opening C.

For a period of 40 seconds the voltage input to the blower increased slowly so that the generated flow increased monotonically from zero. Pressure and flow signals were measured, amplified and anti-alias filtered before digitization and recording. The sampling rate was 60 Hz. To investigate the effect of reversal of flow the blower was switched to suction mode and the same procedure was repeated.

The pressure-flow behavior of opening C is presented in Figure 8-2 and Figure 8-3 for flow into and out of the chamber, respectively. These pressure-flow relationships were characterized as a second order polynomial.

We now develop the mathematical relationship which defines the pressure-flow behavior of opening C. As previously shown (section 4.1.3 Equation 4.18), the flow $\dot{V}$ that leaves the ventilator to the patient through opening A (Figure 4-3) is

$$\dot{V} = \frac{P_a - P_{LC}}{R_a} + \frac{r^2 l\dot{\theta}}{2}(P_{LC} - P_{RC}) + \frac{r^2 l\theta}{2}\left(\dot{P}_{LC} - \dot{P}_{RC}\right) - \frac{r^2 l\pi}{2}\dot{P}_{LC} \qquad (8.1)$$

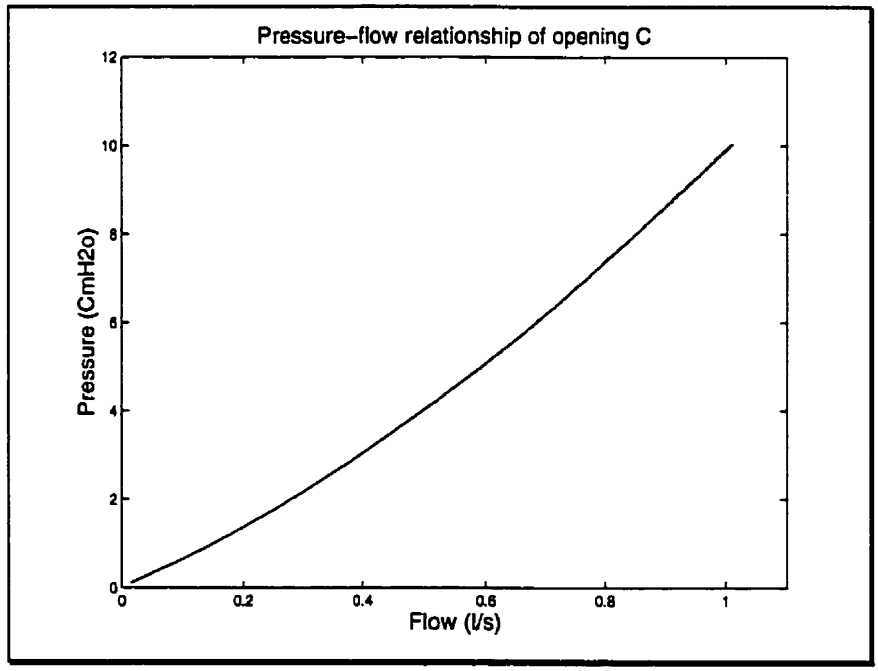

Figure 8-2: Pressure-flow relationship of opening C (flow leaves the chamber through C)

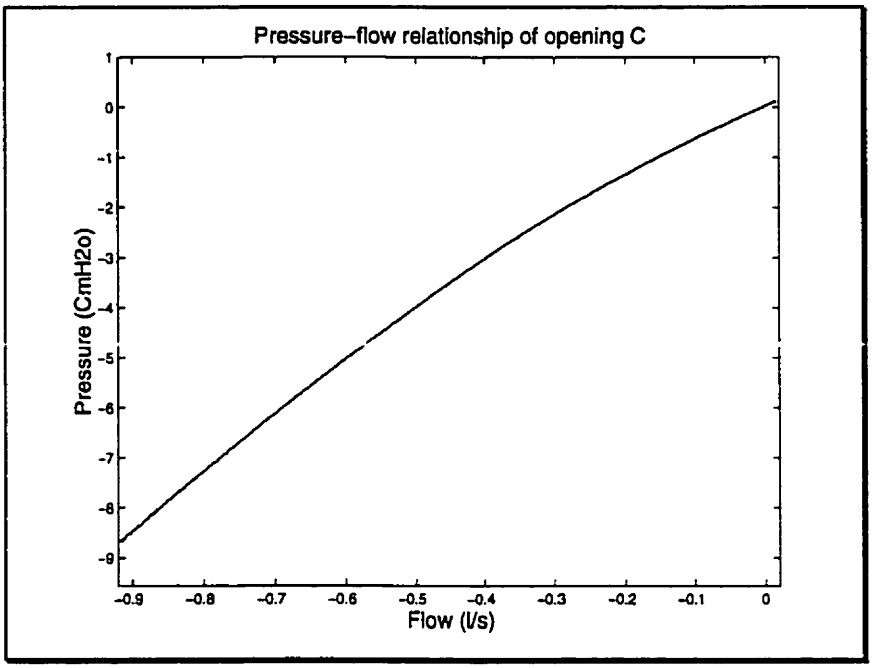

Figure 8-3: Pressure-flow relationship of opening C (flow enters chamber through C)

The term $\frac{P_a - P_{LC}}{R_a}$ in Equation 8.1, designated by $\dot{V}_a$ in Figure 4-3, is the flow through opening C due to the difference between atmospheric pressure and that of P_{LC}. Equation 8-1 can thus be written as

$$\dot{V} = \dot{V}_a + \frac{r^2 l \dot{\theta}}{2}(P_{LC} - P_{RC}) + \frac{r^2 l \theta}{2}\left(\dot{P}_{LC} - \dot{P}_{RC}\right) - \frac{r^2 l \pi}{2}\dot{P}_{LC} \tag{8.2}$$

To characterize $\dot{V}_a$ let

$$\dot{V}m = \left|\dot{V}_a\right| \tag{8.3}$$

For the pressure drop across opening C we can write

$$|P_{LC}| = a\dot{V}_m^{\,2} + b\dot{V}_m + K \tag{8.4}$$

Where a, b and K are some constants. K must be zero because $\dot{V}_a$ is zero when P_{LC} is zero. Therefore:

$$|1 - P_{LC}| = a\left|\dot{V}_a\right|^2 + b\left|\dot{V}_a\right| \tag{8.5}$$

Thus;

$$a\dot{V}_m^{\,2} + b\dot{V}_m - |P_{LC}| = a\dot{V}_m^{\,2} + b\dot{V}_m - M_{LC} = 0 \tag{8.6}$$

where $M_{LC} = |P_{LC}|$. Equation 8.6 is a polynomial of order 2 whose solutions are given by

$$\dot{V}_m = \frac{-b \pm \sqrt{b^2 + 4aM_{LC}}}{2a} \tag{8.7}$$

Because $\dot{V}_m > 0$, we choose the positive solution. Finally, substituting for $\dot{V}_m$ from Equation 8.3, $\dot{V}_a$ is

$$\dot{V}_a = \dot{V}_m \cdot Sig[P_{LC}] \quad \Rightarrow \quad \dot{V}_a = \frac{-b + \sqrt{b^2 + 4aM_{LC}}}{2a} \cdot Sig[P_{LC}] \tag{8.8}$$

A second order polynomial fit to the pressure-flow curve of Figure 8-2 yields the constants a, b and K as follows

$$\begin{aligned} a &= 3.82 \ \ cmH_2O.s^2.l^{-2} \\ b &= 0.621 \ \ cmH_2O.s.l^{-1} \\ K &= 0.0 \ \ cmH_2O \end{aligned} \tag{8.9}$$

The fit has a coefficient of determination equal to 1.000 and the variance accounted for (%VAF) is 99.99 (see Equation 6.20). Note it is not possible to show the polynomial fit on the same plot in Figure 8-2, since the data and fitted curves are indistinguishable.

Equation 8.8 can now be substituted into Equation 8.2 for estimation of $\dot{V}$.

8.2 Validation of flow ($\dot{V}$) computation by RVV

8.2.1. Single frequency sinusoidal volume input waveforms

Having characterized the pressure-flow relationship of opening C, we can now proceed to verify the accuracy of Equation 4.18 for determination of $\dot{V}$. To do this, the experimental setup of Figure 8-4 was used where generated flow was measured with a

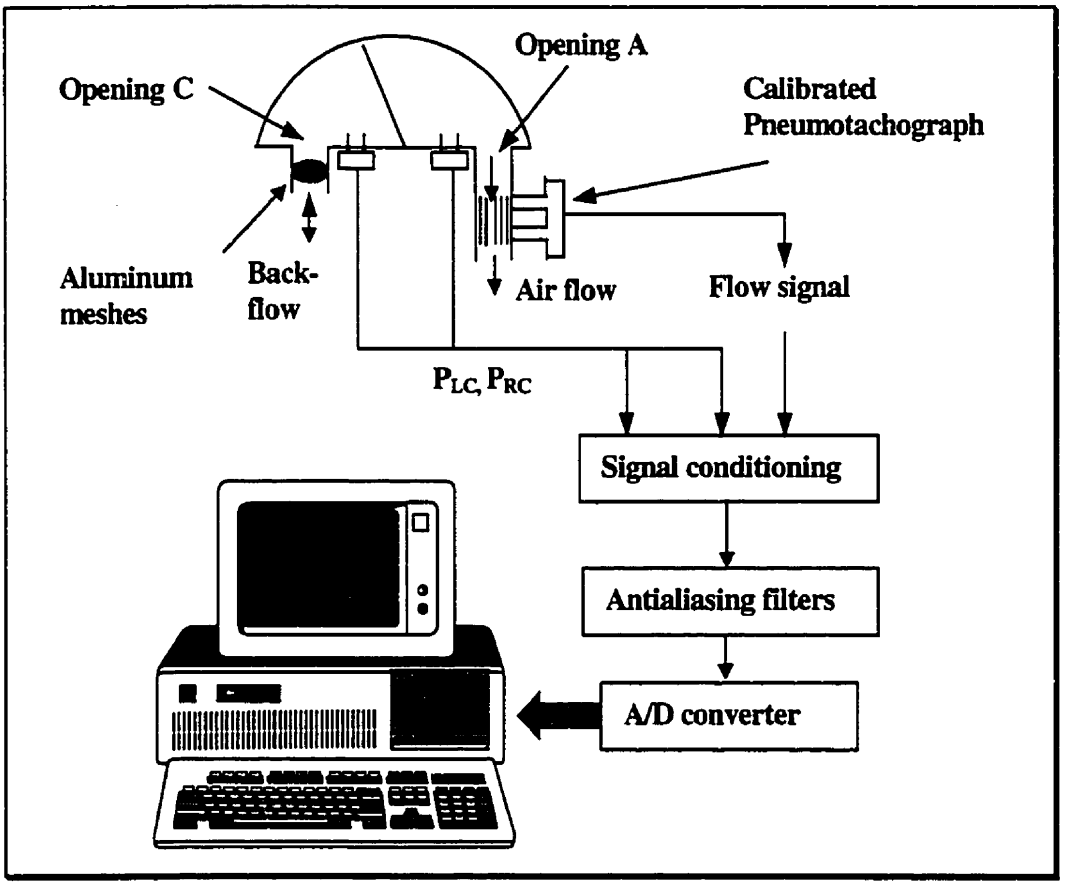

Figure 8-4 : Experimental setup for the validation of flow determined by Equation 4.18

standard calibrated pneumotachograph placed at the opening A as close to the pressure chamber as possible. A sinusoidal waveform signal was input to the ventilator drive to generate flow. The signals from the flow sensor, and pressure sensors from both sides of the vane were amplified and anti-alias filtered at 50 Hz before digitization and recording. Comparisons of the measured flow with $\dot{V}$ obtained from Equation 4.18 were then made.

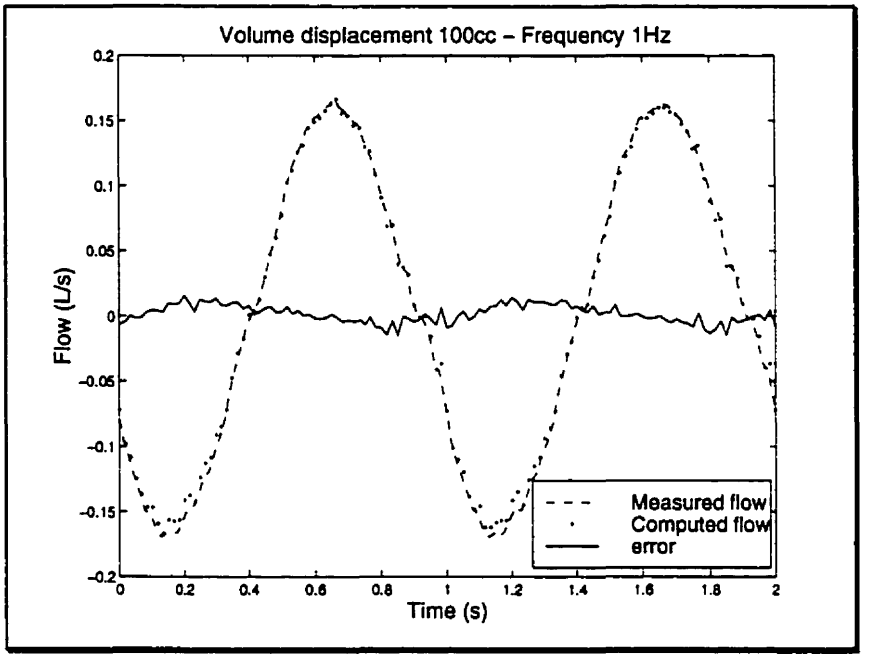

Figure 8-5: Flow measured by the pneumotachograph, computed flow and the error between the two

Figure 8-5 shows the measured flow, $\dot{V}$ and the error between them when a sinusoidal waveform of 100 ml peak-peak at 1Hz, was input to the ventilator vane. Forty seconds of data were sampled at 60 Hz (2 seconds is shown). The entire data record was used in the computation of error measures.

By comparing the two flows the following statistical results were obtained

$$\%VAF = 99.66, \qquad std(error) = 0.066, \qquad \frac{std(error)}{FSD} \times 100\% = 1.94$$

where $std(error)$ is the standard deviation of the calculated error between the measured flow and that determined by Equation 4.18, full scale deflection (FSD) is the peak to peak amplitude of the measured flow signal and $\%VAF$ represents the percentage variance accounted for (see Equation 6.20). Figure 8-6 gives the measured and computed flows for an input waveform signal of 100 ml p-p at 4Hz. The standard deviation of the error is 8.2×10^{-4}, the $\%VAF$ is 95.42 and percentage of $std(error)$ over full-scale flow deviation is 7.08. For smaller amplitude input waveforms these indices of accuracy improved considerably.

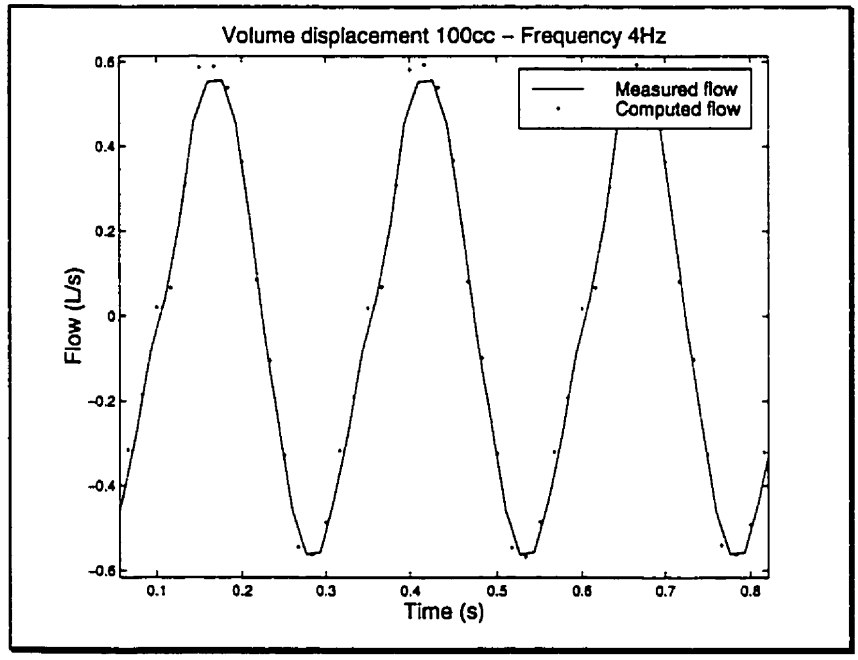

Figure 8-6: Measured and computed flows, input waveform 100 ml p-p amplitude at 4Hz

In Figure 8-7 the measured and computed flows show a $\%VAF$ of 99.19 with standard deviation of error at 9×10^{-3} and $\%\,std(error)$ over FSD of measured flow signal of 3.02. Finally, in a systematic series of tests, when the vane displacement amplitude was varied from 20 ml at 10 Hz to 150 ml at 1 Hz, $\%\,std(error)/\,FSD$ never exceeded 9.1.

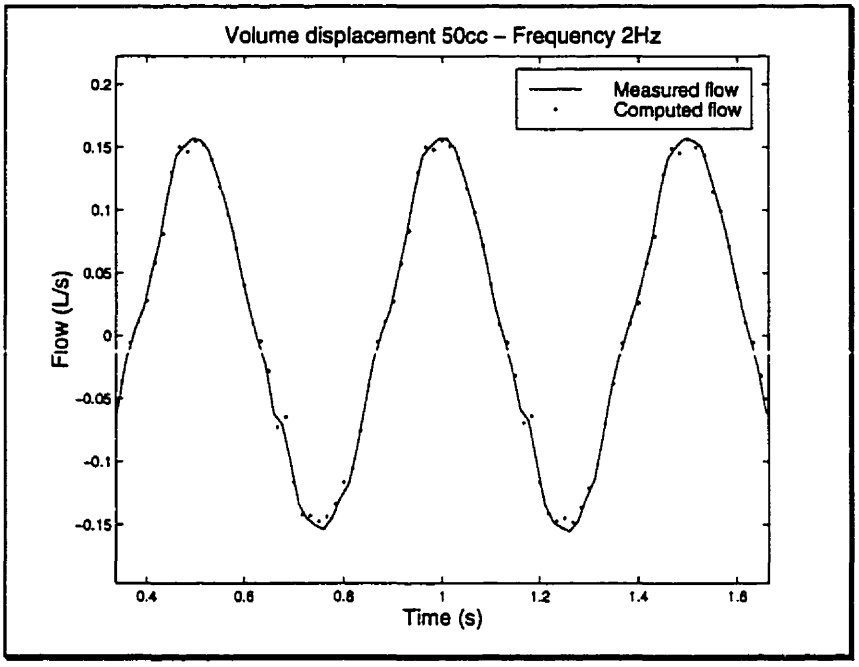

Figure 8-7: Measured and computed flows, input waveform 50 ml p-p amplitude at 2 Hz

8.2.2. Chirp input waveforms

To obtain further confirmation of the accuracy of the algorithm for the computation of flow, two more sets of experiments were carried out. In both experiments the experimental setup of Figure 8-4 was used. In the first test the RVV was not connected to any load. A chirp signal of 0 to 5 Hz frequency with amplitude decreasing with frequency was input to the vane drive. The generated flow was measured with a standard calibrated pnemotachograph placed at the opening A. Figure 8-8 shows the computed flow and the measured flow when the amplitude of the chirp was maximum. The two flows were compared over the eintire 0-5 Hz range and gave the following results

$$std(error) = 0.095\,, \quad \frac{std(error)}{FSD} \times 100\% = 4.093$$

In the second test the RVV was connected to a load (a plastic tank of 56 liters volume) via a pnemotachograph . The same chirp signal as above was used to drive the vane.

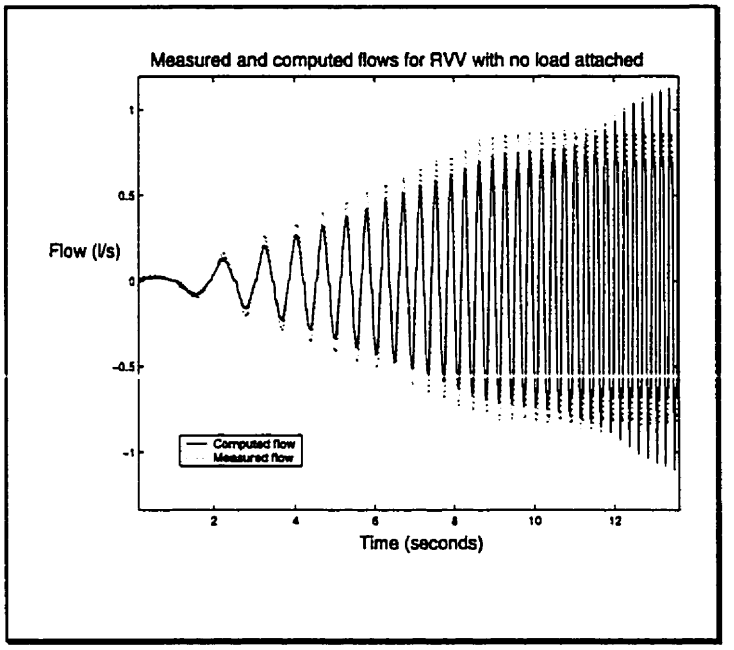

Figure 8-8: Measured and computed flows with no load attached

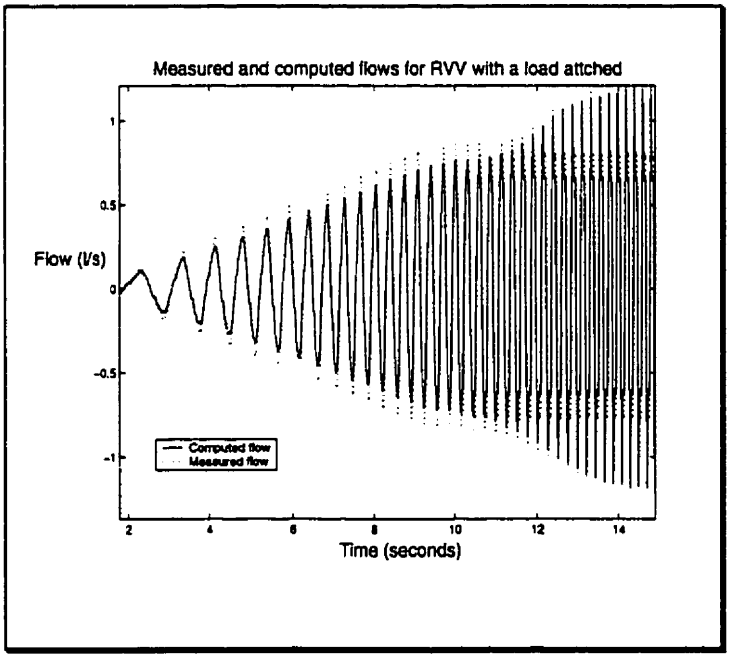

Figure 8-9: Measured and computed flow with a load attached

Figure 8-9 shows the computed flow and the measured flow. Comparing the calculated and measured flows gave

$$std(error) = 0.868, \quad \frac{std(error)}{FSD} \times 100\% = 3.514$$

Note in both tests the $std(error)$ over full-scale flow deviation did not exceed 5%. Results obtained in these two experiments reconfirms the accuracy of the algorithm (Equation 8.2) used to compute patient-flow by RVV

8.3 Load impedance estimation by RVV

To evaluate the load impedance estimation capability of the RVV, a load similar to the respiratory system was tested. This consisted of a container of approximately 56L volume with resistive and elastic properties and a piece of tubing with resistive properties. The outlet of the pressure chamber (opening A in Figure 4-3 or Figure 8-10) was connected to the inspiratory valve through a very short piece of non-compliant plastic tubing with diameter 22 mm and a length of 8 cm. Its negligible impedance was common to all measurements. However, the "patient circuit", that is the piece of tubing between the inspiratory valve and the load, was about 50 cm long and had a diameter of 22 mm. It was also non-compliant and posed a very small load to the RVV that had to be measured separately when a load was connected to the RVV.

The procedure to verify the resolution of the ventilator in measuring small and larger loads was as follows. First, the connecting tube was connected to the RVV and its impedance was measured in isolation. Next, the container impedance was measured on its own. Finally the connecting tube and the container were joined and the impedance of the ensemble was measured.

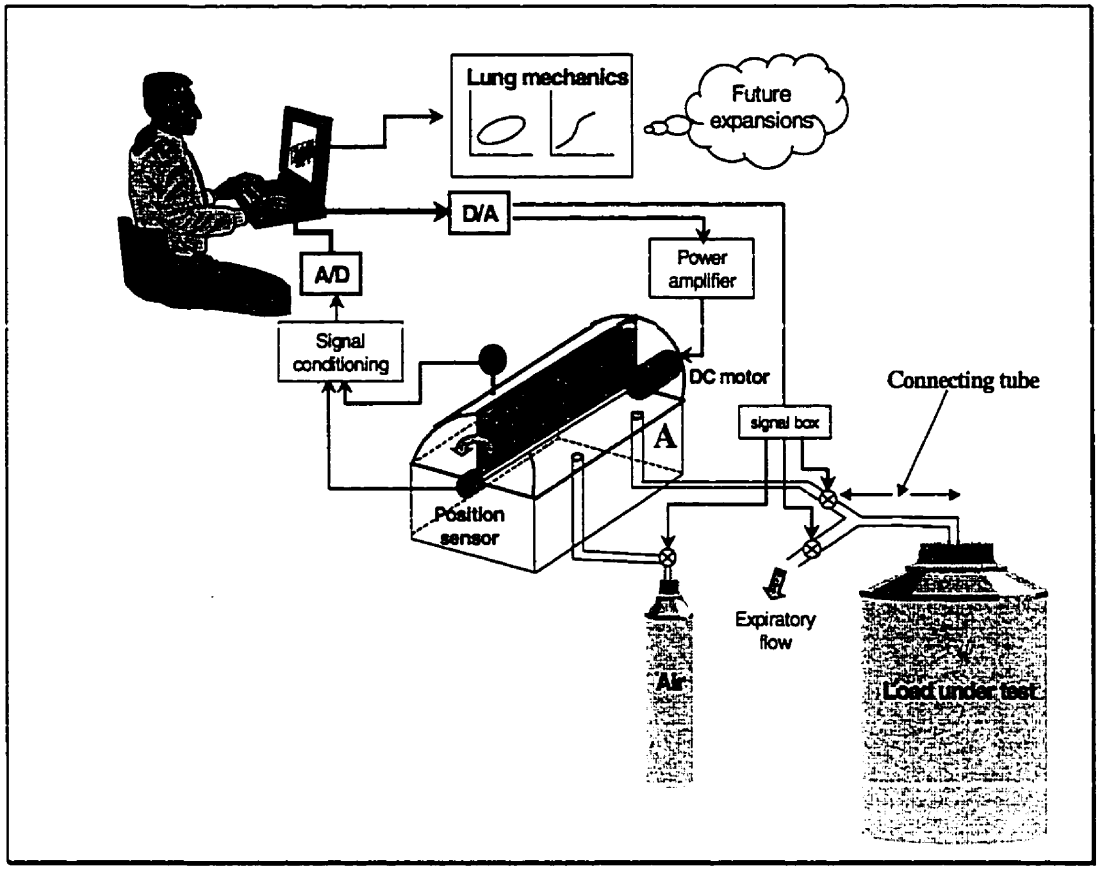

Figure 8-10: RVV's experimental setup for estimation of respiratory mechanics

Figure 8-10 shows the experimental setup for mechanical load measurements. The desired input waveform to the RVV was a chirp signal with a frequency that increased from 0.5 to 5 Hz over 15 seconds. The amplitude of the chirp decreased hyperbolically so that flow amplitude remained constant (Figure 8-1). The data were sampled at 1 kHz. The impedance of the load was obtained by dividing the Fast Fourier Transform (FFT) of P_{RC} by the FFT of $\dot{V}$ (see section 2.6.1).

Figures 8-12 to 8-14 show the measured load impedances of the connecting tube, the container and that of the container plus the tube ensemble. In all cases, the load characteristics obtained are of the form anticipated. For instance, the resistance of the tube is approximately constant as frequency increases while its reactance increases linearly, Figure 8-12. This is expected of a resistive-inertive load. For the container, Figure 8-13, the resistance decreases with frequency presumably due to polytropic gas

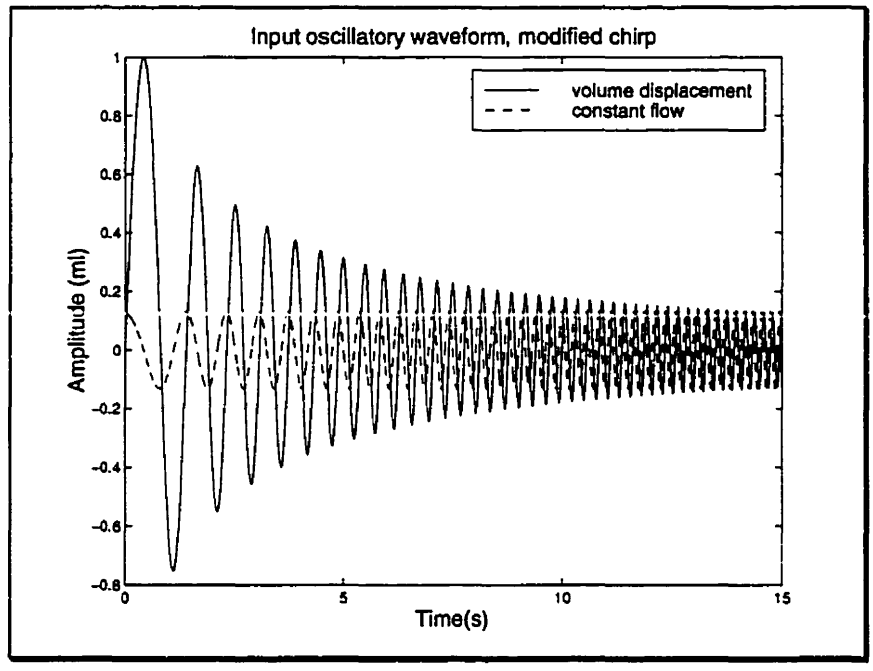

Figure 8-21: Modified Chirp signal used as input signal and the theoretical resulting flow

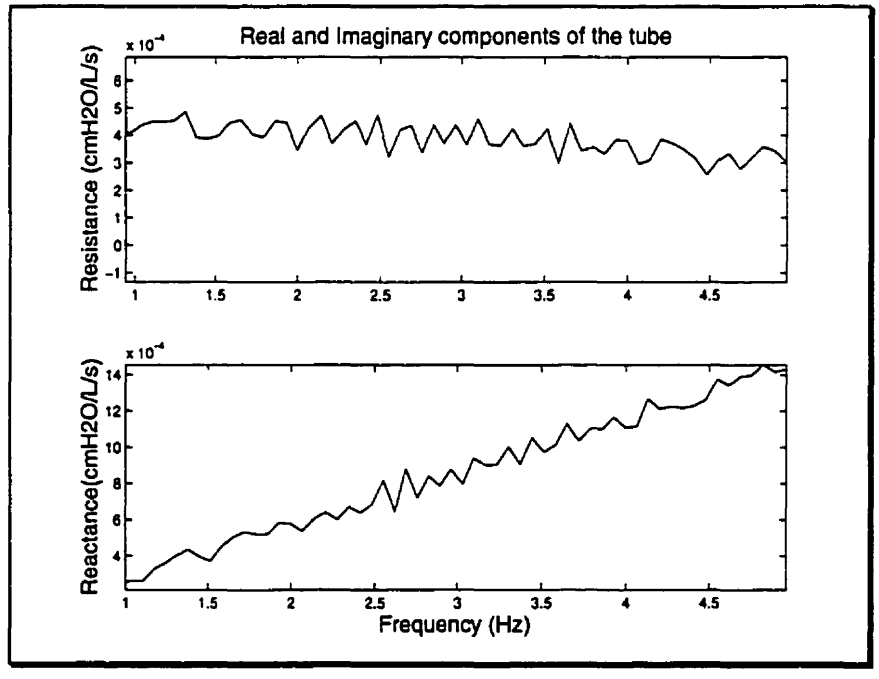

Figure 8-12: Real and imaginary components of the impedance of the connecting tube on its own

compression while its reactance increases in a hyperbolic fashion. Note, the noise in these plots is due to the use of the chirp perturbation signal.

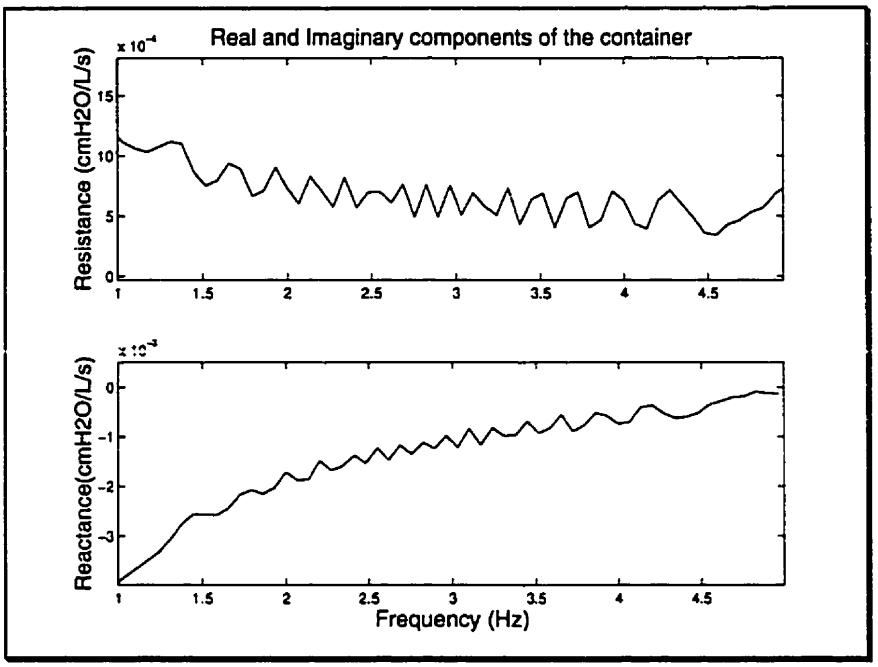

Figure 8-13: Real and imaginary components of the impedance of the container on its own

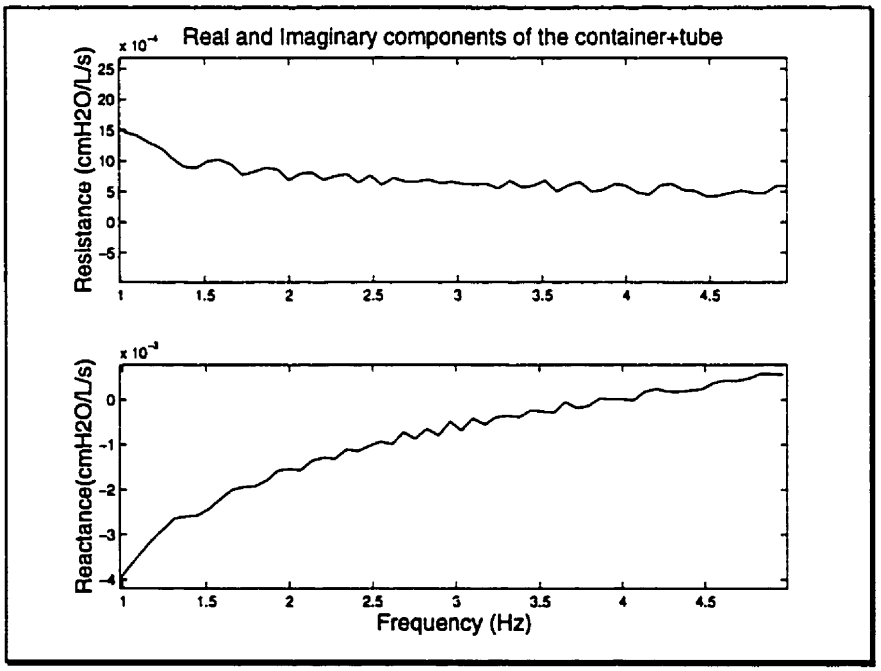

Figure 8-14: Impedance of the container and the connecting tube in series

Figure 8-15 shows the superimposition of the measured impedance of the ensemble load (tube and container in series) and the summed impedances of the individual parts. In general the respective resistive and reactive components of the impedances match well. The resolving power of the RVV is demonstrated by the fact that the ensemble load can be described by the superposition of the characteristics of the individual components.

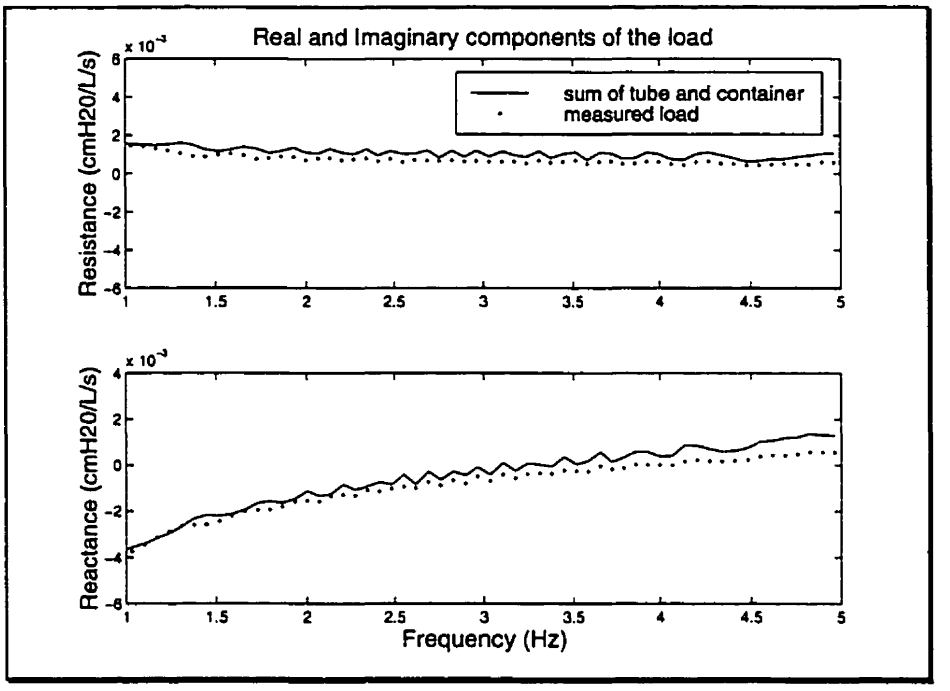

Figure 8-15: Measured impedance of the container plus tube, the sum of their individual impedances

8.3.1. Theoretical analysis of the load

The elastance of the gas in the plastic container used as the load in the following tests is inversely proportional to its volume, and has a value of

$$P\ /V\ = 1000/56=17.9\ cmH_2O.l^{-1} \tag{8.10}$$

where P is the atmospheric pressure and V is the volume of the container.

8.3.2. Estimation of the load by RVV versus the computer controlled piston oscillator

In a further attempt to confirm the accuracy of the load measurements by the RVV a load similar to that used in section 8.3 was chosen and was connected to a computer controlled oscillatory piston. This device consisted of a moving piston inside a

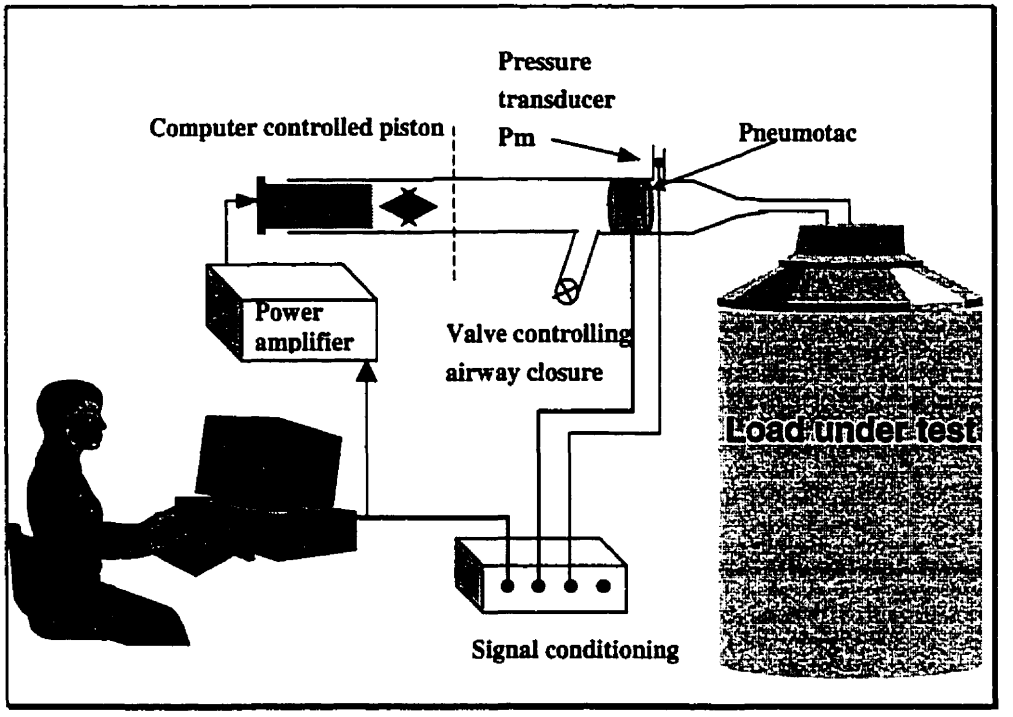

Figure 8-16: The experimental setup for the Piston oscillator

glass syringe. The piston was driven by a linear motor of a fixed magnet, translation coil servo taken from a RK-05 disk drive (DEC). The position of the servo-arm of the linear motor was sensed by a linear variable differential transformer, LVDT (model DC-E 1000, Lucas Schaevitz, Pennsauken, NJ). No amplification was required for the position measurement, due to the matching of the LVDT output to the A/D input dynamic range of ± 5 volts by use of a voltage divider resistor network. For control purposes an unfiltered position signal was sent by the computer. The motor driver amplifier was essentially a PA-12A (Apex μ tech, Tuscon, Arizona) operational amplifier in a noninverting configuration. Piston diameter was 20 mm with a volume displacement of air of up to 50 ml. As the piston moved in the syringe, the volume of air displaced was

equal to the volume displacement of the piston. Since the piston fitting in the syringe is of a bushing nature, the air leak was practically non-existent.

The experimental setup is shown in Figure 8-16. Flow was measured by a pneumotachograph placed at the end of the syringe. The tank was directly connected to the pneumotachograph via a connector tubing of 4 cm length. The pressure signal was measured at the entry of the tank. The input waveform to the piston oscillator was a chirp signal with a frequency that increased from 0 to 5 Hz over 16 seconds. Data were sampled at 200 Hz. The impedance of the load was obtained by dividing the FFT of the pressure signal by the FFT of the flow. Figure 8-17 shows the real and imaginary components of the load when measured by the RVV and the Piston oscillator. The solid lines show the resistive and reactive components of the load measured by the RVV. The dotted lines show that measured by the Piston oscillator. With the exception of small differences at frequencies less than 0.5 Hz due to poor signal-to-noise ratio, the load components measured by the two ventilators match well over the frequency range.

The theoretical (anticipated) value of the reactance of the load is obtained by dividing the elastance of the load (E) by $-2\pi f$ (see 2.6.2). This is shown as the dashed line in Figure 8-17 (middle plot). When the reactance of the load measured by the RVV was compared to the anticipated reactance the $std(error)$ was 1.93 yielding a $\%\, std(error)/\, FSD$ of 4.6. Once again a small difference between the two curves was mostly observed over frequencies less than 0.5 Hz. Figure 8-17 (bottom plot) shows the measured elastance of the load obtained with the RVV and Piston oscillator. Although at lower frequencies the value for elastance given by the RVV, 22 $cmH_2O.l^{-1}$, is higher than that obtained theoretically, 17.9 $cmH_2O.l^{-1}$ nevertheless it approaches that of the theoretical value at higher frequencies. The measured value of elastance by the Piston oscillator was around 20 $cmH_2O/l/s$.

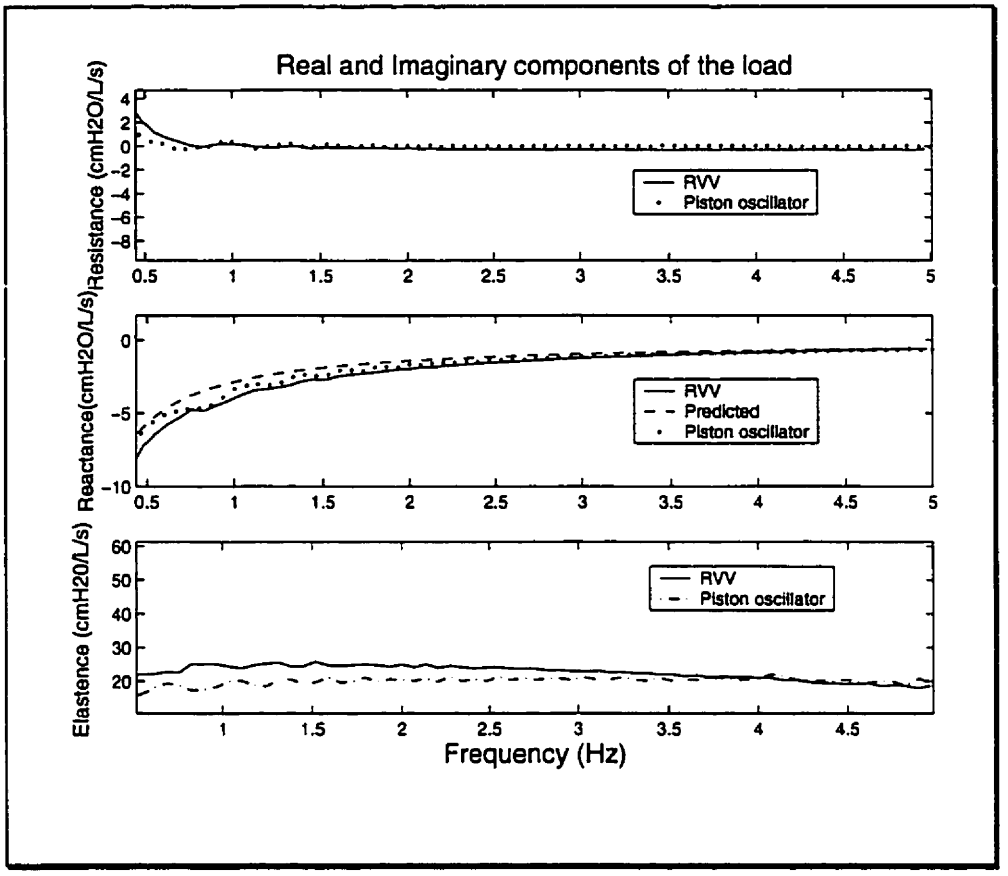

Figure 8-17 :Comparison of the measured impedance of the tank using RVV and the Piston oscillator

8.4 Respiratory impedance in normal subjects

To demonstrate the capability of the RVV in measuring the respiratory impedance of a normal subject, the experimental setup of Figure 8-10 was used. The subject was a healthy male 42 years of age, 1.78 m height and 69 kg in weight. During the experiment he sat in upright position on a chair directly facing the ventilator. A mouthpiece connected him to the RVV while he remained apneic with glottis open for the 16 second duration of the experiment. The input waveform to the RVV was a chirp signal whose frequency increased linearly from 0 to 5 Hz over 16 seconds while its amplitude decreased hyperbolically. Data were anti-alias filtered at 50 Hz and sampled at 200 Hz. To minimize oscillation of the upper airways the subject firmly supported his cheeks with his hands during the measurement.

The calculated impedance (Figure 8-18) shows the expected frequency characteristics (Pelsin and Fredberg, 1986; Hantos et al., 1986). Specifically, resistance shows a strong negative frequency dependence below 2Hz, reflecting the complex rheological properties of the respiratory system tissues, while it plateaus toward airway resistance at higher frequencies. The small peak around 1 Hz is presumably an artifact due to the beating heart. The reactance increases monotonically with frequency and would presumably cross zero at about 9 Hz, the expected resonant frequency of the respiratory system. Elastance (obtained by multiplying reactance by $-2\pi f$) increases slightly with frequency below about 1.5 Hz, again a manifestation of tissue rheology, and then decreases at higher frequencies due to the effects of airway inertance.

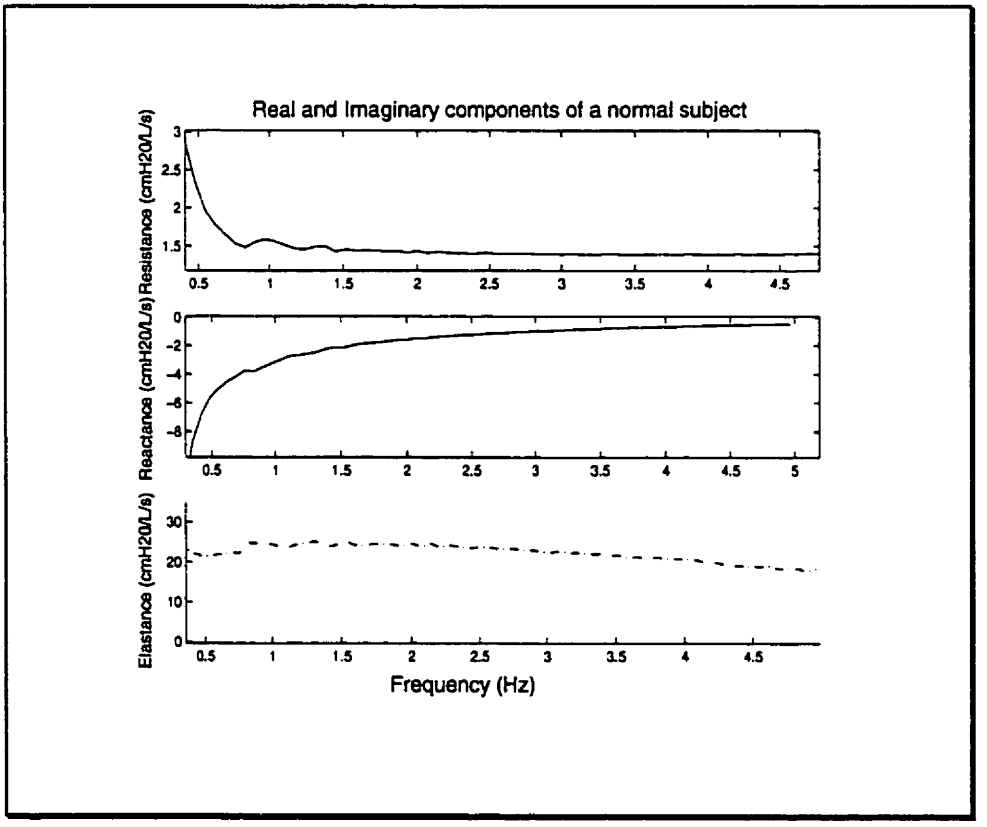

Figure 8-18: Measured impedance of a normal subject

The above experiment was repeated 6 times. When the mean of the impedance was calculated for the best 3 trials the following results were obtained:

mean $std(error)$ for the resistance was found to be 0.461, while $\%\, std(error)/\, FSD$ was 6.8. For reactance the mean $std(error)$ was calculated to be 0.9314 with $\%\, std(error)/\, FSD$ at 5.3. Much of the variation between trials was probably due to variations in the degree of relaxation of the subject at each trial.

8.5 Closing remarks

In this chapter the pressure-flow relationship of opening C was characterized, which in turn enabled the computation of $\dot{V}$. The accuracy of $\dot{V}$ through extensive tests was validated. It was shown that the RVV possesses the ability to resolve small loads in a simple composite system. The RVV was successfully used to estimate the impedance of various loads. Comparison between the RVV and a computer controlled piston oscillator was made. Expected and measured elastence of a load was compared. RVV was successfully used to measure the impedance of a normal subject.

In the next chapter, a discussion and conclusions will be presented. The application scope of the RVV will be illustrated. Recommendations for future directions are discussed. Finally, original contributions are listed.

9

Discussion and conclusions

This thesis describes the design, construction and workings of a prototype flexible computer-controlled rotary vane ventilator suitable for use on large animals as well as human beings. The gas compression mechanism used in the RVV is based on a unique design that permits estimation of flow from the ventilator without the use of any flow transducer. This is significant because it circumvents problems associated with pneumotachographs such as poor response at high frequencies and the inconvenience of sterilization after use. Furthermore, the RVV can apply any desired ventilatory flow waveforms in a flexible and practical manner. The computed flow is determined from vane position and the pressures on either side of the vane. The use of a rotary vane for flow generation has the following advantages:

(i) The actuator can be a rotary dc motor, which is economical and can oscillate at high frequencies easily.

(ii) The vane shaft angular position can be accurately measured with economical transducers.

(iii) The control of delivered air volume is very precise even at higher frequencies.

Another feature of the ventilator is its negligible dead space and the fact that the impedance of the connecting tube between the ventilator and the patient (i.e., the patient circuit) can be precisely determined.

The RVV was designed and developed as a research ventilator with computer flexibility in mind. Its compatibility with standard data analysis packages such as *Matlab* or *Anadat* makes it possible to generate an unlimited variety of volume perturbation signals. Furthermore, real-time safety and diagnostic features can be easily implemented via software, such as the Information Display Panel.

In principal, the RVV is also capable of applying many modes of ventilation; all that is required is an appropriate modification to the software. Another key design feature of the RVV is that it can be used to keep a patient alive while simultaneously applying perturbations for respiratory mechanics measurements; this will permit a wider variety of sophisticated and versatile experimental protocols to be perused while maintaining higher measurement precision and better parameter control.

The RVV is physically compact and the use of a Laptop computer and custom designed supporting box makes it portable. In the present configuration the RVV has a flat frequency response up to 17 Hz for volume amplitudes ≤140 ml. As the amplitude increases the perturbation bandwidth decreases. However, at lower amplitudes a flat frequency response to greater than 17 Hz is easily achievable. The RVV thus has the ability to measure a wide range of load impedances.

Finally, the RVV was designed with expandability in mind. The hardware and software is modular enabling the adaptation and integration of new ideas with relatively little effort.

9.1 Applications scope: present and future

As a flexible research tool, the RVV has various domains of application, principally in the fields of ventilation control research, modeling of respiratory system mechanics and bronchial pharmacology.

9.1.1. Ventilation control

The clinical application of a conventional ventilator with high frequency capability as a viable substitute for high positive pressure ventilators, in the hope of eliminating the problems associated with the latter type, is still an ongoing debate. In certain cases, the use of a high frequency ventilator is advantageous. Patients with treatable forms of diffuse lung injury, or those with neuromuscular disorders that impair the respiratory muscles, fail to respond to conventional ventilation. High frequency ventilation reportedly has the advantages of conventional ventilation, but with a lower risk of barotrauma and cardiac compromise, although to date there has been no clear-cut large prospective clinical study to support this (Nochomovitz et al. 1987).

There are well-defined clinical situations where the high frequency mode of ventilation can offer definite advantages over other modes of ventilation. This can be due to the properties of this mode of ventilation or the actual size of the air delivery orifice that must be inserted in the airway to achieve adequate gas exchange. For example, high frequency ventilation can be delivered through a tiny cannula, which can be very useful during laryngeal surgery by permitting unobstructed access to the operating field. *Bronchoscopy*, *Laryngoscopy*, *Thoracic Surgery*, *Tracheobronchial Distruption*, *Mobilization of Airway Secretions*, *Diffuse Lung Injury*, *Neurosurgical Procedures*, *Unilateral Lung Injury* are examples where HFV has been successfully used in hundreds of patients (Nochomovitz et al. 1987).

9.1.2. Modeling respiratory mechanics

This has been the principal motivation for the development of the RVV. As mentioned before, the computer flexibility of the RVV permits application of different flow waveforms to the respiratory system. Thus, information at low frequencies, principally reflecting rheological properties of the respiratory tissues, can be obtained alongside information about the resistance and inertance of the airway tree that is reflected in the high frequency impedance. Moreover, with precise control over tidal volume, frequency and inspiratory-to-expiratory ratio, and without disconnecting the patient for the ventilator, ambitious and more elaborate experimental protocols can now be carried out.

9.1.3. Evaluation of bronchial pharmacology

The RVV can be used to improve the environment for experiments aimed at studying the responsiveness of the lung to various drugs.

9.2 Future directions

Respiratory ventilators that provide scientists with the means of applying specifically designed ventilatory signals or perturbations into the respiratory system are important research tools. Such ventilators should be able to accurately measure an impedance load up to 10 Hz, and offer good control over ventilatory parameters.

The new air compression chamber design and the computer flexibility of the RVV meet the requirements mentioned above. Nevertheless, future work should be directed at enhancing the modes of ventilation and protocols used to measure load impedance. For example, a useful addition would be a mechanism for allowing computerized setting of positive end expiratory pressure (PEEP). It would also be useful to extend the RVVs performance at higher frequencies (>17 Hz) and amplitudes.

A future RVV prototype should perhaps be built out of an appropriate metal rather than Plexiglass, and the use of a digital incremental encoder for sensing vane position would probably improve performance. This would make the RVV more robust and economical. A more powerful motor and power amplifier would also increase the frequency response of the ventilator. Further compactness in size could be achieved by the use of surface mount technology for all the electronic boards.

When used in a clinical setting for prolonged patient ventilation, the integration of air filters and proper air humidification equipment should be considered. It is hoped tht the RVV will bring a new standard of precision and flexibility to the research field of respiratory mechanics, and that the innovative design concept of its air compression chamber may set the trend for future generations of versatile broad-band computer controlled ventilators.

9.3 Original contributions

The design and construction of the RVV has included a great deal of research, both theoretical and practical. The following summarizes the novel contributions:

- Design and construction of a broad-band rotary vane ventilator capable of measuring load impedance without using a flow meter;
- Realization of the concept of varying the flow waveform applied to a patient without having to disconnect them from the ventilator. For example, perturbation signals can be either superimposed on spontaneous breathing or applied independently;
- Derivation of theoretical expressions for the estimation of the resistance to flow between the vane and the housing as a function of clearance between the two, length of the vane and radius of the housing;
- Development of a mathematical model for estimating the flow generated in a closed semicircular housing due to the rotation of a vane within it.

The following is a list of the key components of the RVV that have been custom designed and constructed for the purpose of meeting performance requirements.

- Gas compression chamber based on movement of a rotary vane having a very fine clearance with respect to its semicircular housing
- Motor power amplifier with variable gain
- Instrumentation-grade dc power supplies for use in various sections of the ventilator
- High-current capacity valve driver circuitry
- Computer controlled information display panel for real time display of key signals
- PCMCIA technology based data acquisition and control system running on a 90 MHz Pentium Laptop computer, featuring eight analog input channels with variable gain amplification and anti-aliasing filters, two analog output channels and sixteen digital I/O lines

- ❖ Comprehensive software package with many features including routines for fast motor position control, data acquisition, unlimited on line data storage, safety features and informative fast real time graphics.
- ❖ Compact custom made box to house the pressure chamber and all other components

9.4 Publications arrising from this work

"Lung volume dependence of bronchial responsiveness in rats." M. Ahmadi, T.F. Schuessler, C. Dolman, D.H. Eidelman and J.H.T. Bates. Presented at the Annual Meeting of the American Thoracic Society, New Orleans, May 11-15, 1996. Abstract in American Journal of Respiratory and Critical Care Medicine. 153:pp. A747, 1996.

"A computer-controlled high-bandwidth mechanical ventilator for the intensive care unit: design and construction." M. Ahmadi, T.F. Schuessler, and J.H.T. Bates. Presented at the Annual Meeting of the American Thoracic Society, San Francisco, May 17-21. Abstract in the American Journal of Respiratory and Critical Care Medicine. 155:pp. A526, 1997.

"Characteristics of a computer-controlled high-frequency ventilator for the intensive care unit." M. Ahamdi, T.F. Schuessler, and J.H.T. Bates. Presented at the Annual Meeting of the American Thoracic Society, Chicago, April 24-29, 1998. Abstract in the American Journal of Respiratory and Critical Care Medicine. 157: pp. A685, 1998.

"A computer-controlled high-bandwidth mechanical ventilator for the intensive care unit: design and construction." M. Ahmadi, J.H.T. Bates. Presented to the Association Québécoise des fabricants de l'industrie médicale, student-researchers contest, Montreal, 17-18 June 1988. Abstract no 9801 in AQFIM publications.

"Measuring pressure and flow delivered by a computer-controlled mechanical ventilator for the intensive care unit." M. Ahmadi and J.H.T. Bates. Presented at the Annual Meeting of the American Thoracic Society, San Diego, April 23-28, 1999.

"Measuring pressure and flow delivered by a computer-controlled rotary vane ventilator for the intensive care unit." M. Ahmadi and J.H. T. Bates, BMES, Atlanta, Oct 1999.

"Design and construction of a high-bandwidth computer controlled rotary vane ventilator." M. Ahmadi, and J.H.T. Bates. To be presented to the Annals of the Biomedical Engineering (in preparation)

"Mechanical Ventilator". J.H.T. Bates, T.F. Schuessler and M. Ahmadi. **Canadian Patent Application**, March 1997, filed by Swabey Ogilvey Renault, Montreal, Quebec (ref 1770-169 KPM/ch).

Alison, B. F. and C. A. Bryan (1987). "High frequency ventilation." American Respiratory Diseases **135**: 1363-1374.

Avanzolini, G. and P. Barbini (1985). "A comparative evaluation of three on-line identification methods for a respiratory mechanical model." IEEE Trans. Biomed. Eng **BME-32**: 957-963.

Bates, J. H. T. and A. M. Lauzon (1992). "A nonstatistical approach to estimating confidence intervals about model parameters: Application to respiratory mechanics." IEEE Trans. Biomedical Engineering **BME-39**: 94-100.

Bates, J. H. T. and T. F. Schuessler (1993). A mobile patient monitoring system for respiraory mechanics. Canadian Medical Biomedical Engineering Society.

Bates, J. H. T., M. S. Ludwig, et al. (1988). "Interrupter resistance elucidated by alveolar pressure measurements in open-chest normal dogs." Journal of Applied Physiology **65**: 408-414.

Bates, J. H. T., T. F. Schuessler, et al. (1993). Monitoring respiratory mechanics during anesthesia. 15th annual International Conference IEEE Engineering Medical Biology Society.

Bates, J. H. T., W. A. Decramer, et al. (1986). "Respiratory resistance with histamine challenge by single breath and forced oscillation methods." journal of Applied Physiology **61**: 873-880.

Boynton, B., F. Mannino, et al. (1984). "Combined high-frequency oscillatory ventilation and intermittent mandatory ventilation in critically ill neonates." Pediatrics **105**: 297-302.

Briscoe, W. A., R. E. Foster, et al. (1954). "Alveolar ventilation at very low tidal volume." Journal of Applied Physiology **7**: 27-30.

Butler, W., D. Bohn, et al. (1980). "Ventilation by high-frequency oscillation in humans." Anesthesioloy Analg **59**: 577-84.

Carlon, C. G. and S. W. Howland (1985). High frequency ventilation in intensive care and during surgery. New York, Marcel Dekker, Inc.

Carlon, G., R. Kahn, et al. (1981). "Clinical experience with high frequency jet ventilation." Critical Care Medicine **9**: 1-6.

Chang, H. K. (1984). "Mechanism of gas transport during ventilation by high-frequency oscillation." Jouranl of Applied Physiology: Respiratory Environment Excise Physiology **56**(3): 553-563.

Chang, H. K. and L. E. Farhi (1973). "Mathematical analysis of gas transport in the lung." Journal of Respiratory Physiology **18**: 370-385.

Chapman, F. W. and J. C. Newell (1989). "Estimating lung mechanics of dogs with unilateral lung injury." IEEE Trans. Biomed. Eng **BME-36**: 405-413.

DuBois, A. B., D. H. L. Brody, et al. (1956). "Oscillation mechanics of lungs and chest in man." J. Appl. Physiology **8**: 587-594.

Dupuis, G. Y. (1992). Ventilators: Theory and clinical applications. St. Louis., Mosby-Year Book, Inc.

El-Baz, N., L. Holinger, et al. (1982). "Hig-frequency positive pressure ventilation for tracheal reconstruction supported by tracheal T-tube." Anesthesia Analg **61**: 796-800.

Electro-Craft, C. (1980). DC Motors Speed Controls Servo Systems. Hopkins, Minn, Electro-Craft Corporation.

Flatau, E., G. Lewinsohn, et al. (1982). "Mechanical ventilation in fiberoptic-bronchoscopy: comparison between high frequency positive pressure ventilation and normal frequency [psitive pressure ventilation]." Critical Care Medicine **10**: 733-5.

Frantz, I. I., J. Werthhammer, et al. (1983). "High-frequency ventilation in premature infants with lung disease." Pediatrics **71**: 483-8.

Fredberg, J. (1980). "Augmented diffusion in the airways can support pulmonary gas exchange." Journal of Applied Physiology **49**: 232-8.

Fredberg, J. J., H. D. Keefe, et al. (1984). "Alveolar noninhomogeneity during small-amplitude high-frequency oscillations." Journal of Applied Physiology **57**: 788-800.

Fredberg, J. J., R. H. Ingram, et al. (1985). "Noninhomogeneity of lung response to histamine assesed with alveolar capsules." Journal of Applied Physiology **58**: 1914-1922.

Goldstein, D., A. S. Slutsky, et al. (1981). "CO2 elimination by high frequency ventilation (4 to 10 Hz) in normal subjects." Am. Rev. Respir. Dis **123**: 251.

Hantos, Z., B. Daroczy, et al. (1982). "Parameter estimation of transpulmonary mechanics by a nonlinear inertive model." Journal of Applied Physiology **52**: 955-963.

Hantos, Z., B. Daroczy, et al. (1990). "Modeling of flow-frequency pulmonary impedance in dogs." Journal of Applied Physiology **68**: 849-860.

Hazelton, F. and P. Scherer (1980). "Bronchial bifurcations and respiratory mass transport." Science **208**: 69-71.

Henderson, Y. H., F. P. Chillingworth, et al. (1915). "The respiratory of dead space." American Journal of Physiology **38**: 1-19.

Hilderbrandt, J. (1970). "Pressure-volume data of cat lung interpreted by plastoelastic, linear viscoelastic model." Journal of Applied Physiology **28**: 365-372.

Hirai, T., K. A. Mckeown, et al. (1999). "Effects of lung volume on lung and chest wall mechanics in rats." Journal of Applied Physiology **86**(1): 16-212.

Jackson, A. and K. R. Lutchen (1987). "Modeling of respiratory system impedance in dogs." Journal of Applied Physiology **62**: 414-420.

Kaczka, D. W., E. P. Ingenito, et al. (1997). "Partitioning airway and lung tissue resistances in humans: effects of bronchoconstriction." Journal of Applied Physilogy **82**(5): 1531-1541.

Klain, M. and B. Smith (1977). "High frequency percutaneous transtracheal jet ventilation." Crit. Care Med. **5**: 280.

Kolton, M. (1984). "A review of high frequency oscillation." Canadian Anesthetist Society **31**: 416-29.

Laubscher, P. T., W. Heinrichs, et al. (1994). "An Adaptive Lung Ventilation Controller." IEEE Transactions on Biomedical egineering **41**(1).

Lauzon, A. M. and J. H. T. Bates (1991). "Estimation of time-varying respiratory mechanical parameters by recursive least squares." Journal of Applied Physiology **71**: 1159-1165.

Lauzon, A. M., G. Dechman, et al. (1992). "Time course of respiratory mechanics during histamine challenge in th dog." Journal of Applied Physiology **73**: 2643-2647.

Ludwig, M. S., P. D. S. Romero, et al. (1990). "Interpretation of interrupter resistance after histamine induced constriction in the dog." Journal of Applied Physiology **68**: 1651-1656.

Lunkenheimer, P. P., W. Rafflenbeul, et al. (1972). "Application of "diffusion respiration"." Br. J. Anaesth. **44**: 627.

Lutchen, K. R., B. Suki, et al. (1994). "Airway and tissue mechanics during physiological breathing and bronchoconstriction in dogs." Journal of Applied Physiology **77**(1): 373-385.

Lutchen, R. K. and H. Gillis (1997). "Relationship between heterogeneous changes in airway morphometry and lung resistance and elastance." Journal of Applied Physiology **83**: 1192-1201.

Lyle, H. H., N. Josef, et al. (1986). High Frequency Ventilation. Boca Raton, Florida, CRC Press.

Macklem, P. T. and J. Mead (1986). Handbook of Physiology. Bethesda, Maryland, American Physiology Society.

Marchak, B. E., W. K. THompson, et al. (1981). "Treatment of RDS by high-frequency oscillatory ventilation: a preliminary report." J. Pediatr. **99:287**.

McPherson, P. S. (1995). Respiratory care equipment. St. Luis, Mosby-Year Book, Inc.

Mead, J. and J. L. Whittenberger (1953). "Physical properties of human lungs measured during spontaneous respiration." Journal of Applied Physiology **5**: 779-796.

Neegaard, K. v. and K. Wirz (1927). "Die Messung der Stromungswiderstande der Atemwedge der Menchen insbesondre bel Asthma und Emphesymen." Zeitschrift fur klinische Medizin **105**: 51-82.

Nochomovitz, L. M. and D. H. Montenegro (1987). Ventilatory support in respiratory failure. Mouny Kisco, New York., Futura Publishing Company, Inc.

Oberg, P. A. and U. Sjostrand (1969). "Studies of blood pressure regulation. Common carotid artery clamping in studies of the carotid-sinus baroreceptor control of the sytemic blood pressure." Acta Physiol. Scand **75**: 276.

Pelsin, R. and J. J. Fredberg (1986). "Oscillation mechanics of the respiratory system." American Physiology Society: handbook of physiology **III, section 3, part 1.**: 145-177.

Ribeiro, P. S., N. L. Tremblay, et al. (1998). High-frequency ventilation Principles and Practice. Physiological basis of ventilatory support. J. J. Marini and S. A. Slutsky. New York, Marcel Dekker AG. **118**.

Rodarte, J. R. and K. Rehder (1986). Dynamics of respiration, American Physiology Society.

Rohrer, F. (1915). "Der Stromungswiderstand in den menschlichen Atemwegen und der Einflub der unregelmabigen verzweigung des Bronchialsystems auf den Atmungsverlauf in verschiedenen Lungebezirken." Pflugers Archiv Gesammelte Physiologie Menschen und Tiere **162**: 225-299.

Rouby, J., J. Fusciardi, et al. (1983). "High-frequency jet ventilation in postoperative respiratory failure: determinants of oxygenation." Anesthesiology **59**: 281-7.

Sato, j., B. L. K. Davey, et al. (1991). "Low frequency respiratory system resistance in the normal dog during mechanical ventilation." J. Appl. Physiology **70**: 1536-1543.

Schied, H. K. and F. R. Haselton (1982). "Convective exchange in oscillatory flow through bronchial tree models." Journal of Applied Physiology **53**: 1023-1033.

Schied, P. and J. Piiper (1980). Intrapulmonary gas mixing and stratification. New York, Academic.

Schuessler, T. F. and J. H. T. Bates (1993). A computer controlled small animal ventilator. 15th Annual International Conference IEEE Engineering Medical Biological Society.

Sjostrand, U. (1980). "High-frequency positive pressure ventilation (HFPPV): a review." Critical Care Medicine.

Slutsky, A. (1981). "Gas mixing by cardiogenic oscillations: a theoretical quantitative analysis." Journal of Applied Physiology: 69-71.

Taylor, G. (1954). The dispersion of matter in turbulent flow through a pipe. Royal Society of London.

Van De Graaff, M. K. and W. R. Rhees (1987). Human anatomy and physiology. New York, McGraw-Hill, Inc.

West, B. J. (1977). Bioengineering Aspects of the Lung. Bethesda, Maryland, Marcel Dekker, Inc.

West, J. B. (1992). Pulmonary pathophysiology. Baltimore, Williams and Wilkins.

Younes, M. (1992). "Proportional assist ventilation, a new approach to ventilatory support. Theory." Americal Reiew of Respiratory Diseases **145**(1): 114-20.